博士論文

Comprehensive evaluation and environmental effects of urbanization process in China

中国における都市化総合評価及び環境への影響に関する研究

北九州市立大学国際環境工学研究科

2018 年 3 月

陳　偉

Wei CHEN

Preface

This thesis research was performed at the Department of Architecture at The University of Kitakyushu. This thesis presents an interdisciplinary study which combines insights from the field of urban dynamics, evaluation system, urban heat island effects, and thermal comfort studies. The focus is set on urbanization and eco-environment assessment, urban sprawl and urban expansion evaluation, urban heat island and its impact factors, urban structure and its effects on thermal comfort.

ABSTRACT

With the rapid development of economic, the sustained growth of the population, the fast urbanization and modernization, a number of metropolises have emerged in the world as Tokyo in Japan, New York in United States, and London in United Kingdom etc. The rate of urbanization all over the world is quite alarming, with the proportion of the world's population living in urban area projected to reach 66% by 2050. Urban area, with better access to health care, education, entertainment, and employment resources have been attracting a continuous flow of people from rural areas. As a result, the world is in the midst of the largest wave of urban growth in history. This remarkable phenomenon is generally known as urbanization. Urbanization may be defined as a social process significant to human society in the 21th century. It is accompanied by an increase in urban population followed by urban growth and urbanism a term referring to the urban life style. Urban development can be viewed as a complex system, urbanization is directly related to expansion of urban areas and growth of the proportion of total population leaving rural areas and moving to live in urban areas. In addition, urbanization always is characterized by their complexity heterogeneity and hybridity.

The rapid urbanization and economic development have caused many problems for the environment, society and governance. The rapid urbanization is associated with a variety of problems such as the loss of farming land, increase of CO_2 emissions, shortage of water resources in urban areas, housing shortages, traffic congestion, rising crime rate, biodiversity reductions, heat island effects, noise, air and water pollution. Many governments, researchers and practitioners have dedicated efforts to developing policies and methods for promoting sustainable urbanization. Recent years, Remote sensing science and technologies emerged as an important new tool for environmental applications over four decade ago. The environmental applications of remote sensing have gained an irreversible momentum ever since. Remote

sensing is now widely recognized as a valuable and often essential means of data collection for urban development applications.

The main aims of this study is to do the comprehensive evaluation on the urbanization processing and eco-environment based on hybrid method, besides, the land cover land use monitoring and its impact on urban heat island effect also have be analyzed.

Chapter 1, **PREVIOUS STUDY AND PURPOSE OF THE STUDY**, investigated research background and significance, In addition, previous study and current situation on the research fields was reviewed and discussed.

Chapter 2, **LITERATURE REVIEW,** provides an in-depth review of prior studies associated with the study which focuses on the following three aspects: urbanization and eco-environment evaluation; urban sprawl assessment, urban heat island investigation

Chapter 3, **INTEGRATED ASSESSMENT OF URBANIZATION AND ECO-ENVIRON--MENT IN CHINA,** maximum entropy method was applied to help generate the evaluation system of eco-environment level and urbanization level at provincial scaleComparison analysis and coordinate analysis was carried through to assess the development of urbanization and eco-environment as well as the balance and health degree of thee city develop. The analysis results show that, in both 2005 and 2015, the most urbanized province in China was Beijing. The highest value of eco-environment index was Qinghai which holds a highest value of eco-environment level indexes in both years. The results also provided that the urbanization level in China is unbalanced, Northwest, Southwest and Central China should pay attention to the urbanization development to catch up with the urbanization level in Eastern China, Eastern China should pay more attention on their eco-environment development with a relative high level of urbanization.

Chapter 4, **MEASUREMENT AND ASSESSMENT OF URBAN SPRAWL IN MAJOR CITIES IN CHINA,** DMSP/OLS stable nighttime light dataset was used to measure and assess the urban dynamics from the extraction of built up area. Urban sprawl was evaluated by analyzing the landscape metrics which provided general understanding of the urban sprawl and distribution pattern characteristics could be got from the evaluation. it can be drawn that the relationship between the NTL indicators and social-economic variables was initially examined through a log-linear regression analysis which proved that DMSP/OLS NTL based urbanization indicators are effective ways to evaluate and monitor the development at city level. Besides, the built-up area extraction of all the selected cities showed an obvious expansion during the period

Chapter 5, **MACRO-SCALE ANALYSIS ON CLIMATE CHANGE AND URBAN HEAT ISLAND EFFECTS,** investigates surface urban heat island effects in Beijing city which derive from land surface temperature retrieval from remote sensing data of Landsat TM. Spatial correlation and relationship between the urbanization level, vegetation coverage and surface urban heat island was also have been carried out. The analysis results show he value of NDVI changed significantly due to urban expansion and the normalized land surface temperature in the downtown area is obviously higher than that in the surroundings. The results also indicate that an area with a higher NTL-DN value (more urbanized area), the mean LST within it would be higher than the surroundings, which provides strong evidence that the surface urban heat island effects are influenced by urban development. Besides, both the medium temperature and low temperature zones had a decrease of area proportion.

Chapter 6, **CONCLUSIONS,** the whole summary of each chapter has been presented

CONTENTS

List of Figure

List of Table

Chapter One: Previous Study and Purpose of the Study

1.1. Introduction

1.2. Research background and significance

1.2.1. Present situation of urbanization worldwide

1.2.2. Present situation of urban environment

1.3. Research objectives

1.4. Purpose of this study

1.1. Introduction

With the rapid development of economic, the sustained growth of the population, the fast urbanization and modernization, a number of metropolises have emerged in the world as Tokyo in Japan, New York in United States, and London in United Kingdom etc. The rate of urbanization all over the world is quite alarming, with the proportion of the world's population living in urban area projected to reach 66% by 2050 (United States. 2014). Urban area, with better access to health care, education, entertainment, and employment resources have been attracting a continuous flow of people from rural areas. As a result, the world is in the midst of the largest wave of urban growth in history (Shen, et al.2017). This remarkable phenomenon is generally known as urbanization (United States. 2010). Urbanization may be defined as a social process significant to human society in the 21th century. Cities grow due to the continues flow of people into cities, Hiroshi Morikawa defines urbanization as a transformation of life style of the rural population combined with expansion of urban built-up area (Hiroshi.1989). Urbanization is accompanied by an increase in urban population followed by urban growth and urbanism a term referring to the urban life style. Urban development can be viewed as a complex system, urbanization is directly related to expansion of urban areas and growth of the proportion of total population leaving rural areas and moving to live in urban areas. In addition, urbanization always be characterized by their complexity heterogeneity and hybridity.

As to the situation in China, since its open door policy in 1978, China has experienced rapid urban transformation and expansion, created by the world's largest rural-urban migration flow after the government's strict regulation of intra-country migration slackened. China's urban population increased from 170 million in 1978 to 670 million in 2010, and the urban proportion rose from 18% to 50% during this period (Chen, et al.2016). China's road to urbanization has been considered unique due to it is neither identical with that of developed economies nor does it duplicate the model found in developing countries (Tan, et al.2016). China's process of urbanization followed its own peculiar pattern until the early 1980s due to the government's strict regulation of intra-country migration. A great amount of ink has been spilled to paint the picture of China's urbanizations by economists, planners, geographers in recent decades (Lin and Du.2015).

However, the rapid urbanization and economic development have caused many problems for the environment, society and governance. The rapid urbanization is associated with a variety of problems such as the loss of farming land, increase of CO_2 emissions, shortage of water resources in urban areas, housing shortages, traffic congestion, rising crime rate, biodiversity reductions, heat island effects, noise, air and water pollution (Li, et al.2009). People are increasingly realizing the importance of a sustainable urban environment that will mitigate or eliminate these problem (Shearer, et al.2006). The challenges brought by urbanization have led to global recognition of the need for effectively implementing sustainable development principles in urbanization process. Many governments, researchers and practitioners have dedicated efforts to developing policies and methods for promoting sustainable urbanization, such as developing indicators to guide policy makers and planners in order to make adequate decisions to implement urban development towards the mission of sustainable development (Palme and Tillman.2008). Urban ecosystems affect the quality of life for the majority of the planet's residents. Urbanization produces radical changes in the quantity, type, and spatial distribution patterns of land use. Rapid changes from agricultural to non-agricultural use of land lave led to changing land use and earth surface cover patterns, and the carbon source and sink functions of different land use types change accordingly (Xu, et al.2016). During the last 50 years, urban and transport networks have spread at the expense of former natural or agricultural spaces, frequently occupying the lands most suitable for agriculture. Although urban built-up areas cover only a small proportion of the land, their impact on ecosystems is significant. For example, in the United States, roads occupy only 1% of the territory, but they highly alter the structures and ecological functions of at least 20% of the territory (Forman.2000).

Urbanization and city growth are caused by a number of different factors including rural-urban migration, natural population increase, and annexation (Cohen.2006). Urban growth is characterized by the transformation of natural land covers into built up areas. It causes depletion of greenery in the cities and subsequent increase in the impervious surface. Cities experience unprecedented change in land use and land cover patterns due to urban growth (Rajasekar and Weng.2009). Urban growth has adverse impact on land surface characteristics including its thermal capacity. The increased thermal storage capacity creates

so called urban heat island effect, observed as an elevated temperature of urban areas relative to rural areas, which is one of the most important research topic related to urban climate and environmental studies (Wei, et al.2017).

Recent years, the remote sensing techniques had been applied to get the information of the world from the space after rapid development. Remote sensing is a technique to observe the earth surface or the atmosphere from out of space using satellites or from the air using aircrafts. Remote sensing science and technologies emerged as an important new tool for environmental applications over four decade ago. The environmental applications of remote sensing have gained an irreversible momentum ever since. Remote sensing is now widely recognized as a valuable and often essential means of data collection for urban development applications. The most significant recent advance in the use of remote sensing data is in the area of geographic information systems where spatial data from disparate sources are integrated into one system (Bhatta, et al.2010). Whilst allowing users to access and relate different types of information more effectively, a predictive capability is now also possible. By using the remote sensing products, the detailed information and changing situation could be presented spatial-temporally (Wei, et al.2017). To understand the impact of human activities on the ecosystems it has long been recognized the need to obtain and employ detailed data from remote sensing.

Urbanization is an integrated complex processing which is associated with population transformation combined with expansion of urban built-up area. It is very difficult to quantify urbanization, which is basically a process of progressive concentration, as the cities evolve from an agrarian to industrial society. In recent years, scholars have begun to study the theoretical relationship between urbanization and the eco-environment (He, et al.2017). According to practical and theoretical analysis, the dynamic change process of interaction between urbanization level and eco-environment shows to be closely associated (Wang, et al.2014). To make it clear, it is necessary to establish an evaluation system to evaluate the urbanization level and eco-environment level which would have guiding significance for the future development of the cities.

Over the years, many studies on urban climate and thermal comfort have been conducted in different outdoor spaces and under different climatic conditions. Examining the urban thermal

environment is really important in order to establish the life quality of an urban context, which in turn affects the image of a city. Scholars applied remote sensing products to discuss the urban climate change and urban thermal problems such as urban heat island from the satellite observing (Rajasekar and Weng.2009). Monitoring spatial-temporal changes in large urban/suburban areas will therefore become increasingly important as the number and proportion of urban residents continues to increase. The urban thermal environment is influenced by the physical characteristics of the land surface and by human socio-economic activities. The thermal environment can be considered to be the most important indicator for representing the urban environment.

1.2. Research background and significance

1.2.1. Present situation of urbanization worldwide

World population has grown exponentially in the 20th century from around 1.6 billion in 1900 to around 7.4 billion today, with each additional billion people being added more rapidly than the last (Cohen.2006). The vast majority of this growth has occurred in the developing world. Achieving the United Nation's Millennium Development Goals (MDGs), cities are currently home to nearly half of the world's population and over the next 20 years most of the two-billion-plus person increase in global population is expected to occur in urban area in the developing world.

Table 1-1 shows the urban population and distribution by major geographic area. In 1950, just over one-half of the population of the developed world and just under one-third of the

Table 1- 1 Urban population and distribution by major geographic area, 1950-2030

Region	**Period**			
	1950	1975	2000	2030
Total polulation(millions)				
World	2519	4068	6071	8130
More developed regions[a]	813	1047	1194	1242
Less developed regions[b]	280	3021	4877	6888
Urban population(millions)				
World	733	1516	2857	4945
More developed regions	427	703	822	1015
Less developed regions	306	813	1974	3930
Rural population(millions)				
World	1786	2552	3214	3185
More developed regions	386	344	311	228
Less developed regions	1400	2208	2902	2958
Percentage of population living in urban areas (%)				
World	29.1	37.3	47.1	60.8
More developed regions	52.5	67.2	73.9	81.7
Less developed regions	17.9	26.9	40.5	57.1
Distribution of the world's urban population (%)				
World	100	100	100	100
More developed regions	58.3	46.4	30.9	20.5
Less developed regions	41.7	53.6	69.1	79.5

[a] The more developed regions comprise Europe, North America, Austrilia/New Zealand and Japan.

[b] The less developed regions comprise all regions of Africa, Asia (except Japan), Latin American and the Caribbean, plus Melanesia, Micronesia and Polynesia.

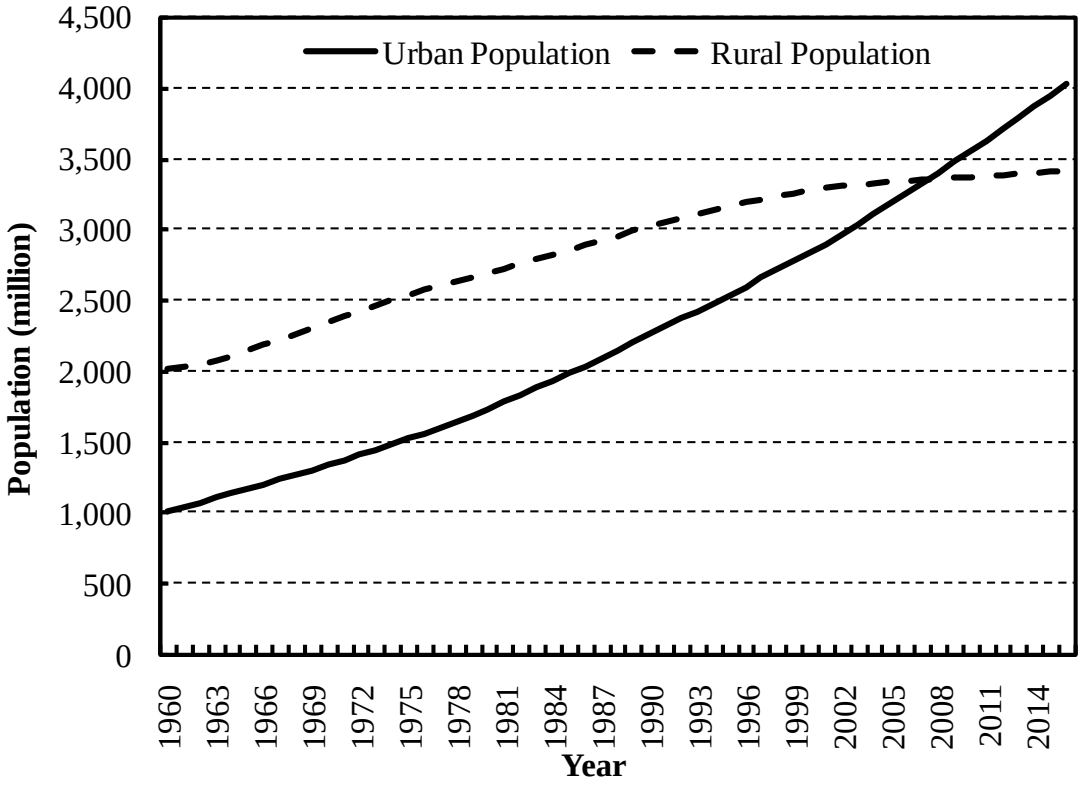

Figure 1- 1 The world's urban and rural populations, 1960-2016.

(Source: United Nations World Urbanization Prospects. 2017 revision.)

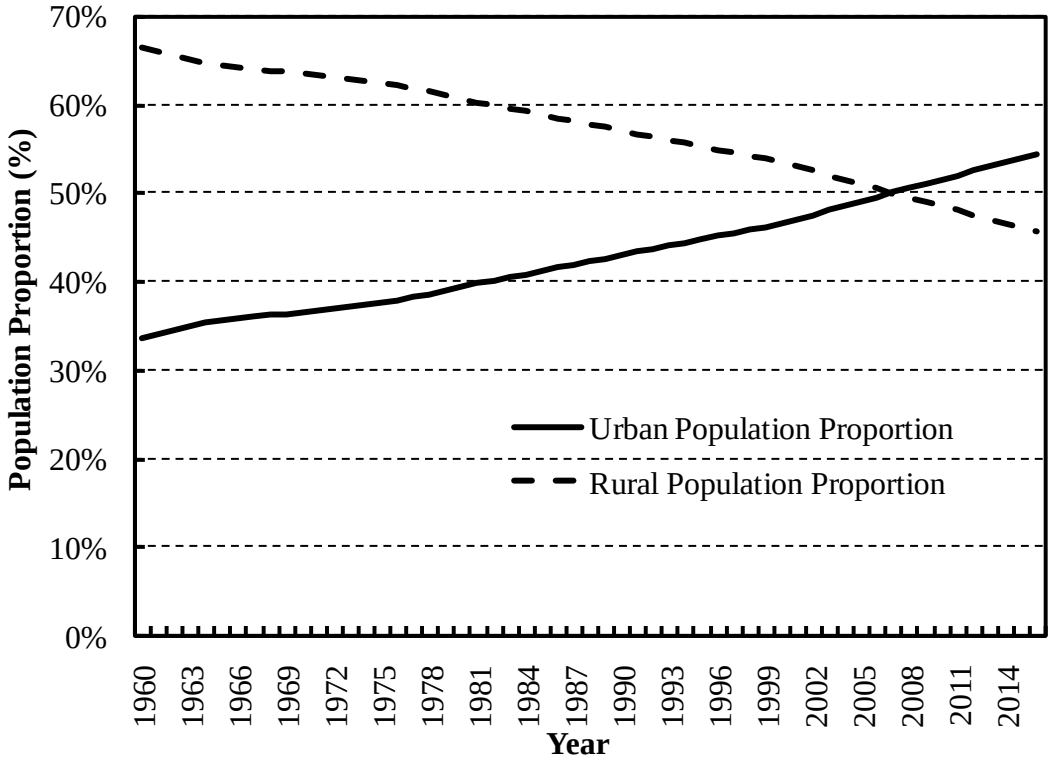

Figure 1- 2 The world's urban and rural population proportions, 1960-2016.

(Source: United Nations World Urbanization Prospects. 2017 revision.)

population of the entire world lived in urban areas. At that time, there were only around 733 million people living in urban areas around the world and 83 cities in the world that could boast a million or more residents. Continued urbanization over the last 50 years has resulted in a situation whereby close to 54.3% of the world population now live in urban areas. In absolute terms, the numbers of urban resident almost quadrupled between 1950 and 2000 going from 733 million to 2.857 billion. Especially during the last three decades, globalization driven by advances in transportation and telecommunications, and a positive political climate has created a global economy characterized by unprecedented levels of urbanization and more and bigger cities than ever before.

In the near future until 2030, the world's population is projected to grow at an annual rate of 1.8 percent (United States. 2014). At this rate of growth, by 2030, demographers predict that around 61 percent of the world's population will be living in urban areas, at which time the world's urban population will be approaching 5 billion (Table 1-1).

Figure 1-1 shows the change of the world's urban and rural populations from 1960 to 2010. Compared with the rapid rise in the urban population, the growth of the world's rural population has been relatively slow. While the world's urban population increased four-fold between 1960 and 2016, the world's rural population less than doubled which going from 2.0 million in 1960 to 3.4 billion in 2016. In addition, the world's urban population is expected to increased by almost 2 billion over the next 30 years, the world's rural population is actually expected to decline slightly falling. Thus, all future population growth for the foreseeable is expected to be absorbed in urban areas.

On the other hand, Figure 1-2 shows the variation of the world's urban and rural population proportions during 1960 to 2016. The urban population proportion increased from 33.6% in 1960 to 54.3% in 2016. To the contrary, the proportion of world rural population decreased from 66.4% in 1960 to 45.7% in 2016. The rural-urban migration has taken place during this period and this trend is expected to be continued in the near future. The proportion of the urban population exceeded the rural population proportion at around 2007, after that, the urban population proportion kept sustainable growing until now.

Table 1-2 shows the distribution of large cities by major geographic area from 1950 to 2015. In most cases, most of the world's largest cities are located in countries with the world's

Table 1-2 Distribution of large cities by major geographic area, 1950-2015

Region	Period			
	1950	1975	2000	2015
Distributiion of the world's 30 largest cities				
Africa	1	1	2	3
Asia	7	14	16	15
Europe	12	6	3	2
Latin America and Caribbean	4	4	6	6
Northern America	6	5	3	3
Oceania	0	0	0	0
Number of Cities with more than one million residents				
Africa	2	8	35	63
Asia	27	86	194	288
Europe	20	47	62	60
Latin America and Caribbean	7	21	49	73
Northern America	14	31	41	51
Oceania	2	2	6	6
Total	72	195	387	541

largest economies. In 1950, there were 12 world's largest cities located in Europe, however, there were only 2 cities in 2015 that located in Europe. To the contrary, many cities in Pacific Asia have experienced dramatic economic growth, reflecting the fact that the region is completely integrated into the new global economy. In 1950, 7 of the world's thirty largest urban agglomerations were located in Asia while this number increased into 15, half of the thirty largest cities located in Asia. Cities on the forefront of global restructuring such as Hong Kong, Singapore, Seoul, and Taipei have enjoyed unprecedented growth rate of more than 10 percent per annum throughout the 1970s and early 1980s.

Urbanization has been imposing substantial global environmental changes. It affects the environment by directly fragmenting the landscape in human habitats and by indirectly changing the biophysical properties of the landscape that cause numerous environmental impacts across different spatial and temporal scales, such as ecosystem services reduction, resource and energy depletion and climate change (Han, et al.2017). In 2050, over 67% of the world population will reside in urbanized areas, with most of the net increase in urban residents expects to occur in the urbanized regions of developing countries such as China, India, Mexico, and Brazil (United States. 2014). Thus, understanding the urbanization process and its consequence on eco-environment on a regional scale, especially in developing

countries such as China, is crucial to addressing the significant challenges of achieving regional sustainability and mitigation global climate change (Han, et al.2017).

1.2.2. Present situation of urban environment

Urban environment was founded in 1975 by visionary architects and activists who believed that cities should serve both people and nature. From the beginning, urban environment has used urban planning, ecology, and participation to help design and build healthier cites. Urban environment's mission has always involved local change within a global perspective.

Urban environment is the investigation of living organisms in relation to their environment in towns and cities, as in ecological studies of forests or the sea. The ecological approach considers a city as an ecosystem, characterized by its history, its structure and function, including both biotic and abiotic components, and the cycling and conversion of energy and materials (Kumar, et al.2011). Cities also have their own spatial organization and distinctive patterns of change through time, which result in patterns of species behavior, population dynamics and the formation of communities, each of which is specific to the urban environment. In policy and planning the term urban environment is synonymous with sustainable cities.

Nowadays, one of the hottest topics of urban environment research is to understand the interactions between the natural and the socioeconomic system. The aim of the research is not only to supply suggestions for a more reasonable urban planning in order to bring nature closer to humans , but also to understand in more detail how human beings perceive urban nature and what the benefits are for both systems, the natural and the socioeconomic.

For millions of people living in cities, increased temperatures are a growing fact and concern. The so called urban heat island has come into sight and became one of the most serious urban environment issues. The urban heat island effect is the most obvious atmospheric modification attributable to urbanization, the most studied of climate effects of cities and an iconic phenomenon of urban climate. It can be found in settlements of all sizes in all climatic regions. The evaluation of the influence of settlements on the local climate has been an important task for a long time, and the thermal environment in particular has received widespread attention because it has practical implication for energy use, human comfort and productivity, air pollution and urban ecology (Taleb and Abu-Hijleh.2013). After years of development, observational and modeling approaches are used to investigate the urban thermal environment. Field observations provide descriptive information about the urban heat

island and the processes causing it, and methods differ for each urban heat island type. Observations are also essential to evaluate the full range of physical, statistical or numerical models used to research these processes and predict urban heat island behavior (Fan, et al.2017).

On the other hand, city modifies meteorological conditions surrounding significantly, increasing radiation higher, average temperature of the city become hotter than the surroundings, decreasing wind speed due to the presence of building in the city, therefore make relative humidity much lower than surrounding. Along with global climate change and the existence of several urban development and uncontrolled industrial area at this time will result in a very detrimental to society. The impact can be felt, its impact on the atmosphere with heat island or island formation above the city. With the gathering of human beings, the thermal comfort conditions in many place become very significant at the same time. Outdoor thermal comfort of people is affected by outdoor thermal environment, and outdoor thermal environment is significantly affected by the design of built environment(Hwang, et al.2011). Thus, there is a need to understand the relationship between urban design and outdoor thermal comfort to develop bioclimatic urban design guidelines. It would be meaningful to evaluate the importance of climate change by specific design details for predicting the effect of a particular change in a climatic element on the comfort of persons staying outdoor (Givoni, et al.2003). Nowadays, urban designers in China still have not understood or considered how the design strategies can reduce the occurrence of thermal discomfort and lengthen the comfort time of an outdoor urban space. It still has a long way to go for the urban designers to detection, simulate, and design better living conditions for the residents.

1.3. Research objectives

The main aims of this study can be divided into three aspects. One is comprehensive evaluation on the urbanization processing and eco-environment based on hybrid method, one is the land cover land use monitoring and its impact on urban heat island effect.

a) Comprehensive evaluation on urbanization and eco-environment

In the 21st century, urbanization is a very dynamic process worldwide which is forecasted by experts to increase even further in the future. As the urbanization and land sprawl had draw more and more attention, it is meaningful and useful to have an investigation of the urbanization processing in China in recent decades. In addition, environmental issues arose along with the urbanization, it is essential to do more in-depth study to explore the relationship between the urbanization and eco-environment to provide guidance for sustainable development. The investigation of urbanization could help us to get a comprehensive understanding of what happened in the study region and promote better health and quality of life. The information it produces is helping urban residents and policymakers make informed decisions and take actions before the eco-environment get worse. After the investigation and evaluation, not only can we get the advantages and benefits from the development, but also present the imbalance and weakness to remind us what we should do for our cities to get better condition and better eco-environment. The evaluation also can provide us the urban development trend where more attention should be paid to make sure the steady development of the cities.

b) Monitoring the urban sprawl and its impact on urban heat island effect

Land use and land cover change is one of the most important indicators in understanding the impact of human activities on the environment, which seem unprecedented despite profoundly affecting the earth's ecological systems. Global urban areas are rapid expanding nowadays, as ecosystems in urban areas are strongly influenced by anthropogenic activities, considerable attentions is currently directed towards monitoring changes in urban land use and land cover. It is particularly important because the spatial characteristics of land use and land cover are useful for understanding various impacts of human activities on ecological conditions in urban environment. As with the global warming and environment issues appeared, urban heat island had grown into prominent problem for the modern society. The

urban heat island has so many bad influences such as energy consumption increasing, air pollution, water pollution, etc. Urban heat island is considered to be one of the major problems in the 21st century, it also be considered as one of the climatic disasters in urban areas and very harmful for citizens. Therefore monitoring the urban heat island effects is crucial for protecting the urban ecological and residential environment from being totally damaged.

1.4. Purpose of this study

This study focuses on the urbanization and eco-environment assessment, urban sprawl and urban expansion evaluation, urban heat island and its impact factors, urban structure and its effects on thermal comfort. Based on the previous study and theory analysis, the evaluation and simulation method is developed. The application research is executed for various considerations.

a) Previous study

In Chapter one, research background and significance is investigated. In addition, previous study and current situation on the research fields was reviewed and discussed. The environmental issues caused by urbanization processing have became more and more serious, it is essential to do more in-depth study to explore the relationship between the urbanization and eco-environment to provide guidance for sustainable development.

b) Literature review

In Chapter two, an in-depth review of prior studies associated with the research topic was conducted. The literature review was carried out from three aspects: urbanization and eco-environment evaluation and coordination, urban sprawl assessment, urban heat island investigation.

c) Assessment of urbanization and eco-environment in China

In Chapter three, maximum entropy method was applied to help generate the evaluation system of eco-environment level and urbanization level at provincial scale in 2005 and 2015 in China. Comparison analysis and coordinate analysis was carried through to assess the development of urbanization and eco-environment as well as the balance and health degree of thee city develop.

d) Measurement of urban sprawl

In Chapter four, DMSP/OLS stable nighttime light dataset was used to measure and assess the urban dynamics from the extraction of built up area. Detailed information of data processing, method selection, dataset validation and evaluation system was introduced here. Urban sprawl was evaluated by analyzing the landscape metrics a general understanding of the urban sprawl and distribution pattern characteristics could be got from the evaluation.

e) Urban heat island effects investigation

In Chapter five, investigation of surface urban heat island effects in Beijing city which derive from land surface temperature retrieval from remote sensing data of Landsat TM was carried out in this chapter. Spatial correlation and relationship between the urbanization level, vegetation coverage and surface urban heat island was carried out in this chapter. The analysis method in this chapter was composed of three parts: spatial relationship analysis, temporal comparison analysis and urban heat island analysis, respectively.

f) Conclusions

In Chapter seven, all the works has been summarized and a conclusion of whole thesis is deduced.

Reference

[1] World Urbanization Prospects: The 2014 Revision; New York: United Nations.

[2] Liyin Shen, Zhenyu Zhang, Xiaoling Zhang, Hang Yan, Bei He, Measuring incoordination-adjusted sustainability performance during the urbanization process: Spatial-dimensional perspectives, Journal of Cleaner Production, 143 (2017) 731-743.

[3] World Urbanization Prospects: The 2010 Revision; New York: United Nations.

[4] Morikawa Hiroshi, Urbanization and urban system. Damingtang Press; 1989., (1989).

[5] Yingbiao Chen, Kang-tsung Chang, Fuzhuang Han, David Karacsonyi, Qinglan Qian, Investigating urbanization and its spatial determinants in the central districts of Guangzhou, China, Habitat International, 51 (2016) 59-69.

[6] Yongtao Tan, Hui Xu, Xiaoling Zhang, Sustainable urbanization in China: A comprehensive literature review, Cities, 55 (2016) 82-93.

[7] Boqiang Lin, Zhili Du, How China′s urbanization impacts transport energy consumption in the face of income disparity, Renewable and Sustainable Energy Reviews, 52 (2015) 1693-1701.

[8] Feng Li, Xusheng Liu, Dan Hu, Rusong Wang, Wenrui Yang, Dong Li, Dan Zhao, Measurement indicators and an evaluation approach for assessing urban sustainable development: A case study for China's Jining City, Landscape and Urban Planning, 90 (2009) 134-142.

[9] Allan W. Shearer, David A. Mouat, Scott D. Bassett, Michael W. Binford, Craig W. Johnson, Justin A. Saarinen, Examining development-related uncertainties for environmental management: Strategic planning scenarios in Southern California, Landscape and Urban Planning, 77 (2006) 359-381.

[10] Ulrika Palme, Anne-Marie Tillman, Sustainable development indicators: how are they used in Swedish water utilities?, Journal of Cleaner Production, 16 (2008) 1346-1357.

[11] Qian Xu, Ren Yang, Yu-Xiang Dong, Yan-Xu Liu, Lin-Run Qiu, The influence of rapid urbanization and land use changes on terrestrial carbon sources/sinks in Guangzhou, China, Ecological Indicators, 70 (2016) 304-316.

[12] Richard T. T. Forman, Estimate of the Area Affected Ecologically by the Road System in the United States

Estimación del Area Ecológicamente Afectada por el Sistema Carretero de los Estados Unidos, Conservation Biology, 14 (2000) 31-35.

[13] Barney Cohen, Urbanization in developing countries: Current trends, future projections, and key challenges for sustainability, Technology in Society, 28 (2006) 63-80.

[14] Umamaheshwaran Rajasekar, Qihao Weng, Urban heat island monitoring and analysis using a non-parametric model: A case study of Indianapolis, ISPRS Journal of Photogrammetry and Remote Sensing, 64 (2009) 86-96.

[15] Yehua Dennis Wei, Han Li, Wenze Yue, Urban land expansion and regional inequality in transitional China, Landscape and Urban Planning, 163 (2017) 17-31.

[16] B. Bhatta, S. Saraswati, D. Bandyopadhyay, Urban sprawl measurement from remote sensing data, Applied Geography, 30 (2010) 731-740.

[17] Jinqiang He, Shaojian Wang, Yanyan Liu, Haitao Ma, Qianqian Liu, Examining the relationship between urbanization and the eco-environment using a coupling analysis: Case study of Shanghai, China, Ecological Indicators, 77 (2017) 185-193.

[18] ShaoJian Wang, Haitao Ma, YaBo Zhao, Exploring the relationship between urbanization and the eco-environment—A case study of Beijing–Tianjin–Hebei region, Ecological Indicators, 45 (2014) 171-183.

[19] Xiaoshan Yang, Lihua Zhao, Michael Bruse, Qinglin Meng, Evaluation of a microclimate model for predicting the thermal behavior of different ground surfaces, Building and Environment, 60 (2013) 93-104.

[20] Teresa Zölch, Johannes Maderspacher, Christine Wamsler, Stephan Pauleit, Using green infrastructure for urban climate-proofing: An evaluation of heat mitigation measures at the micro-scale, Urban Forestry & Urban Greening, 20 (2016) 305-316.

[21] Ji Han, Xing Meng, Xiang Zhou, Bailu Yi, Min Liu, Wei-Ning Xiang, A long-term analysis of urbanization process, landscape change, and carbon sources and sinks: A case study in China's Yangtze River Delta region, Journal of Cleaner Production, 141 (2017) 1040-1050.

[22] Amit Kumar, Arvind Chandra Pandey, Najmul Hoda, A. T. Jeyaseelan, Evaluation of urban sprawl pattern in the tribal-dominated cities of Jharkhand state, India, International Journal of Remote Sensing, 32 (2011) 7651-7675.

[23] Dana Taleb, Bassam Abu-Hijleh, Urban heat islands: Potential effect of organic and structured urban configurations on temperature variations in Dubai, UAE, Renewable Energy, 50 (2013) 747-762.

[24] Chao Fan, Soe Myint, Shai Kaplan, Ariane Middel, Baojuan Zheng, Atiqur Rahman, Huei-Ping Huang, Anthony Brazel, Dan Blumberg, Understanding the Impact of Urbanization on Surface Urban Heat Islands—A Longitudinal Analysis of the Oasis Effect in Subtropical Desert Cities, Remote Sensing, 9 (2017) 672.

[25] Ruey-Lung Hwang, Tzu-Ping Lin, Andreas Matzarakis, Seasonal effects of urban street shading on long-term outdoor thermal comfort, Building and Environment, 46 (2011) 863-870.

[26] Baruch Givoni, Mikiko Noguchi, Hadas Saaroni, Oded Pochter, Yaron Yaacov, Noa Feller, Stefan Becker, Outdoor comfort research issues, Energy and Buildings, 35 (2003) 77-86.

Chapter Two: Literature Review

2.1. Introduction

2.2. Literature review of urbanization and eco-environment evaluation

2.2.1. Previous field studies on urbanization and eco-environment evaluations

2.2.2. Method of assessment

2.3. Literature review of urban sprawl

2.3.1. Impacts of LULC change on climate

2.3.2. Urban sprawl from remote sensing data

2.3.3. Quantization assessment of urban sprawl

2.4. Literature review of UHI studies

2.4.1. Definition of UHI effect

2.4.2. Formation of UHI effect

2.4.3. Types of urban heat island

2.4.4. Impacts of urban heat island

2.5. Summary

2.1. Introduction

This chapter aims to provide an in-depth review of prior studies associated with our study. The literature review focuses on the following three aspects: urbanization and eco-environment evaluation; urban sprawl assessment, urban heat island investigation.

In the 21st century, urbanization is a very dynamic process worldwide which is forecasted by experts to increase even further in the future. Recent years, Chinese scholars have begun to study the theoretical relationship between urbanization and the eco-environment. More in-depth researches are needed to explore the relationship between the urbanization and eco-environment to provide guidance for sustainable development. A comprehensive review on the assessment method has been conducted in this chapter.

Land use and land cover (LULC) change and urban sprawl are important indicators in understanding the impact of human activities on the environment. Scholars around the world have pay attention to monitor and predict the change of urban land dynamics. In addition, with the rapid development of the remote sensing technology, which can provide a synoptic and comprehensive view from the space, have been applied into such kind of research topics in recent years. Here we carried out a comprehensive review on the acquirement and quantization of the monitoring of urbanization dynamics.

As with the global warming and environment issues appeared, urban heat island had grown into prominent problem for the modern society. Monitoring the urban heat island effects is crucial for protecting the urban ecological and residential environment from being totally damaged. The third parts of the review focus on the urban heat island effects. The formation of the classification and impacts of the urban heat island effects has been discussion in this chapter.

2.2. Literature review of urbanization and eco-environment evaluation

2.2.1. Previous field studies on urbanization and eco-environment evaluations

Since its reform and opening up, China has been undergoing a rapid and large-scale process of urban expansion. The strategic roles and effects of urbanization to social and economic development have been well recognized in previous studies. For example, urbanization can provide new opportunities to improve social services and promote economic development (Shen, et al.2015). In addition, urbanization process helps upgrade industrial structure and increase life quality of the residents. The equally rapid increases in urban sprawl that have resulted from this phenomenal growth pose tremendous challenges for China through the pressure that they place upon the environment. This rapid urbanization has led to resource depletion and a number of environmental and ecological problems and disasters. Appearance of such kind of problems have had complicated effects on the modernization of China and have caused concerns among experts and researchers (Cohen.2006, Wang, et al.2014). As a result, it is crucial to obtain accurate and timely information about the dynamics of urbanization to clarify the driving forces of urbanization, to estimate its effects and to promote an effective urbanization process in China (Gao, et al.2015). Methods must be developed to enable this rapid development to occur in a sustainable manner that maintains a good quality of life for China's population. The coordination of urbanization and the ecological environment ("eco-environment") is critical to this task.

Presently, two main types of data are used to obtain information of the urbanization dynamics. One is socioeconomic statistical data based on administrative units from the government. The other one is by using the remote sensing data to monitor the urbanization dynamics from the space.

In recent years, Chinese scholars have begun to study the theoretical relationship between urbanization and the eco-environment. Researchers have proved that an interactive coercing relationship exists between urbanization and eco-environment (Wang, et al.2014). Examination and quantification of the coupling process between urbanization and the eco-environment is crucial for the realization of sustainable and healthy forms of urbanization.

Examination and quantification of the coupling process between urbanization and the eco-environment is crucial for the realization of sustainable and healthy forms of urbanization. The relationship between urbanization and the level of economic development in terms of geography, economics and demography is a classic topic of discussion. Chenery et al. systematically analyzed the relationship patterns between urbanization and economic development level in the 1970s, and Chinese scholar proposed the logarithm regression model for urbanization and per capita GDP (Chenery H.1988). In general, there is a strong correlation between urbanization and the level of economic development, and it seems that each country or region conforms to this rule to a certain degree (Henderson, et al.2003). This has become a fruitful empirical research domain, which implies the complexity of this relationship. Urbanization in China is not like the parallel urbanization of Western countries, nor like the over-urbanization in many developing countries, which falls into the categories of under-urbanization that urbanization lags behind economic development level (Ebanks G E.1990). While some research has pointed out that urbanization did not lag behind the level of economic development before 1978, it has become more prevalent than under-urbanization with the surges in rural–urban immigration that have occurred in the mid and later periods of the Reform and Opening-up Policy. Furthermore, some scholars hold the view that the urbanization of China is increasing dramatically, at breakneck speed, and that it displays the characteristics of the rapid growth of urban scale and peri-urbanization.

2.2.2. Method of assessment

In line with these developments, studies have introduced various models and mechanisms to assess the eco-environment and urbanization. For example, Hunter et.al introduced the ecological footprint (EF) method to evaluate sustainable tourism in the United Kingdom (UK) (Hunter.2007). The EF method is a quantitative tool that helps assess the resource consumption and waste assimilation requirements of a defined economy in terms of a corresponding productive land area. Another method, data envelopment analysis (DEA), has been adopted by many researchers to evaluate the sustainable development capacity of a specific city based on the input and output of every decision-making unit (DMU) (Wu and He.2006). However, the result obtained via the DEA method only presents the relevant efficiency of individual indicators. Other methods evaluate urbanization performance based

on a single aspect such as speed or quality. The assessment results of using mono-parameter-based methods nevertheless present difficulty for city decision-makers to select a suitable development strategy.

Urbanization strategy has ever been an important aspect of world economic and social development. Doubtless, accurate urbanization level evaluation has played important guiding roles in better urbanization strategic development. The importance of urbanization level evaluation has encouraged numerous researches on the methods of ULE during past decades. At present, the methods used in urbanization level evaluation are mainly divided into two categories. One is single indicator method such as population ratio method and proportional method of urban land-use. Another is comprehensive indicator method such as AHP, projection pursuit comprehensive evaluation and data envelopment analysis, fuzzy comprehensive evaluation method, principal component analysis and cluster analysis, gray relational analysis etc. (Zhao and Chai.2015).

Since urbanization systems are complex dynamic systems influenced by many indicators or factors, single indicator method has some shortcomings in reflecting urbanization level objectively and comprehensively. In contrast, comprehensive indicator method, which can take the effects of many indicators or factors into account, has many advantages over single indicator method. Nevertheless, we still notice most existing comprehensive indicator methods have many theoretical shortcomings and applicable restrictions. Two most serious problems exist for most available comprehensive indicator methods. One is that they cannot mathematically–physically treat the interactions between indicators. They are usually subjective in setting interaction weights between indicators. The other is that they have not given a mechanistic definition of urbanization level from comprehensive indicators. Being incapable of mechanistically treating the interactions between indicators and yielding a definition of urbanization level from comprehensive indicators, these methods often encounter many problems in urbanization level evaluation.

2.3. Literature review of urban sprawl

2.3.1. Impacts of LULC change on climate

Land use and land cover (LULC) change is one of the most important indicators in understanding the impact of human activities on the environment, which seem unprecedented despite profoundly affecting the Earth's ecological systems (Dewan and Yamaguchi.2009). f the LULC changes induced by humans, urbanization manifests itself as the most widespread anthropogenic causes of the loss of arable land, habitat destruction and the decline in natural vegetation cover. Significant population increase, migration, and accelerated socioeconomic activities have intensified these environmental changes over the last several centuries. The climate impacts of these changes have been found in local, regional, and global trends in modern atmospheric temperature records and other relevant climatic indicators (Pielke.2005). Global urban areas are rapidly expanding and nowadays, the majority of the world's population lives in cities.

Land use and land cover change (LULCC) has been a key research priority with multi-directional impacts on both human and natural systems yet also a challenging research theme in the field of land change science. LULCC can affect biodiversity, hydrology, and ecosystem services (Teferi, et al.2013). LULCC can also affect climate through its influence on surface energy budgets (e.g. albedo change) and biogeochemical cycling mechanisms (e.g. carbon cycle) (Teferi, et al.2013, Imhoff, et al.2010). The changing dynamics of land use and land cover brought by human activity at any ecosystem scale seems to have incremental and unconscious, could lead to an undesirable modification of the native environment.

The unusual changes in land use and expansion of urbanized surface could substantially decrease half of the diurnal temperature range and could warm the mean earth surface temperature by 0.27 °C per century (Estoque, et al.2017). Moreover, the immediate effects of environmental changes are more prominent at regional and local scale than that of globally averaged values. UHI phenomenon could be the extreme case of land use alteration at regional and local scale, where the unprecedented changes of vegetation cover, impervious surface area, and complex geometry of building in an urban landscape lowering the evaporative cooling, store the excess heat and hence, warm the earth surface (Dos Santos, et al.2017). In addition, the sensitivity of land use and land cover changes and earth surface

temperature found to be zero or close to zero in globally, however, the dynamics of land surface temperature, precipitation, and other climate components can be as large as or greater than those that result from the anthropogenic increase of well-mixed greenhouse gases. Hence, detecting the change of LULC has increasingly become a topic of paramount importance for national and international research programs examining global environmental change (Li, et al.2017). In addition, Therefore, the detail investigation of long run LULC changes at any ecosystem scale could help us to explain the discrepant and unprecedented modification of earth surfaces, and also contribute to describing the directions and degree of other human-related environmental changes (Weng.2012).

Urban areas constitute just a small subset of the world's overall land mass; however, population density and resource utilization intensity are very high in these areas as compared to their surroundings, compelling improved resource management practices (Cohen.2006). As a result, it is essential to Understanding the spatial distribution and growth of urban areas for better urban planning and resource management, one of the basic activities required for this purpose is mapping the built-up areas. Such mapping activity requires a lot of resources if carried out through conventional means like ground surveying and aerial photography (Weng, et al.2004).

2.3.2. Urban sprawl from remote sensing data

Remote sensing data from satellite observing, which is an invaluable resource for mapping land cover and land use, can provide a synoptic and comprehensive view that is impossible from the ground surveys (Zhang, et al.2011). In addition, the application of remote sensing data for urban studies made mapping and understanding urban sprawl over time possible, due to the availability of historical archives. Thus, during the past several decades, satellite observing remote sensing data has been increasingly used for urban studies, one of the hottest topics of its application is the detection of the land use and land cover change.

Researchers have long been using different types of remote sensing data to derive land cover patterns, such as Landsat, ASTER, SPOT, DMSP/OLS and IKONOS (Li, et al.2017) . Among this, Landsat (TM, ETM, OLI) provides the most commonly used remote sensing data because of it is quite accessible for researchers, in addition, the world-wide coverage with medium spatial resolution (30×30 m) has widened the range of application. Most importantly,

the long-term temporal coverage (available since 1972) which enables researchers to monitor changes over a much needed longer time span (Goodwin, et al.2008).

2.3.3. Quantization assessment of urban sprawl

Sprawl can be measured in relative and absolute scales. Many metrics and statistics have been used to quantify the sprawl. These metrics are generally known as spatial metrics. Spatial metrics are numeric measurements that quantify spatial patterning of land cover patches, land cover classes, or entire landscape mosaics of a geographic area. These metrics have long been used in landscape ecology (which also known as landscape metrics) to describe the ecologically important relationship such as connectivity and adjacency of habitat reservoirs (Bhatta, et al.2010). Spatial or landscape metrics, in general, can be defined as quantitative indices to describe structures and patterns of a landscape defined it as measurements derived from the digital analysis of thematic-categorical maps exhibiting spatial heterogeneity at a specific scale and resolution .

Landscape metrics have been proved to be an important tool in quantifying urban growth, sprawl and fragmentation (Bhatta, et al.2010). Based on the work of O'Neill et al. (O'Neill, et al.1988), sets of different spatial metrics have been developed, modified and tested. Many of these quantitative measures have been implemented in the public domain statistical package FRAGSTATS (McGarigal.2002). Spatial metrics can be grouped into three broad classes:

a) Patch metrics;
b) Class metrics;
c) Landscape metrics.

Patch metrics are computed foe every patch in the landscape, class metrics are computed for every class in the landscape and landscape metrics are computed for entire patch mosaic. There are numerous types of spatial metrics that are found in the existing literature, for example: area/density/edge metrics (patch area, patch perimeter, class area, number of patches, patch density, total edge, edge density, landscape shape index, largest patch index, patch area distribution); shape metrics (perimeter-area ratio, shape index, fractal dimension index, linearity index, perimeter-area fractal dimension, core area metrics (core area, number of core areas, core area index, number of disjunct core areas, disjunct core area density, core area distribution); isolation/proximity metrics (proximity index, similarity index, proximity index

distribution, similarity index distribution); contrast metrics (edge contrast index, contrast-weighted edge density, total edge contrast index, edge contrast index distribution); contagion/interspersion metrics (percentage of like adjacencies, clumpiness index, aggregation index, interspersion and juxtaposition index, mass fractal dimension, landscape division index, splitting index, effective mesh size); connectivity metrics (patch cohesion index, connectance index, traversability index); and diversity metrics (patch richness, patch richness density, relative patch richness, Shannon's diversity index, Simpson's diversity index, Shannon's evenness index, Simpson's evenness index) (Bhatta, et al.2010, McGarigal.2002) Landscape metrics provided a comprehensive view of the overall landscape structure, including area, density, boundary, shape, core area, isolation/closeness, difference, spread, connection, and diversity

2.4. Literature review of UHI studies

2.4.1. Definition of UHI effect

For millions of peoples living in cities, increased temperatures are a growing fact and concern. The urban heat island (UHI) is a phenomenon whereby urban regions experience warmer temperature than their rural, undeveloped surroundings. The concept of UHI was introduced by Howard (1820) (GARTLAND.2011). The UHI is the most obvious atmospheric modification attributable to urbanization, the most studied of climate effects of cities and an iconic phenomenon of urban climate. It can be found in settlements of all sizes in all climatic regions and arises from the introductions of artificial surfaces characteristic of those of a city that radically alters the aerodynamic, radiative, thermal, and moisture properties in the urban region compared to the natural surroundings.

Urban and suburban areas have recorded higher temperature than their surroundings for a long time. UHI results in a difference of temperature between urban and rural areas of almost

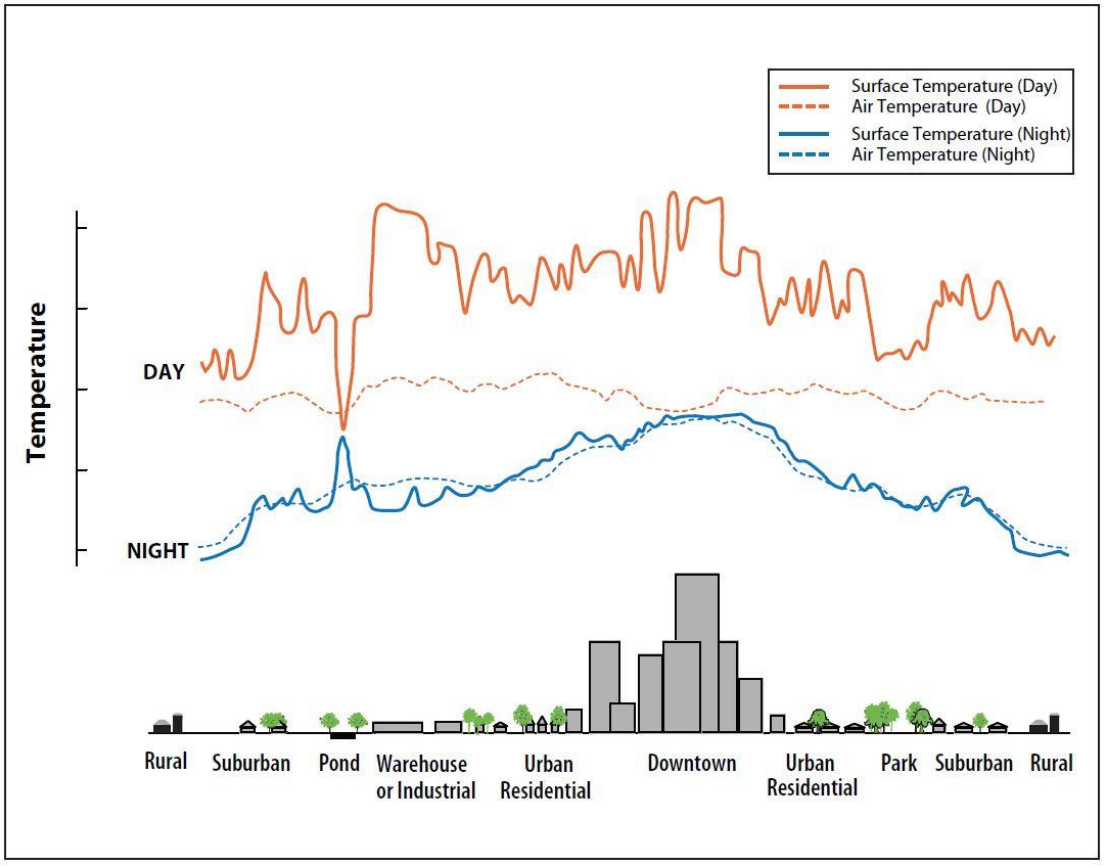

Figure 2-1 Variation of surface and atmospheric temperatures

(Source: United States Environmental Protection Agency (EPA.2016))

10 to 15℃ in the daytime and 5 to 10 ℃ at nighttime (Oke.1982). Figure 2-1 shows the variations of surface and atmospheric temperatures (EPA.2016). Surface and atmospheric temperatures vary over different land use areas. Surface temperatures vary more than air temperatures during the daytime, but they both are fairly similar at nighttime. The dip and spike in surface temperatures over the pond show how water maintains a fairly constant temperature day and night due to its high heat capacity.

There are two main reasons for the UHI effects. Firstly, the urban materials are mostly impermeable; consequently, moisture is not available to dissipate the sun's heat. For instance, the temperature of dry urban surface under a clear sky can reach up to 88 ℃, while vegetated areas with low moisture and in the same conditions experience a temperature of 18 ℃. Secondly, dark materials in cities with canyon like configurations trap more of the sun's energy. Moreover, factors such as human-made heat, low wind speed and air pollution increase the UHI effect dramatically (GARTLAND.2011).

2.4.2. Formation of UHI effect

The formation of the UHI is related to the energy balance of the urban area. Urban structures and materials, land cover change, and human activity alter the individual components of the energy balance in urban areas and subsequently the atmospheric state. The UHI must therefore be the result of urban/rural energy balance differences. The surface urban energy balance is defined as follows (Oke.1988):

$$R_n + F = H + LE + S \cdots\cdots\cdots\cdots\cdots\cdots\cdots\cdots\cdots\cdots (1)$$

Where

R_n is the net radiation, the energy generated by the sun and earth system;

F is the anthropogenic heating, the heat from buildings and vehicles;

H stands for sensible heat, the heat that causes change of temperature in an object;

LE is latent heat, the heat required to convert a solid into a liquid or vapour;

S represents heat storage.

Figure 2-2 shows the partitioning of energy fluxes in a city and a rural area. During the daytime, cities experience heat emitted from the sun (R_n) together with anthropogenic heat (F). As a recycling process, this amount of heat or energy is transferred into three alternative energies:

a) Stored in the city (S), such as absorbed by the building and road materials;

b) Caused evapo-transpirations (LE)

c) Heats the atmosphere.

In urban areas, the generated heat ($R_n + F$) is mostly stored in rough and low albedo materials such as concrete and asphalt whereas vegetated areas acts as a significant heat sink. Urban areas thus experience a higher temperature than the vegetated areas which is the formation of the urban heat island effect (Roth.2013).

The formation of the phenomenon of urban heat island is complex. The two major causes of urban heat islands are the the absent of vegetation and presence of more impervious surfaces.

a) Reduction of vegetation

In rural areas, vegetation and open land typically dominate the landscape, the absence of vegetation contributes to the formation of urban heat islands because it can no longer provide

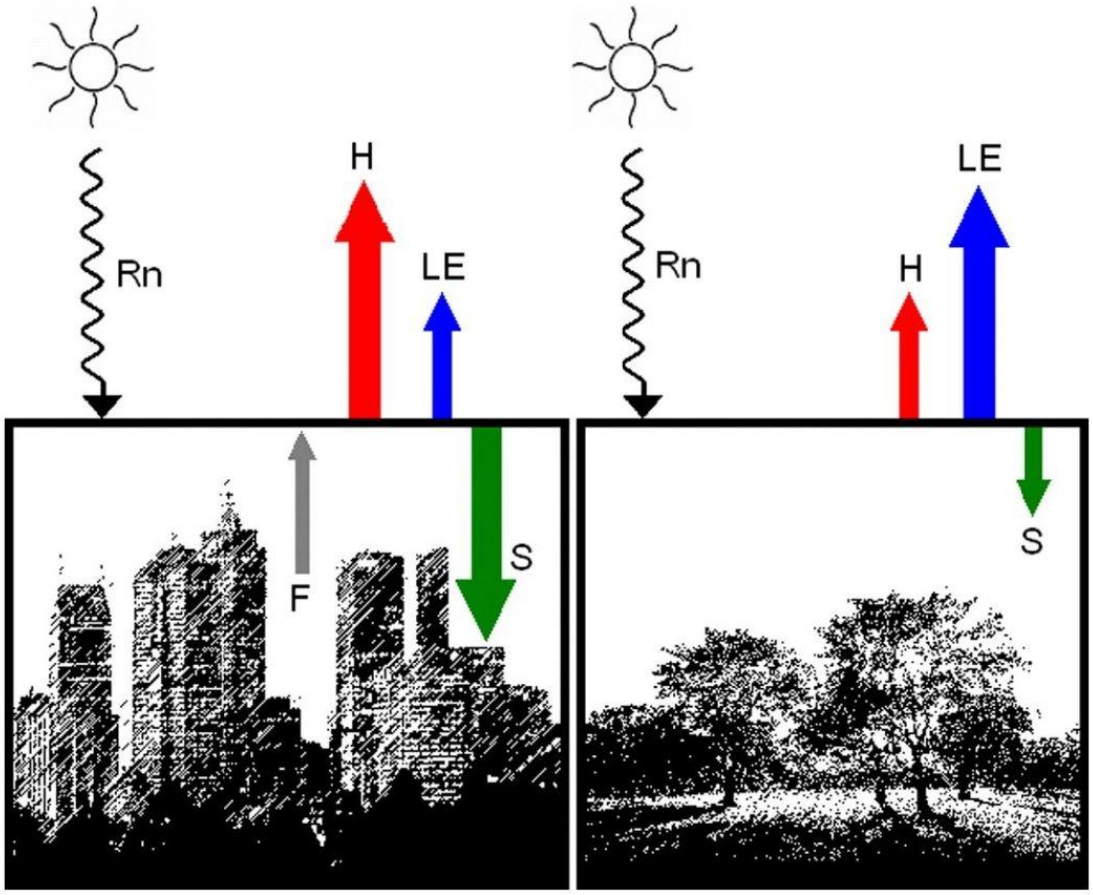

Figure 2-2 Partitioning of energy fluxes in a city (left) and a rural area (right)

(Source: The image was modified from Coutts et al. (Coutts, et al.2010))

two important cooling mechanisms: shade and evapo-transpiration. Shade can help cools the air by blocking solar radiation from low albedo surfaces, this reduces thermal energy and prevents the surface and ambient temperature from greatly increasing. Vegetation's evapo-transpiration cools the atmosphere because as the leaves of vegetation sweat water in their natural processes, they remove heat from the air.

b) Presence of more impervious surfaces

In contrast, urban areas are characterized by dry, impervious surfaces, such as conventional roofs side-walks, roads, and parking lots. Dark surfaces contribute to heat islands due to their low reflectivity. Albedo is ratio of the amount of light reflected from a material to the amount of light shone on the material. Dark and dry surfaces, such as pavements and buildings, absorb sunlight. This produces thermal energy, causing the surface to become hotter. Light and dry surfaces, such as natural ground and forest, which have a high albedo, they reflect sunlight and therefore, have a cooler surface temperature. The low overall albedo of the urban fabric is a major cause of the urban heat island effect. The heat that is stored in dark surfaces causes the overall ambient temperature to rise.

As cities develop, more vegetation is lost and more surfaces are covered with buildings, the change in ground cover results in less shade and moisture to keep urban area cool. Built up areas evaporate less water, which contributes to elevated surface and air temperatures.

c) Additional factors

An additional factor that influences urban heat island development is urban geometry. Urban geometry influences wind flow, energy absorption, and a given surface's ability to emit long-wave radiation back to space. Moreover, anthropogenic heat produced by human activities and additional factors such as the weather and geographic location also contribute to the phenomenon of urban heat island.

2.4.3. Types of urban heat island

Scholars have classified UHI into three categories based on the altitude that the UHI is measured (Zhang, et al.2009). The three types are surface urban heat island, canopy layer heat island and boundary layer heat island (Oke and Hannell.1970). The surface urban heat island (SUHI) measures temperature differences between urban and non-urban areas at the surface of the earth. The canopy layer UHI is derived at altitudes ranging from the rooftop to the

surface of the earth (Roth.2013). Boundary layer UHI measures temperature differences at altitudes ranging from general rooftops to the atmosphere (Table 2-1).

The surface UHI is defined by the temperature of the surface that extends over the entire 3-D envelope of the surface. It is a surface energy balance phenomenon and involves all urban facets (street, vertical walls, roofs, trees, etc.). In general, SUHI is measured using remote sensing data. The canopy-layer UHI is found within the atmosphere below the tops of buildings and trees (i.e., in the urban canopy). It is an expression of the surface energy balance that influences the air volume inside the canyon, primarily through sensible heat transfer from the surface into the canyon to change the temperature. The urban warmth extends into the urban boundary layer (above the roughness sub-layer) through convergence of sensible heat plumes from local scale areas and the entrainment of warmer air from above the urban boundary layer to create the boundary-layer UHI.

Table 2-1 Classification of urban heat island

UHI Types	Spatial Scale	Processes	Timing and Magnitude	Impacts
Surface	1-100 m	Day: surface energy balance; strong radiation absorption and heating by exposed dry and dark surfaces;	Day: very large and positive	Thermal comfort, planning and mitigation measures, temperature of storm water runoff, and health of aquatic ecosystems
		Night: surface energy balance; roofs—large cooling (large sky view); canyon facets—less cooling (restricted sky view)	Night: large and positive	
Canopy-Layer	1 -< 10 Km	Day: strong positive sensible heat flux at surface; sensible heat flux convergence in canyon	Day: small, sometimes negative if shading is extensive	Thermal comfort, building energy use, water use (irrigation), thermal circulation if winds are light, air quality, urban ecology, and ice and snow
		Night: often positive sensible heat flux supported by release of heat from storage in ground and buildings, longwave radiative flux convergence, and anthropogenic heat	Night: large and positive, increases with time from sunset, maximum between a few hours after sunset to predawn hours	
Boundary-Layer	> 10Km	Day: bottom-up sensible heat flux through top of RSL, top-down heat entrainment into UBL, and radiative flux divergence due to polluted air	Day/night: small and positive, decreasing with height in UBL	Air quality, photochemical pollutants, local circulation, precipitation and thunderstorm activity downwind, and plant growing season
		Night: Similar to day, but intensity of processes is reduced anthropogenic heat under special conditions		

2.4.4. Impacts of urban heat island

The adverse effect of UHI has been widely documented in the literature. For example, it increases temperature of cities; contributes to global warming (EPA.2016), initiates storms/precipitation events (Bornstein and Lin.2000), increasing energy demand of cities, and contributes to heat related mortality (Rajasekar and Weng.2009).

The city temperature, especially the land surface temperature (LST), is the most essential factor which affect the urban environment. As the urban heat island center with high land surface temperature, the atmosphere rises upward. Elevated temperature from urban heat islands, particularly during the summer, can affect a community's environment and quality of life. The impacts of UHI are listed as follows:

a) Effect on urban climate

   Urban climate is different from rural climate due to human activities. The climate factors such as sunshine, radiation, air temperature, humidity, rain, wind are related to each other (Imhoff, et al.2010). The urban heat island has a strong correlation with the urban dry island, urban wet island, urban dark island, and urban rain island. The urban heat island will result in local circulation, making the features of urban wind field complex. The snowfall, the frequency of snow, the frost quantity and other snow climate phenomenon are significantly lower in the urban heat island area compared with rural areas (Oke and Hannell.1970).

b) Effect on urban hydrological characteristics

   The urban heat island effect will affect the formation and movement of clouds. The precipitation and the surface runoff in urban areas is significantly larger than surrounding rural areas (Yang, et al.2017). However, the evaporation and the underground water runoff is lower than surrounding rual areas. Generally, the urban heat island effect will increase the precipitation.

c) Effect on soil physicochemical characteristics

   Due to the urban heat island effect, the urban soil temperature is higher than surrounding natural soil temperature (Kohler, et al.2017). The change of soil temperature affect soil temperature and humidity environment, active nutrient, microbial activities and so on.

d) Effect on atmospheric environment

Due to the existence of urban heat island, around the urban heat island center, there is a strong warm updraft, rising while radiate outward, when reaching the surrounding rural areas, it will become downdraft, and the cold air blows to the city, finally forming a closed circulation circle, resulting in a vicious circle of pollutants between suburbs(Sannigrahi, et al.2017) .

e) Effect on urban energy consumption

The urban heat island effect will affect the urban energy consumption (Oke.1982). In summer, the energy consumption of air conditioning is quite big due to the effect make the city hotter. Although the energy consumption for heating is lower in winter, the total energy consumption is increasing (Oke.1982).

f) Effect on residents health

Thermohygrometrix index (THI) is often being used to evaluate the degree of uncomfortableness of human toward heat environment (Kohler, et al.2017). People feel hot if THI is greater than 20. Previous studies found that the digestive system diseases occur more frequently on urban residents.

2.5. Summary

In this chapter, an in-depth review of prior studies associated with our study was conducted. The literature review carried from three aspects: urbanization and eco-environment evaluation; urban sprawl, urban heat island.

a) Review on the previous field study on urbanization and eco-environment evaluation was carried out which presented detailed information on the research processes and popular field relate to the assessment. In addition, methods of assessment, selection of indicators also have been discussed to make evaluation evidence based.

b) Literature review on urban sprawl expounded the impacts of land cover change on climate, as well as the quantization assessment of urban sprawl. Detailed introduction of landscape metrics have been conducted which help providing a comprehensive view of the overall landscape structure.

c) As with the global warming and environment issues appeared, urban heat island had grown into prominent problem for the modern society. Urban heat island effect studies also have been reviewed in this chapter which including the definition, formation, classification and effects of UHI phenomenon.

Reference

[1] Liyin Shen, Jingyang Zhou, Martin Skitmore, Bo Xia, Application of a hybrid Entropy–McKinsey Matrix method in evaluating sustainable urbanization: A China case study, Cities, 42 (2015) 186-194.

[2] Barney Cohen, Urbanization in developing countries: Current trends, future projections, and key challenges for sustainability, Technology in Society, 28 (2006) 63-80.

[3] ShaoJian Wang, Haitao Ma, YaBo Zhao, Exploring the relationship between urbanization and the eco-environment—A case study of Beijing–Tianjin–Hebei region, Ecological Indicators, 45 (2014) 171-183.

[4] Bin Gao, Qingxu Huang, Chunyang He, Qun Ma, Dynamics of Urbanization Levels in China from 1992 to 2012: Perspective from DMSP/OLS Nighttime Light Data, Remote Sensing, 7 (2015) 1721-1735.

[5] Shaojian Wang, Chuanglin Fang, Xingliang Guan, Bo Pang, Haitao Ma, Urbanisation, energy consumption, and carbon dioxide emissions in China: A panel data analysis of China's provinces, Applied Energy, 136 (2014) 738-749.

[6] Syrquin M Chenery H, The Development Style: 1950–1970. In: Li Xinhua et al. Beijing: Economic Science

Press. (in Chinese), (1988).

[7] M. Henderson, E. T. Yeh, P. Gong, C. Elvidge, K. Baugh, Validation of urban boundaries derived from global night-time satellite imagery, International Journal of Remote Sensing, 24 (2003) 595-609.

[8] Cheng C Ebanks G E, China: A unique urbanization model. Asia-Pacific Population Journal, 5: 29–50., (1990).

[9] C. Hunter, & Shaw, J. , The ecological footprint as a key indicator of sustainable tourism. Tourism Management, 28(1), 46–57., (2007).

[10] Y. Y. Wu, X. J. He, Evaluation of Beijing sustainable development based on DEA model, Xitong Gongcheng Lilun yu Shijian/System Engineering Theory and Practice, 26 (2006) 117-123.

[11] Jingjing Zhao, Lihe Chai, A novel approach for urbanization level evaluation based on information entropy principle: A case of Beijing, Physica A: Statistical Mechanics and its

Applications, 430 (2015) 114-125.

[12] Ashraf M. Dewan, Yasushi Yamaguchi, Land use and land cover change in Greater Dhaka, Bangladesh: Using remote sensing to promote sustainable urbanization, Applied Geography, 29 (2009) 390-401.

[13] LA Pielke, Land use and climate change. Science 310(November):1625–1626., (2005).

[14] Ermias Teferi, Woldeamlak Bewket, Stefan Uhlenbrook, Jochen Wenninger, Understanding recent land use and land cover dynamics in the source region of the Upper Blue Nile, Ethiopia: Spatially explicit statistical modeling of systematic transitions, Agriculture, Ecosystems & Environment, 165 (2013) 98-117.

[15] Marc L. Imhoff, Ping Zhang, Robert E. Wolfe, Lahouari Bounoua, Remote sensing of the urban heat island effect across biomes in the continental USA, Remote Sensing of Environment, 114 (2010) 504-513.

[16] R. C. Estoque, Y. Murayama, S. W. Myint, Effects of landscape composition and pattern on land surface temperature: An urban heat island study in the megacities of Southeast Asia, Sci Total Environ, 577 (2017) 349-359.

[17] A. R. Dos Santos, F. S. de Oliveira, A. G. da Silva, J. M. Gleriani, W. Goncalves, G. L. Moreira, F. G. Silva, E. R. F. Branco, M. M. Moura, R. G. da Silva, R. S. Juvanhol, K. B. de Souza, Caas Ribeiro, V. T. de Queiroz, A. V. Costa, A. S. Lorenzon, G. F. Domingues, G. E. Marcatti, N. L. M. de Castro, R. T. Resende, D. E. Gonzales, L. A. de Almeida Telles, T. R. Teixeira, Gmada Dos Santos, P. H. S. Mota, Spatial and temporal distribution of urban heat islands, Sci Total Environ, 605-606 (2017) 946-956.

[18] Hui Li, Cuizhen Wang, Cheng Zhong, Zhi Zhang, Qingbin Liu, Mapping Typical Urban LULC from Landsat Imagery without Training Samples or Self-Defined Parameters, Remote Sensing, 9 (2017) 700.

[19] Qihao Weng, Remote sensing of impervious surfaces in the urban areas: Requirements, methods, and trends, Remote Sensing of Environment, 117 (2012) 34-49.

[20] Qihao Weng, Dengsheng Lu, Jacquelyn Schubring, Estimation of land surface temperature–vegetation abundance relationship for urban heat island studies, Remote Sensing of Environment, 89 (2004) 467-483.

[21] Qian Zhang, Yifang Ban, Jiyuan Liu, Yunfeng Hu, Simulation and analysis of urban growth scenarios for the Greater Shanghai Area, China, Computers, Environment and Urban Systems, 35 (2011) 126-139.

[22] Nicholas R. Goodwin, Nicholas C. Coops, Michael A. Wulder, Steve Gillanders, Todd A. Schroeder, Trisalyn Nelson, Estimation of insect infestation dynamics using a temporal sequence of Landsat data, Remote Sensing of Environment, 112 (2008) 3680-3689.

[23] B. Bhatta, S. Saraswati, D. Bandyopadhyay, Urban sprawl measurement from remote sensing data, Applied Geography, 30 (2010) 731-740.

[24] R. V. O'Neill, J. R. Krummel, R. H. Gardner, G. Sugihara, B. Jackson, D. L. DeAngelis, B. T. Milne, M. G. Turner, B. Zygmunt, S. W. Christensen, V. H. Dale, R. L. Graham, Indices of landscape pattern, Landscape Ecology, 1 (1988) 153-162.

[25] K. McGarigal, FRAGSTATS: spatial pattern analysis program for categorical maps. www.umass.edu/landeco/
research/fragstats/fragstats.html., (2002).

[26] L. GARTLAND, Heat islands: understanding and mitigating heat in urban areas, Routledge., (2011).

[27] EPA, Heat Island Impacts. United States Environmental Protection, (2016).

[28] T. R. Oke, The energetic basis of the urban heat island, Quarterly Journal of the Royal Meteorological Society, 108 (1982) 1-24.

[29] T. R. Oke, The urban energy balance, Progress in Physical Geography, 12 (1988) 471-508.

[30] Andrew Coutts, Jason Beringer, Nigel Tapper, Changing Urban Climate and CO2 Emissions: Implications for the Development of Policies for Sustainable Cities, Urban Policy and Research, 28 (2010) 27-47.

[31] Matthias Roth, Urban Heat Islands. In: FERNANDO, H. J. S. (ed.) Handbook of Environmental Fluid Dynamics. CRC Press/Taylor & Francis., (2013).

[32] Xiuying Zhang, Taiyang Zhong, Xuezhi Feng, Ke Wang, Estimation of the relationship between vegetation patches and urban land surface temperature with remote sensing, International Journal of Remote Sensing, 30 (2009) 2105-2118.

[33] T. R. Oke, F. G. Hannell, The form of the urban heat island in Hamilton, Canada, WMO

Tech Note, 108 (1970) 113-126.

[34] Robert Bornstein, Qinglu Lin, Urban heat islands and summertime convective thunderstorms in Atlanta: three case studies, Atmospheric Environment, 34 (2000) 507-516.

[35] Umamaheshwaran Rajasekar, Qihao Weng, Urban heat island monitoring and analysis using a non-parametric model: A case study of Indianapolis, ISPRS Journal of Photogrammetry and Remote Sensing, 64 (2009) 86-96.

[36] Xuchao Yang, L. Ruby Leung, Naizhuo Zhao, Chun Zhao, Yun Qian, Kejia Hu, Xiaoping Liu, Baode Chen, Contribution of urbanization to the increase of extreme heat events in an urban agglomeration in east China, Geophysical Research Letters, (2017).

[37] Manon Kohler, Cécile Tannier, Nadège Blond, Rahim Aguejdad, Alain Clappier, Impacts of several urban-sprawl countermeasures on building (space heating) energy demands and urban heat island intensities. A case study, Urban Climate, 19 (2017) 92-121.

[38] Srikanta Sannigrahi, Shahid Rahmat, Suman Chakraborti, Sandeep Bhatt, Shouvik Jha, Changing dynamics of urban biophysical composition and its impact on urban heat island intensity and thermal characteristics: the case of Hyderabad City, India, Modeling Earth Systems and Environment, 3 (2017) 647-667.

[39] Limor Shashua-Bar, Ioannis X. Tsiros, Milo E. Hoffman, A modeling study for evaluating passive cooling scenarios in urban streets with trees. Case study: Athens, Greece, Building and Environment, 45 (2010) 2798-2807.

[40] Erica Correa, María Angélica Ruiz, Alicia Canton, Graciela Lesino, Thermal comfort in forested urban canyons of low building density. An assessment for the city of Mendoza, Argentina, Building and Environment, 58 (2012) 219-230.

[41] 2010 ASHRAE, ASHRAE Handbook-Fundamentals. American Society of Heating, Refrigerating and Air-Conditioning Engineers, Atlanta.

[42] Peter Höppe, Different aspects of assessing indoor and outdoor thermal comfort, Energy and Buildings, 34 (2002) 661-665.

[43] 1R. Emmanuel, An Urban Approach to Climate Sensitive Design: Strategies for the Tropics, 2005.

[44] 1P.O. Fanger, Thermal comfort: Analysis and applications in environmental engineering, Danish Technical Press, 1970.

[45] Mohamed H. Elnabawi, Neveen Hamza, Steven Dudek, Numerical modelling evaluation for the microclimate of an outdoor urban form in Cairo, Egypt, HBRC Journal, 11 (2015) 246-251.

[46] Mohammad Taleghani, Laura Kleerekoper, Martin Tenpierik, Andy van den Dobbelsteen, Outdoor thermal comfort within five different urban forms in the Netherlands, Building and Environment, 83 (2015) 65-78.

[47] P. Höppe, The physiological equivalent temperature – a universal index for the biometeorological assessment of the thermal environment, International Journal of Biometeorology, 43 (1999) 71-75.

[48] Jennifer Spagnolo, Richard de Dear, A field study of thermal comfort in outdoor and semi-outdoor environments in subtropical Sydney Australia, Building and Environment, 38 (2003) 721-738.

[49] Mohamad Fahmy, Stephen Sharples, On the development of an urban passive thermal comfort system in Cairo, Egypt, Building and Environment, 44 (2009) 1907-1916.

[50] Peter Bröde, Dusan Fiala, Krzysztof Błażejczyk, Ingvar Holmér, Gerd Jendritzky, Bernhard Kampmann, Birger Tinz, George Havenith, Deriving the operational procedure for the Universal Thermal Climate Index (UTCI), International Journal of Biometeorology, 56 (2012) 481-494.

[51] Peter Bröde, Eduardo L. Krüger, Francine A. Rossi, Dusan Fiala, Predicting urban outdoor thermal comfort by the Universal Thermal Climate Index UTCI—a case study in Southern Brazil, International Journal of Biometeorology, 56 (2012) 471-480.

[52] H. Mayer, P. Höppe, Thermal comfort of man in different urban environments, Theoretical and Applied Climatology, 38 (1987) 43-49.

[53] Peter R. Höppe, Hermann A. J. Seidl, Problems in the assessment of the bioclimate for vacationists at the seaside, International Journal of Biometeorology, 35 (1991) 107-110.

[54] Marialena Nikolopoulou, Nick Baker, Koen Steemers, Thermal comfort in outdoor urban spaces: understanding the human parameter, Solar Energy, 70 (2001) 227-235.

[55] Baruch Givoni, Mikiko Noguchi, Hadas Saaroni, Oded Pochter, Yaron Yaacov, Noa Feller, Stefan Becker, Outdoor comfort research issues, Energy and Buildings, 35 (2003) 77-86.

[56] Sofia Thorsson, Maria Lindqvist, Sven Lindqvist, Thermal bioclimatic conditions and patterns of behaviour in an urban park in Göteborg, Sweden, International Journal of Biometeorology, 48 (2004) 149-156.

[57] Ayman Hassaan Ahmed Mahmoud, Analysis of the microclimatic and human comfort conditions in an urban park in hot and arid regions, Building and Environment, 46 (2011) 2641-2656.

[58] Liang Chen, Edward Ng, Outdoor thermal comfort and outdoor activities: A review of research in the past decade, Cities, 29 (2012) 118-125.

[59] JiFu Yin, YouFei Zheng, RongJun Wu, JianGuo Tan, DianXiu Ye, Wei Wang, An analysis of influential factors on outdoor thermal comfort in summer, International Journal of Biometeorology, 56 (2012) 941-948.

[60] Igor Knez, Sofia Thorsson, Influences of culture and environmental attitude on thermal, emotional and perceptual evaluations of a public square, International Journal of Biometeorology, 50 (2006) 258-268.

[61] Ingegärd Eliasson, Igor Knez, Ulla Westerberg, Sofia Thorsson, Fredrik Lindberg, Climate and behaviour in a Nordic city, Landscape and Urban Planning, 82 (2007) 72-84.

[62] Sofia Thorsson, Fredrik Lindberg, Ingegärd Eliasson, Björn Holmer, Different methods for estimating the mean radiant temperature in an outdoor urban setting, International Journal of Climatology, 27 (2007) 1983-1993.

[63] Mahesh Kumar Jat, P. K. Garg, Deepak Khare, Monitoring and modelling of urban sprawl using remote sensing and GIS techniques, International Journal of Applied Earth Observation and Geoinformation, 10 (2008) 26-43.

[64] Tzu-Ping Lin, Richard de Dear, Ruey-Lung Hwang, Effect of thermal adaptation on seasonal outdoor thermal comfort, International Journal of Climatology, 31 (2011) 302-312.

[65] Noémi Kántor, Lilla Égerházi, János Unger, Subjective estimation of thermal environment in recreational urban spaces—Part 1: investigations in Szeged, Hungary, International Journal of Biometeorology, 56 (2012) 1075-1088.

[66] Emmanuel Lubango Ndetto, Andreas Matzarakis, Effects of Urban Configuration on Human Thermal Conditions in a Typical Tropical African Coastal City, Advances in Meteorology, 2013 (2013) 1-12.

[67] Akinyemi Gabriel Omonijo, Clement Olabinjo Adeofun, Olusegun Oguntoke, Andreas Matzarakis, Relevance of thermal environment to human health: a case study of Ondo State, Nigeria, Theoretical and Applied Climatology, 113 (2013) 205-212.

[68] Younha Kim, Seung An, Jeong-Hee Eum, Jung-Hun Woo, Analysis of Thermal Environment over a Small-Scale Landscape in a Densely Built-Up Asian Megacity, Sustainability, 8 (2016) 358.

[69] Andreas Matzarakis, Frank Rutz, Helmut Mayer, Modelling radiation fluxes in simple and complex environments—application of the RayMan model, International Journal of Biometeorology, 51 (2007) 323-334.

[70] Fredrik Lindberg, Björn Holmer, Sofia Thorsson, SOLWEIG 1.0 – Modelling spatial variations of 3D radiant fluxes and mean radiant temperature in complex urban settings, International Journal of Biometeorology, 52 (2008) 697-713.

[71] Andreas Matzarakis, Olaf Matuschek, Sky view factor as a parameter in applied climatology rapid estimation by the SkyHelios model, Meteorologische Zeitschrift, 20 (2011) 39-45.

[72] Michael Bruse, Heribert Fleer, Simulating surface–plant–air interactions inside urban environments with a three dimensional numerical model, Environmental Modelling & Software, 13 (1998) 373-384.

[73] Fazia Ali-Toudert, Helmut Mayer, Numerical study on the effects of aspect ratio and orientation of an urban street canyon on outdoor thermal comfort in hot and dry climate, Building and Environment, 41 (2006) 94-108.

Chapter Three: Integrated Assessment of Urbanization and Eco-Environment in China

3.1. Introduction

The urbanization process involves rural people migrating to urban areas. More than half of the world populations were living in urban areas. As one of the most remarkable countries in the world, China have been experiencing large-scale urbanization since the application of the reform and open policy, and this phenomenon is expected to continue into the foreseeable future, with the ratio of China's urban population being predicted to reach 65% by 2025 and 77% by 2050 (Shen, et al.2015).

As the urbanization processing draws more and more attention, it is meaningful and useful to have an investigation of the urbanization processing in China in recent decades. In addition, environmental issues arose along with the urbanization, it is essential to do more in-depth study to explore the relationship between the urbanization and eco-environment to provide guidance for sustainable development. The investigation of urbanization could help us to get a comprehensive understanding of what happened in the study region and promote better health and quality of life.

Urbanization and eco-environment system is rather complicated to evaluate, based on the literature review on the evaluation method and indicator system, in this study, the urbanization evaluation was carried out from four aspects: economic urbanization, demographic urbanization, spatial urbanization and social urbanization. The same with urbanization indexes, the eco-environment indicator system was composed of three sub-level: eco-environment pressure, eco-environment level and eco-environment control.

In this research, available statistic from the China Statistic Yearbook in 2005 and 2015 were used to conduct the evaluation in each year and comparison analysis was then carried out to explore the development of urbanization and eco-environment after ten years. Meanwhile, 30 provinces were divided into 5 regions to explore the unbalance and difference in different geographical location. The indexes selection was based on the previous study and the availability of the dataset. Principle component analysis was then applied to do the data reduction and mining.

Maximum entropy method was applied to generate the evaluation systems. The processing including data standardization, calculating proportion of datum, information entropy, weights etc. To explore the eco-environment level and urbanization level in China at provincial

scale.24 eco-environment related indexes and 32 urbanization related indexes was selected. The weight of each indicator was obtained from entropy calculation. Then the urbanization level indexes and eco-environment level indexes was got for further analysis. Comparison analysis and coordinate analysis was then applied in this research. The research flow of this chapter was shown in Figure 3-1 below.

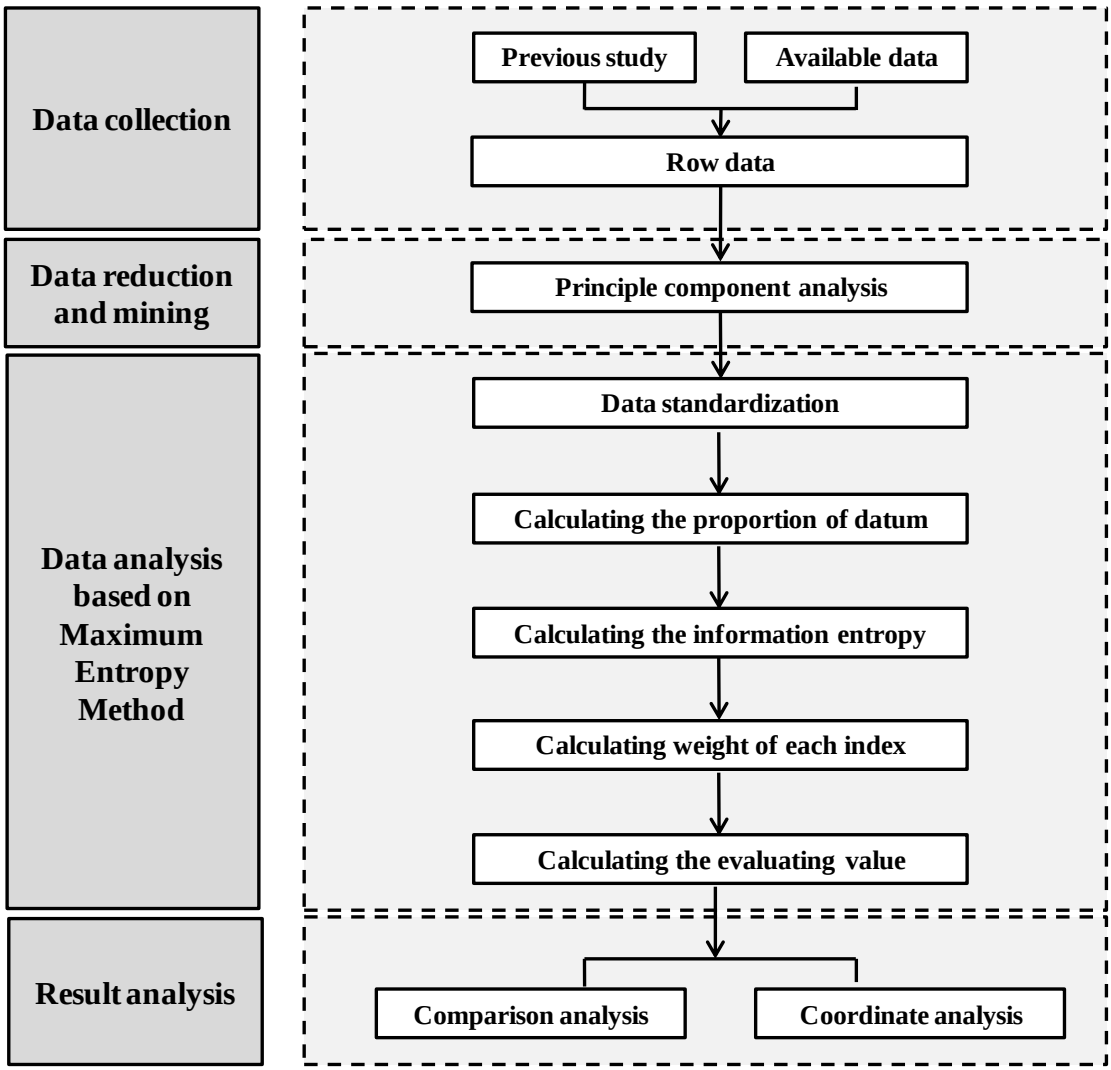

Figure 3-1 Research Flow

3.2. Method and data

3.2.1. Data mining and index system

In this study, we first picked up all indices which could reflect main characteristics of eco-environment and urbanization. For the differences exist in the dimension and the magnitude of the selected indicators, all indicators were required for pro-processing. Therefore, we applied the Entropy Method to determine the weight of selected indicators to evaluate the urbanization and eco-environment systems of China's provinces.

The required data were collected from the Statistical Yearbook. We conducted preliminary indexes of the eco-environment and urbanization system at first. As repeatable information

Table 3-1 Total variance explained of eco-environment related indices

Component	Initial Eigenvalues			Extraction Sums of Squared Loadings		
	Total	% of Variance	Cumulative %	Total	% of Variance	Cumulative %
1	7.13	29.73	29.73	7.13	29.73	29.73
2	4.71	19.63	49.35	4.71	19.63	49.35
3	2.94	12.27	61.62	2.94	12.27	61.62
4	2.46	10.25	71.86	2.46	10.25	71.86
5	1.43	5.96	77.83	1.43	5.96	77.83
6	1.15	4.81	82.64	1.15	4.81	82.64
7	0.90	4.59	87.23	1.10	4.59	87.23
8	0.67	2.78	90.01			
9	0.51	2.11	92.11			
10	0.40	1.68	93.79			
11	0.32	1.32	95.11			
12	0.25	1.06	96.17			
13	0.19	0.79	96.95			
14	0.16	0.65	97.61			
15	0.14	0.58	98.19			
16	0.10	0.40	98.59			
17	0.09	0.36	98.96			
18	0.09	0.36	99.31			
19	0.07	0.27	99.59			
20	0.05	0.20	99.78			
21	0.03	0.14	99.92			
22	0.01	0.06	99.98			
23	0.01	0.02	100.00			
24	0.00	0.00	100.00			

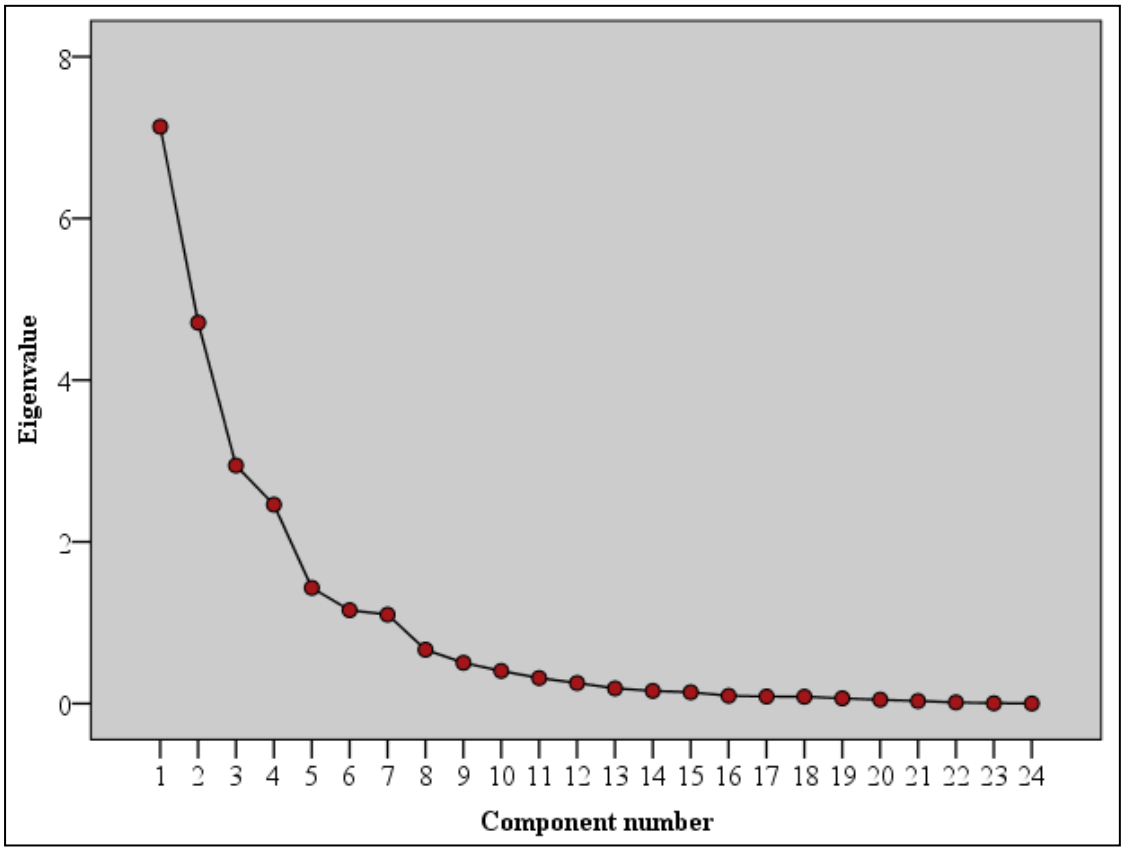

Figure 3-2 Scree plot of principal components on eco-environment indexes

existed among preliminary indices, the indices were further selected through principle analysis to extract the indices which are relatively typical, independent and integrated assessment and aim to gather a better understanding of the relationship between the eco-environment and the urbanization process.

As Table 3-1 shows result of total variance explained of the indices related to eco-environment. Based on Table 3-1, the scree plot between component number and eigenvalue was established shown as Fig.3-2.As it shown in Table 3-1 and Fig. 3-2, the cumulative variance of the first seven components was greater than 85%, and the slope of the broken line is relative high (Kasman and Duman.2015). The broken line becomes smooth from the eighth component. Therefore, we selected the first seven components as principal components.

Then we carried out the variance-max orthogonal rotation toward the contribution matrix of principal component, and then we found out original indices with contribution higher than 0.70 of each principal component, finally to gather these screened original indices, as shown

Table 3-2 Contribution Matrix of Rotated Component of eco-environment indexes

Index	Component number						
	1	2	3	4	5	6	7
X1	0.072	0.886	-0.135	-0.112	0.476	-0.335	0.490
X2	0.721	-0.130	0.408	-0.059	-0.002	0.154	0.309
X3	0.077	0.350	-0.808	-0.135	0.234	0.076	0.004
X4	0.482	0.238	-0.056	0.320	0.434	-0.051	0.328
X5	0.712	0.580	-0.172	0.080	-0.066	-0.075	-0.028
X6	0.387	0.586	0.313	-0.236	-0.008	-0.241	-0.173
X7	0.470	0.328	-0.701	0.179	0.127	-0.016	-0.205
X8	0.840	-0.020	0.277	-0.052	0.127	-0.060	-0.005
X9	0.864	-0.040	0.277	-0.103	0.060	0.022	-0.235
X10	-0.157	0.705	-0.233	0.125	0.304	0.270	-0.302
X11	-0.222	0.045	0.119	0.721	0.464	0.274	-0.136
X12	-0.456	0.749	0.404	0.013	-0.080	0.144	0.079
X13	-0.348	0.871	0.249	-0.169	-0.057	0.046	0.060
X14	-0.450	0.767	0.387	0.006	-0.065	0.149	0.068
X15	-0.202	0.431	0.174	-0.280	-0.106	0.042	-0.035
X16	-0.177	-0.279	0.487	0.634	0.184	0.343	0.026
X17	0.426	0.249	0.445	0.511	-0.209	-0.226	-0.204
X18	0.823	-0.137	0.351	-0.158	0.096	-0.005	0.081
X19	0.914	0.142	0.130	0.111	0.088	-0.111	-0.092
X20	0.690	-0.070	0.203	-0.465	0.268	0.274	-0.006
X21	0.270	-0.165	-0.031	-0.667	0.112	0.539	-0.188
X22	0.703	0.260	-0.303	0.317	-0.311	0.056	-0.116
X23	0.712	0.216	-0.288	0.297	-0.396	0.173	0.048
X24	0.346	0.149	-0.278	0.151	-0.395	0.411	0.543

in Table 3-2, the detailed processing is as follows: for the first principal component, positive indices with the contribution greater than 0.70 are: X2, X5, X8, X9, X18, X19, X22, X22, X23; for the second principal component, positive indices with the contribution larger than 0.70 are: X1, X10, X12, X13; for the third principal component, negative indices with the contribution larger than 0.70 are: X3, X7; for the fourth principal component, positive index with the contribution larger than 0.70 is: X11； contribution larger than 0.75 are: X14、X31. The results of principal component analysis showed that, these original indices (X4, X6, X15, X16, X17, X20, X21, and X24) with repeatable information in eco-environment elementary

assessment index system should be screened out. Thus, the final indices which could represent the entire principal components and overall information of original eco-environment related data were extracted.

Table 3-3 Total Variance Explained of urbanization related indices

Component	Initial Eigenvalues			Extraction Sums of Squared Loadings		
	Total	% of Variance	Cumulative %	Total	% of Variance	Cumulative %
1	17.20	53.76	53.76	17.20	53.76	53.76
2	3.52	10.99	64.76	3.52	10.99	64.76
3	2.27	7.10	71.85	2.27	7.10	71.85
4	1.34	4.17	76.03	1.34	4.17	76.03
5	1.24	3.87	79.90	1.24	3.87	79.90
6	0.91	2.85	82.75	0.91	2.85	82.75
7	0.80	2.49	85.24	0.80	2.49	85.24
8	0.72	2.26	87.50			
9	0.65	2.03	89.53			
10	0.58	1.83	91.36			
11	0.53	1.65	93.00			
12	0.41	1.29	94.29			
13	0.36	1.13	95.42			
14	0.25	0.77	96.19			
15	0.23	0.71	96.91			
16	0.19	0.58	97.49			
17	0.16	0.51	98.00			
18	0.13	0.41	98.41			
19	0.11	0.33	98.74			
20	0.08	0.25	98.99			
21	0.07	0.22	99.21			
22	0.06	0.20	99.41			
23	0.06	0.17	99.58			
24	0.03	0.11	99.69			
25	0.03	0.08	99.78			
26	0.02	0.07	99.84			
27	0.02	0.06	99.90			
28	0.01	0.04	99.94			
29	0.01	0.03	99.97			
30	0.01	0.02	99.99			
31	0.00	0.01	100.00			
32	0.00	0.00	100.00			

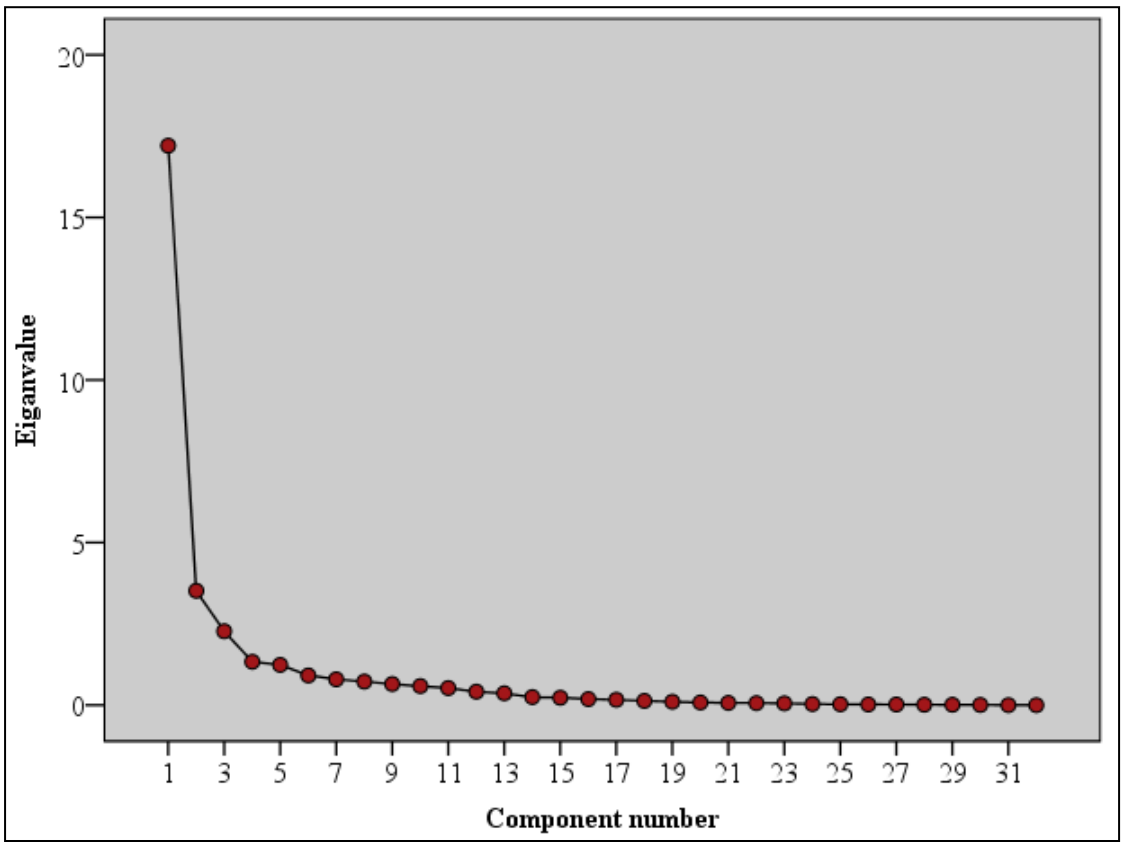

Figure 3-3 Scree plot of principal components on urbanization indexes

As Table 3-3 shows result of total variance explained of the indices related to urbanization. Based on Table 3-3, the scree plot between component number and eigenvalue was established shown as Figure 3-3 As it shown in Table 3-3 and Figure 3-3, the cumulative variance of the first seven components was greater than 85%, and the slope of the broken line is relative high (Kasman and Duman.2015). The broken line becomes smooth from the eighth component. Therefore, we selected the first seven components as principal components.

Then we carried out the variance-max orthogonal rotation toward the contribution matrix of principal component, and then we found out original indices with csontribution higher than 0.70 of each principal component, finally to gather these screened original indices, as shown in Table 3-4s, the detailed process is as follows: for the first principal component, positive indices with the contribution larger than 0.70 are: Y1, Y2, Y3, Y4, Y5, Y6, Y9, Y11, Y18, Y19, Y20, Y22, Y23,Y25, Y28, Y29, Y30, Y32, negative index with the contribution larger than 0.70 is Y10; for the second principal component, negative index with the contribution larger than 0.70 are: Y10; for the fourth principal component, positive index with the contribution larger than 0.70 is:Y12, Y13. There are 22 indices been selected in total.

Table 3-4 Contribution Matrix of Rotated Component of urbanization indexes

Index	Component number						
	1	2	3	4	5	6	7
Y1	0.951	-0.127	-0.005	-0.017	0.114	-0.023	-0.075
Y2	0.759	-0.149	0.08	-0.194	-0.082	0.304	0.148
Y3	0.933	-0.161	0.087	-0.196	0.026	-0.012	-0.097
Y4	0.876	0.151	-0.051	-0.105	0.02	-0.036	0.014
Y5	0.971	-0.068	0.097	-0.095	0.033	-0.04	-0.037
Y6	0.906	-0.26	-0.041	-0.046	-0.008	-0.044	0.018
Y7	0.831	0.187	0.27	-0.344	-0.014	0.07	-0.056
Y8	0.945	-0.265	-0.032	0.064	0.02	-0.005	-0.015
Y9	0.687	0.394	0.255	-0.105	-0.21	0.149	0.089
Y10	0.2	-0.306	0.376	0.542	0.26	0.049	0.275
Y11	0.95	-0.133	-0.045	-0.13	0.053	0.02	-0.013
Y12	-0.504	-0.022	0.347	0.416	-0.148	-0.059	0.051
Y13	0.513	0.161	-0.156	-0.153	0.531	0.041	0.353
Y14	-0.144	-0.09	-0.14	-0.237	0.618	-0.148	0.082
Y15	0.139	0.582	0.633	0.053	0.043	-0.193	-0.173
Y16	0.465	-0.169	0.478	0.099	0.072	0.209	0.251
Y17	0.759	-0.002	-0.458	0.086	0.01	0.13	0.118
Y18	0.925	-0.198	0.01	-0.033	0.05	-0.019	-0.059
Y19	0.822	0.03	-0.131	-0.057	-0.14	-0.185	0.068
Y20	0.806	0.322	-0.119	0.258	-0.028	-0.148	-0.059
Y21	0.81	0.382	0.043	0.146	0.053	-0.292	-0.063
Y22	0.809	0.439	0.127	0.07	-0.053	-0.246	-0.095
Y23	0.811	0.059	0.216	-0.175	-0.01	-0.208	-0.158
Y24	0.059	0.473	-0.381	0.474	0.296	0.021	-0.224
Y25	0.366	0.404	-0.462	0.18	-0.103	0.395	0.286
Y26	-0.135	0.369	0.391	0.124	0.431	0.458	-0.078
Y27	0.42	0.458	0.035	-0.28	-0.198	0.356	0.093
Y28	0.829	0.085	-0.005	0.363	-0.046	-0.082	0.06
Y29	0.814	-0.412	0.02	0.122	0.1	0.006	-0.131
Y30	0.791	-0.405	0.114	0.155	0.073	0.176	-0.05
Y31	0.761	0.084	-0.442	0.203	-0.089	-0.002	0.213
Y32	0.553	-0.275	0.117	0.395	-0.284	0.131	0.404

3.2.2. Entropy method

Shannon introduced the Entropy method into the study of the information management discipline in 1948 for entropy can express the information or uncertainty of a set of data . The method is based on the principle that greater uncertainty about outcomes, results in a more uniform probability assigned to them. At present, the Entropy method has been applied to various disciplines and fields such as energy utilization, urban landscape analysis, the growth of economy, and environment related study (Xu and Zhang.2016). The Entropy principle can be used to evaluate the performance of appointed index between a set of indicators. Previous studies and current practice have recognized that this method can be used effectively for performance evaluation based on a group of indicators by determining properly the weightings of evaluation indicators (Zhou, et al.2015). In this study, we used the Entropy method to assess the development index of eco-environment and urbanization, and the coordination between the eco-environment index and the urbanization index of China provinces.

After data mining through the principal component analysis, we applied the Entropy method to recognize and evaluate the process of China's eco-environment and urbanization. The Entropy method was first introduced into the information management discipline by Shannon in 1948 for the entropy can express the amount of information base on the dispersion of the data. This method has been widely used various disciplines such as energy utilization, LULC analysis, and economic development. Previous studies have shown great effectiveness of the application of this method.

For the dimensions and magnitudes differences exist among the indices, in addition, the effect of the indices is positive or negative are required to be determined, we first standardized the data of the indices using formulas (3-1) and (3-2), formulas (3-1) is used to standardize the positive indicators and formulas (3-2) is used to standardize the negative indicators.

$$X'_{ij} = \frac{X_{ij} - \min\{X_j\}}{\max\{X_j\} - \min\{X_j\}} \qquad (3-1)$$

$$X'_{ij} = \frac{\max\{X_j\} - X_{ij}}{\max\{X_j\} - \min\{X_j\}} \qquad (3-2)$$

$$Y_{ij} = \frac{X'_{ij}}{\sum_{i=1}^{n} X'_{ij}} \quad (3-3)$$

$$k = -\frac{1}{\ln(n)} \quad (3-4)$$

$$e_j = -k \times \sum_{i=1}^{n} \left(Y_{ij} \times \ln\left(Y_{ij}\right)\right) \quad (3-5)$$

$$d_j = 1 - e_j \quad (3-6)$$

$$W_j = \frac{d_j}{\sum_{j=1}^{n} d_j} \quad (3-7)$$

$$Y_{ij} = W_j \times X'_{ij} \quad (3-8)$$

$$Y_i = \sum_{j=1}^{m} Y_{ij} \quad (3-9)$$

Where:

i is China's provinces, j is the indicator, X'_{ij} is the standardized value, X_{ij} is the original value, $\min\{X_j\}$ and $\max\{X_j\}$ represent the minimum and maximum value of the indicator j in all of the provinces studied, Y_{ij} is the proportion of indicator j in provinces i, n is the total number of selected provinces, e_j is the information entropy of the indicator j, d_j is the redundancy of information entropy of the indicator j, W_j is the weight of the indicator j, and Y_i is the mark of province i.

3.2.3. Quadrant scatter method

Cartesian plane rectangular coordinate system divided an area into 4 quadrants, centered on the origin, with the X, Y axis as the basis: the first quadrant (X > 0, Y > 0), the second quadrant (X < 0, Y > 0), the third quadrant (X < 0, Y < 0), the fourth quadrant (X > 0, Y < 0). And there are four main the types of relationships between urbanization and eco-environment development level: senior coordination, low-level coordination, excessive urbanization, and lag urbanization. We set the value of X axis represent the marks of eco-environment, and the value of Y axis is the marks of urbanization. Therefore, the types of the relationship between urbanization and eco-environment development match the four quadrants and can be divided into: the first quadrant: senior coordination model, it has high level of eco-environment and the urbanization level; The second quadrant, excessive urbanization, the eco-environment development level is relative low, while the urbanization level is high; The third quadrant: low-level coordination model, it has low level of eco-environment and the urbanization level; The fourth quadrant, lag of urbanization, eco-environment development level is high, while the urbanization level is relative low (Figure 3-4).

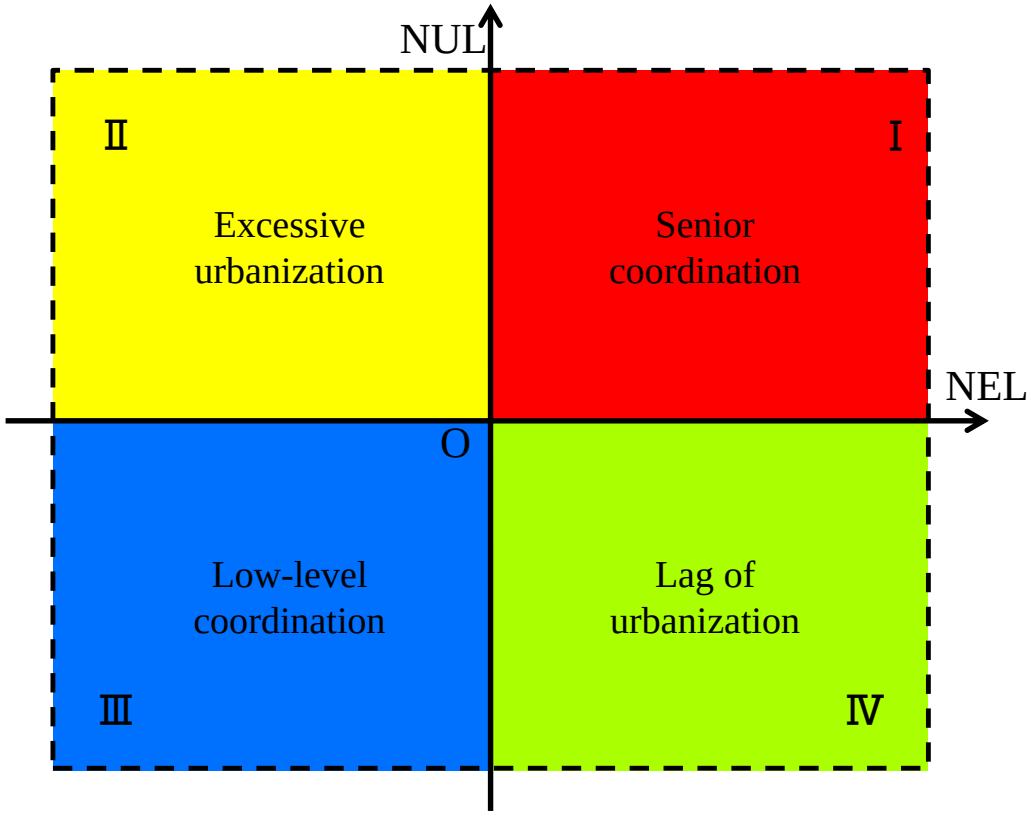

Figure 3-4. The classification of urbanization and eco-environment level

In this study, we applied the quadrant scatter method to classify the eco-environment and urbanization level of China's provinces. And try to get a comprehensive understanding of the situation of China's development.

The revised quadrant scatter method proceeds as follows:

1) Calculating the marks on eco-environment level (EL) and urbanization level (UL) for China's Provinces using the Entropy method;

2) Normalize EL and UL and generate new variables, named NEL and NUL， with the standardization process being conducted using the equation:

$$n = \frac{X_i - \bar{X}}{s} \qquad (3-10)$$

$$X_i = \sum \frac{X}{n} \qquad (3-11)$$

$$s = \sqrt{\sum \frac{(X_i - \bar{X})^2}{n-1}} \qquad (3-12)$$

Where:

i is the observed data;

$\bar{X}$ is the average value of X_i,

s is the standard deviation,

3) Define NEL as the X axis and NUL as the Y axis. Generate a point set for normalized eco-environment level and normalized urbanization level of each provinces (NEL, NUL), and the quadrant scatter would be generated on this point set.

3.2.4. Study area

Take the availability of the data into consideration, 30 provinces in China were selected to carry through the evaluation except Tibet and Taiwan (Figure 3-5). In addition, due to its vast geographic expanse, the development of China has been highly uneven. To give a comprehensive understanding on the regional difference of urbanization and eco-environment development, here, we divided the study area into five zones according to the classification method from the Physical Geography of China:

a) Northeast China: Heilongjiang, Jilin, Liaoning.

b) Eastern China: Beijing, Fujian, Guangdong, Hainan, Hubei, Jiangsu, Shandong, Shanghai, Tianjin, Zhejiang.

c) Central China: Anhui, Henan, Hubei, Hunan, Jiangxi, Shanxi.

d) Northwest China: Gansu, Inner Mongolia, Ningxia, Qinghai, Shaanxi, Xinjiang.

e) Southwest China: Chongqing, Guangxi, Guizhou, Sichuan, Yunnan.

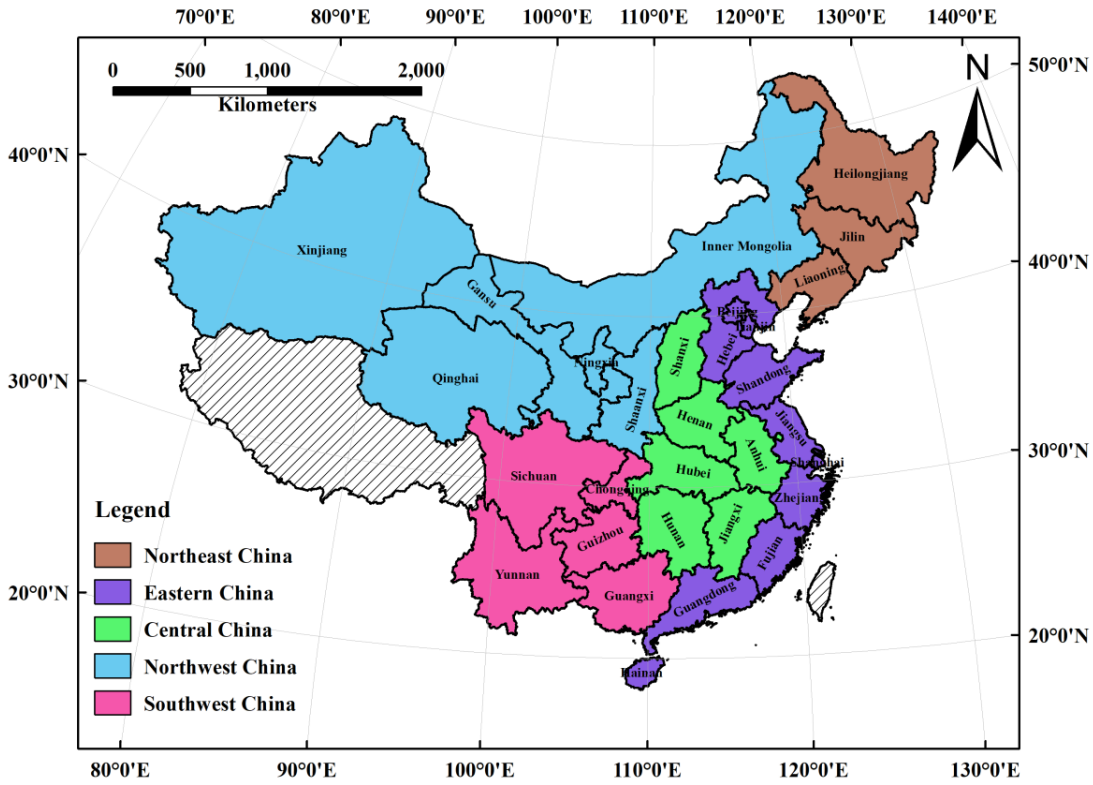

Figure 3-5 Study area and geographic zones

3.3. Results analysis

3.3.1. Results of Index system selection

Table 3-5 shows the indices system of eco-environment assessment and the weight of each index. The indices system was composed of 5 negative indices and 11 positive indices. To the eco-environment assessment, the weights of eco-environment pressure, eco-environment level, and eco-environment control are 6.57%, 64.75%, and 28.67% respectively. The four impact indicators that had the greatest effect wsere per capita green area (0.128), per capita surface water resources (0.109), per capita water resources (0.106) and volume of SO_2 emission per 10,000 Yuan of industrial output (0.103). On the contrary, the weights of the indicators related to eco-environment pressure are relative low for differences among the provinces are not that big compared with other indicators related to eco-environment level and eco-environment control.

3.3.2. Results of eco-environment and urbanization assessment

Table 3-6 shows the indices system of urbanization assessment and the weight of each index. The indices system was composed of 2 negative indices and 20 positive indices. To the urbanization assessment, the weights of economic urbanization, demographic urbanization, spatial urbanization, and social urbanization are 30.33%, 8.85%, 27.38%, and 33.44% respectively. Per capita private car number (0.121) is the only impact indicators that had the greatest effect over 0.1. As a whole, the differences of the weights of the indices are not that big.

As Figure 3-6 shows the provinces ranking eco-environment index in 2005, Qinghai province comes first, for the eco-environment level of Qinghai province is the highest (0.404). The population of Qinghai province is relative small, which result in the per capita value of each indicator is higher than that of other provinces. Therefore, the index of eco-environment control is relative low (0.018). Beijing province comes second and Tianjin province comes third. The eco-environment index of Beijing and Tianjin are 0.382 and 0.361 respectively. These two provinces get high eco-environment control index for the two cities pay very attention to pollutant treatment such as garbage treatment, road cleaning etc. The last three provinces are Hebei, Anhui, and Henan, which located in the central of China. The spatial distribution map of eco-environment index was shown in Figure 3-7.

Table 3-5 Indices system for eco-environment assessment

Level 1	Level 2	Weight	Level 3		Effect	Weight
Eco-environment	Eco-environment pressure	6.57%	X1	Per capita water use (m3)	negative	0.74%
			X2	Per capita waste water discharge (m3)	negative	1.22%
			X3	Per capita emission of SO2 (tons)	negative	1.52%
			X4	Per capita electricity comsupmtion (kWh)	negative	1.96%
			X5	Per capita coal consumption (tons)	negative	1.13%
	Eco-environment level	64.75%	X6	Per capita green area (m2)	positive	8.42%
			X7	Per capita park area (m2)	positive	7.61%
			X8	Per capita forest area (m2)	positive	9.73%
			X9	Per capita artificial green area (m2)	positive	4.76%
			X10	Per capita surface water resources (m2)	positive	10.88%
			X11	Per capita groundwater resources (m2)	positive	12.78%
			X12	Per capita water resources (m2)	positive	10.57%
	Eco-environment control	28.67%	X13	Sewage garbage treatment rate (%)	positive	6.02%
			X14	Road clearing area (m2)	positive	4.58%
			X15	Volume of SO2 emission per 10,000 Yuan of industrial output (kg)	positive	10.28%
			X16	Volume of industrial solid wastes produced per 10,000 Yuan of industrial output (kg)	positive	7.78%

Table 3-6 Indices system for urbanization assessment

Level 1	Level 2	Weight	Level 3		Effect	Weight
Urbanization	Economic urbanization	30.33%	Y1	Per capita Total Social Retail Sales (Yuan)	positive	4.28%
			Y2	Percentage of GDP of the added value of secondary and tertiary	positive	1.20%
			Y3	Per capita wholesale retail value added (Yuan)	positive	6.95%
			Y4	Per capita transportation/warehousing and postal services added value	positive	2.30%
			Y5	Per capita GDP (Yuan)	positive	4.35%
			Y6	The average financial income	positive	7.78%
			Y7	Per capita fixed assessment (Yuan)	positive	3.46%
	Demographic urbanization	8.85%	Y8	Unemployment rate (%)	negative	2.04%
			Y9	Proportion of urban population (%)	positive	3.68%
			Y10	Growth rate of population (%)	positive	2.24%
			Y11	Illiterate Rate (%)	negative	0.90%
	Spatial urbanization	27.38%	Y12	The number of public toilets per person	positive	3.88%
			Y13	Per capita water supply pipeline length (m)	positive	6.84%
			Y14	Per capita natural gas pipeline length (m)	positive	4.16%
			Y15	Per capita build-up area (m2)	positive	4.02%
			Y16	Per capita road area (m2)	positive	2.71%
			Y17	Per capita drainage length (m)	positive	5.78%
	Social urbanization	33.44%	Y18	Per capita hosipital beds	positive	2.37%
			Y19	Per capita private car	positive	4.65%
			Y20	per capita volume of express delivery	positive	12.04%
			Y21	per capita volume of posts and telecommunications	positive	7.86%
			Y22	Per capita public bus number	positive	7.52%

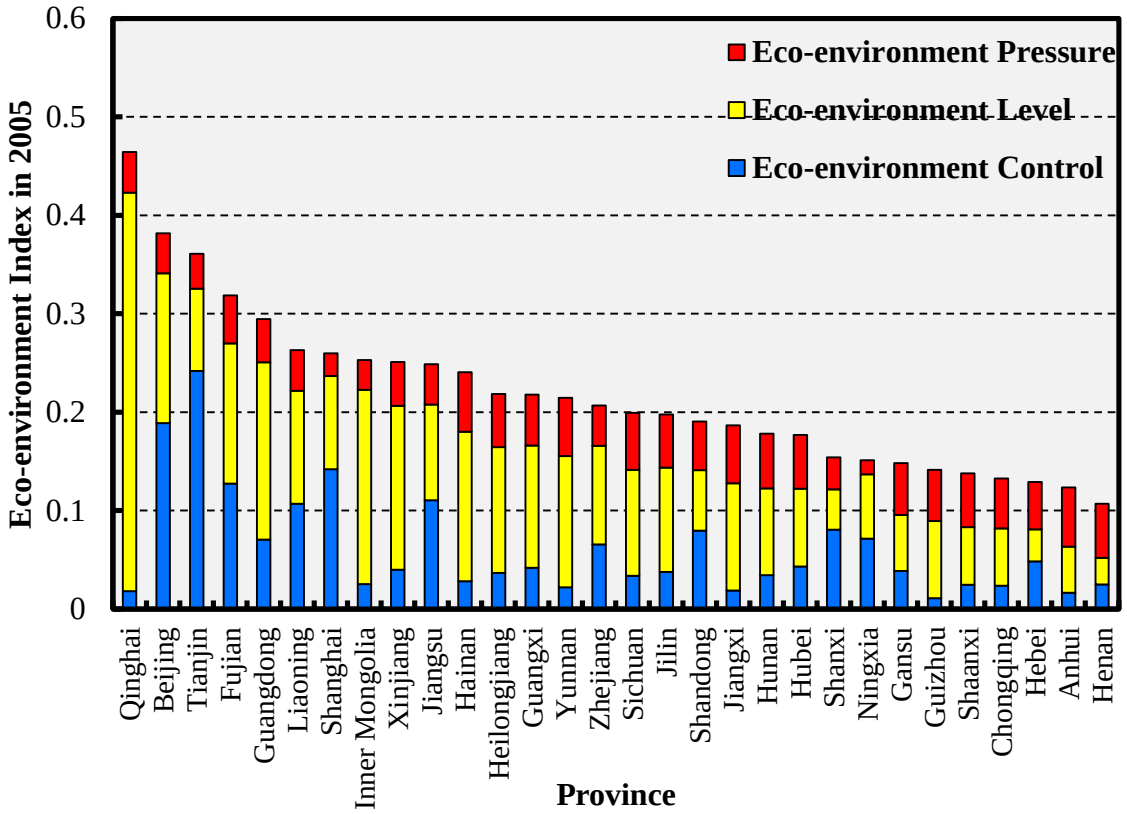

Figure 3-6 Ranking of the eco-environment index in 2005

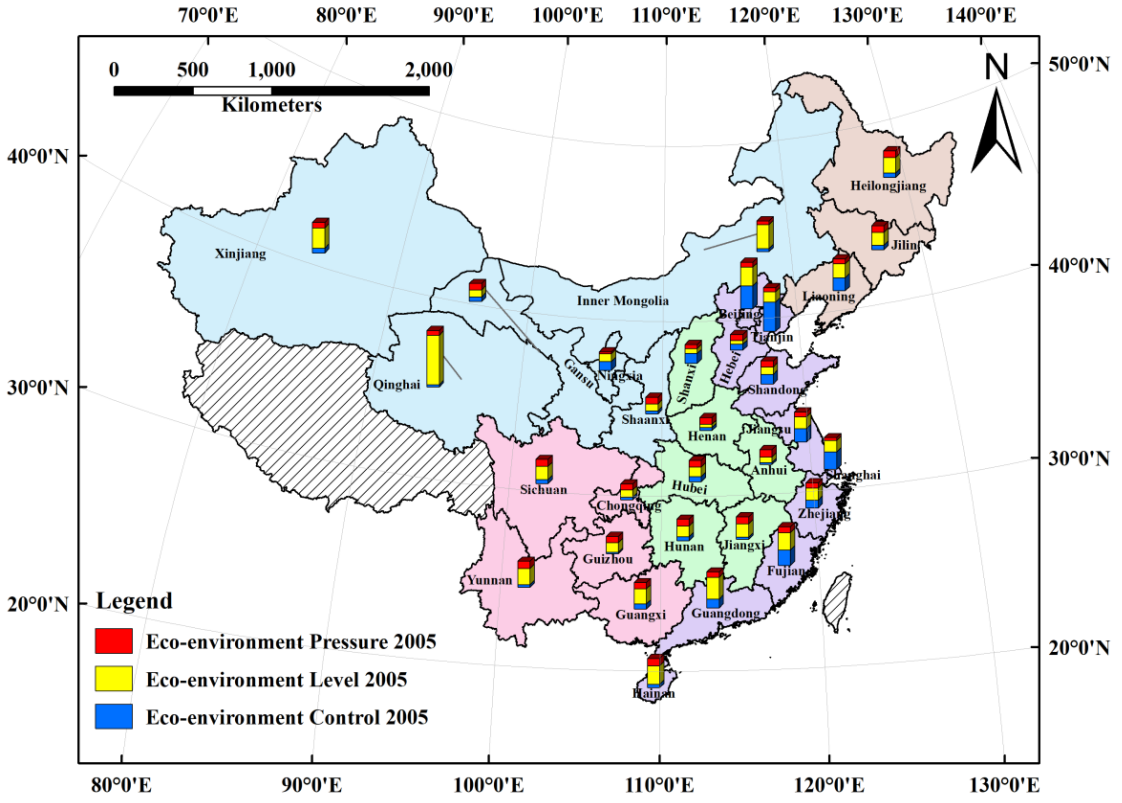

Figure 3-7 Distribution map of eco-environment index in 2005

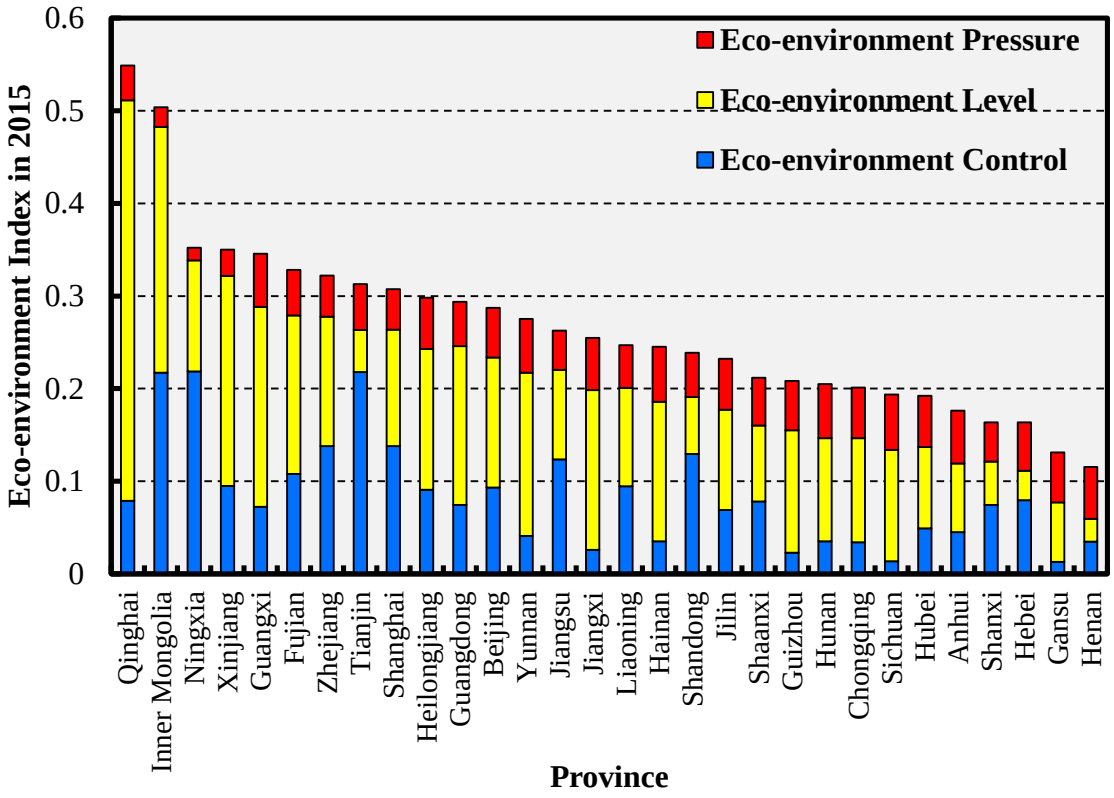

Figure 3-8 Ranking of the eco-environment index in 2015

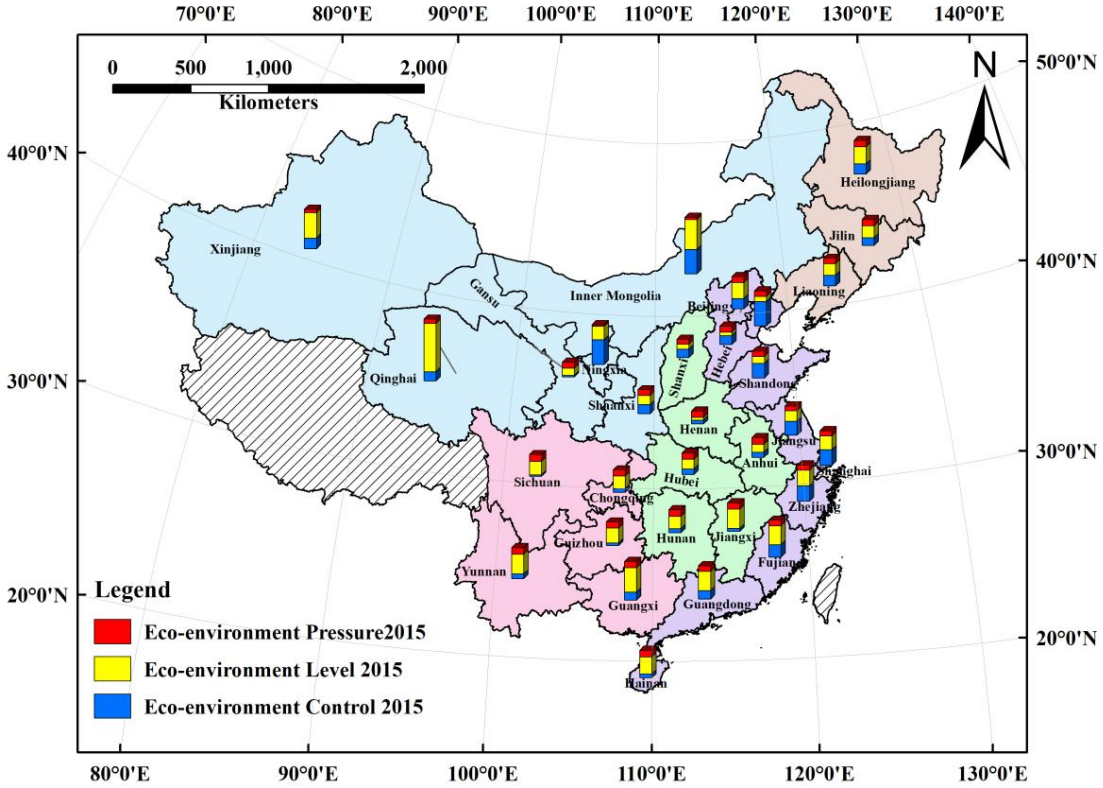

Figure 3-9 Distribution map of eco-environment index in 2015

Figure 3-8 shows the ranking of eco-environment index in 2015, Qinghai province remained the first place, in addition, the eco-environment index increased to 0.55 from 0.46 in 2005. The second place and third place of the eco-environment ranking changed into Inner Mongolia and Nignxia province, respectively. The mainly reason of the increasing of ranking is account of an increasing of eco-environment control in this two provinces. In addition, the last three provinces are Hebei, Gansu, and Henan. Two of the provinces are located in central China and one in Northwest China. Figure 3-9 shows the distribution of the eco-environment from which provided a combination visual result for the evaluation.

On the other hand, Figure 3-10 shows the ranking of urbanization index in 2005. The most urbanized province based on our evaluation system was Beijing. All of the sub-urbanization indexes in Beijing is relative high within China, especially the spatial urbanization and social urbanization, ranking the first place in their field, respectively. Shanghai, Tianjin and Guangzhou ranked the 2nd, 3rd and 4th after Beijing, which is no difference with our common sense. Guizhou province located in last place of the ranking based on the assessment, which can be interpreted as the lag of urbanization in each field. Figure 3-11 shows the distribution map of urbanization index in 2005.

Figure 3-12 shows the information of province ranking on urbanization assessment in 2015. The 1st and 2nd place of the ranking remained unchanged: Beijing and Shanghai. Highest value of urbanization index was 0.84 in Beijing. The ranking of Zhejiang province increased from 5th in 2005 to 3rd place. In depth investigating, all of the four sub-urbanization indexes had a growth after 10 years' development. The urbanization index of Guangzhou province raised from 0.33 in 2005 to 0.46 in 2015, however, the ranking of the urbanization decreased but rising. The lowest urbanization level in 2015 was remained Guizhou province, which holds a value of 0.08. Figure 3-13 showed the distribution map of urbanization level in 2015.

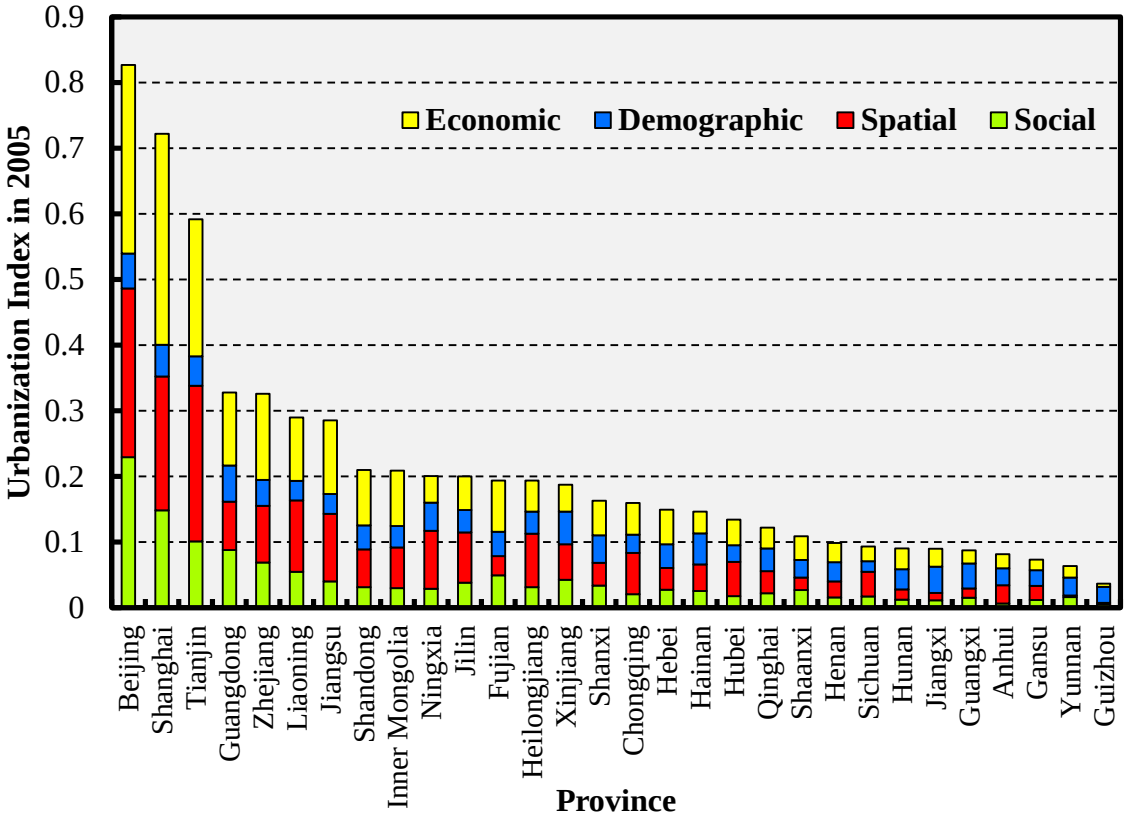

Figure 3-10 Ranking of the urbanization index in 2005

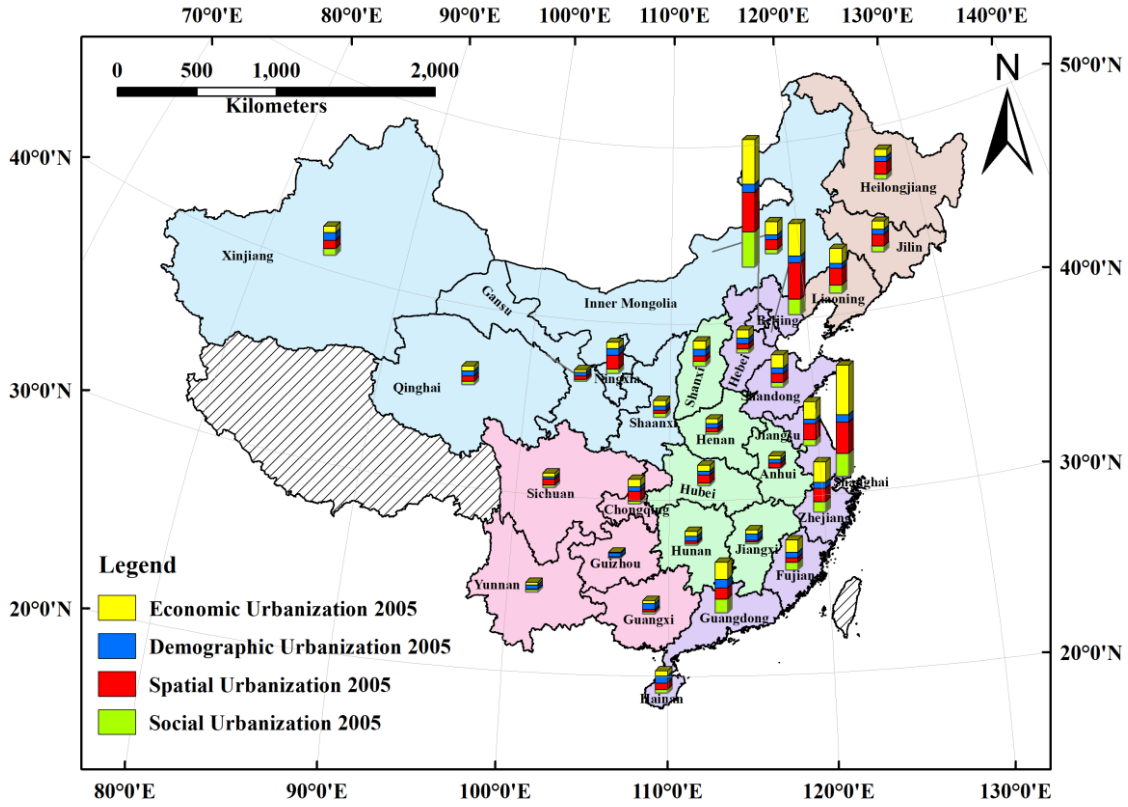

Figure 3-11 Distribution map of urbanization index in 2005

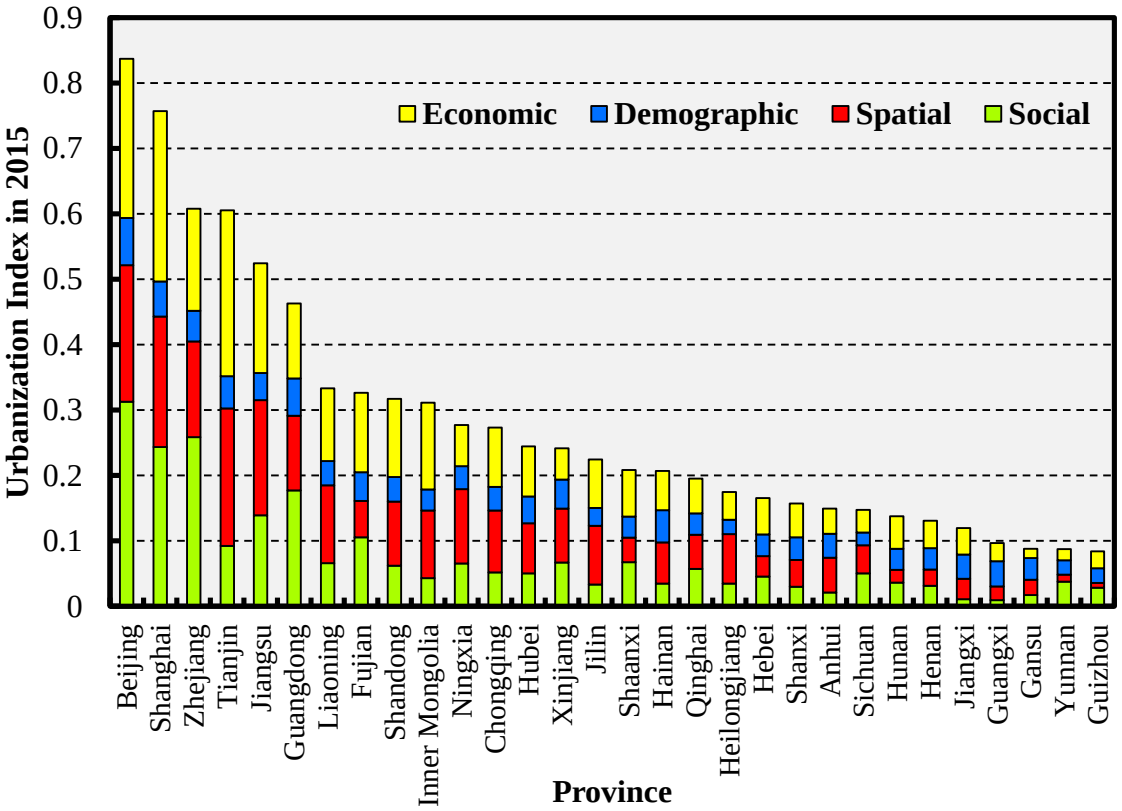

Figure 3-12 Ranking of the urbanization index in 2015

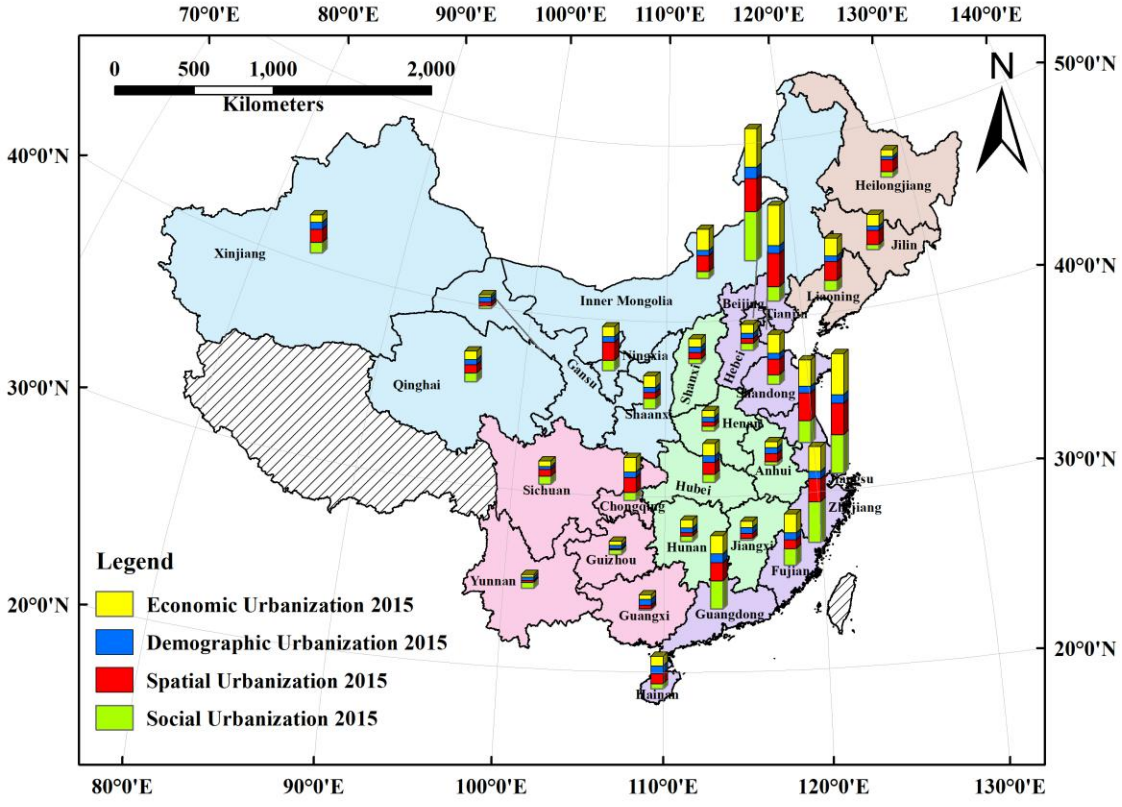

Figure 3-13 Distribution map of urbanization index in 2015

3.3.3. Results of comparison analysis

3.3.3.1. Comparison analysis between 2005 and 2015

Comparison analysis of the eco-environment index and urbanization index between 2005 and 2015 was then carried out to explore the development in each province.

Figure 3-14 shows the result of comparison analysis of the eco-environment. Among the 30 provinces, there are 6 provinces have a decrease in eco-environment value: Beijing, Tianjin, Gansu, Liaoning, Sichuan and Guangzhou province. The value of eco-environment in Beijing decreased from 0.38 in 2005 to 0.29 in 2010. Most of the provinces have an increase in the eco-environment index. The fastest growing province was Inner Mongolia which increased from 0.25 in 2005 to 0.50 in 2015, which was due to a sharp increasing of the eco-environment control index from 0.03 in 2005 to 0.21 in 2015. Furthermore, the increasing in Ningxia province also should not be ignored. The eco-environment index increased from 0.15 in 2005 to 0.35 in 2015, by 2.3 times after ten years' development.

Figure 3-15 shows the comparison result of the urbanization index. From the distribution map, it could be easily got that the uneven development exists in China in both 2005 and 2015. By visual judgment, eastern China has relative higher value of urbanization index in both years than the other regions. Among the 30 provinces, Zhejiang, Jiangsu, Guangdong holds the highest value of urbanization index increasing during the 10 year. Urbanization index of Zhejiang province increased from 0.33 in 2005 to 0.61 in 2015, the fastest increased aspect of urbanization was social urbanization which increased from 0.07 to 0.26, which indicated a fast development of the social urbanization. On the other hand, Heilongjiang province had a not too clear decrease of urbanization index from 0.19 in 2005 to 0.17 in 2015.

3.3.3.2 Regional comparison analysis

Average value of eco-environment index and urbanization index in different regions was calculated to explore the geographical distribution differences in China.

Figure 3-16 shows the eco-environment index of the five regions. Result showed that all of the five regions had an increase on the eco-environment index. The fastest growth on eco-environment index was the Northwest China, which increased from 0.24 in 2005 to 0.35 in 2015. Central China has the lowest value of eco-environment index in both years. Difference between the regions in 2015 became much more obvious than that in 2005.

Figure 3-17 shows the regional comparison results of urbanization index. In both years, Eastern China holds the highest level of urbanization, meanwhile, the urbanization index in Eastern China increased from 0.38 to 0.48 from 2005 to 2015. The lowest urbanization region in both 2005 and 2015 was Southwest China even though the urbanization index increased from 0.08 to 0.14. The results provided strong evidence that the urbanization level in China is unbalanced, Northwest, Southwest and Central China should pay attention to the urbanization development to catch up with the urbanization level in Eastern China.

Figure 3-18 shows the regional comparison of eco-environment aspects in 2005, The eco-environment pressure in all regions showed slight discrepancy where Eastern and Northwest China is less than the other 3 regions. The eco-environment level index varies in the 5 regions. Central China holds the lowest eco-environment level in 2005, while the Northwest China has the highest value of eco-environment level index. The reason was due to that the permanent resident population in the Central China is much larger than that of Northwest that lead to a low eco-environment level which is determined by several per capita indexes. The eco-environment control also showed im-balanced distribution. The eco-environment control level in Eastern China is much higher than the other four regions. Figure 3-19 shows the situation in 2015 of eco-environment which regularities of distribution of eco-environment pressure and level indexes are similar with that of 2005. However, there is an obvious increasing of eco-environment level in both Northwest China and Northeast China, the Central and Southwest are little fall behind of eco-environment control.

Figure 3-20 shows the regional comparison of urbanization aspects in 2005. Economic urbanization index in Eastern China is much higher than the other four regions. In the same time, the Eastern China also takes the lead to the situation of spatial urbanization and social urbanization. The demographic urbanization in all regions showed slight discrepancy, the difference between the five regions was relative low. Figure 3-21 shows the regional comparison of eco-environment aspects in 2015. Same with the situation in 2005, Eastern China take the first place of all aspect of urbanization indexes. Compared with the indexes in 2005, the social urbanization in Eastern China has a great increase from 0.08 to 0.15. In addition, Northwest China and Southwest China also have a considerable increase in social urbanization development.

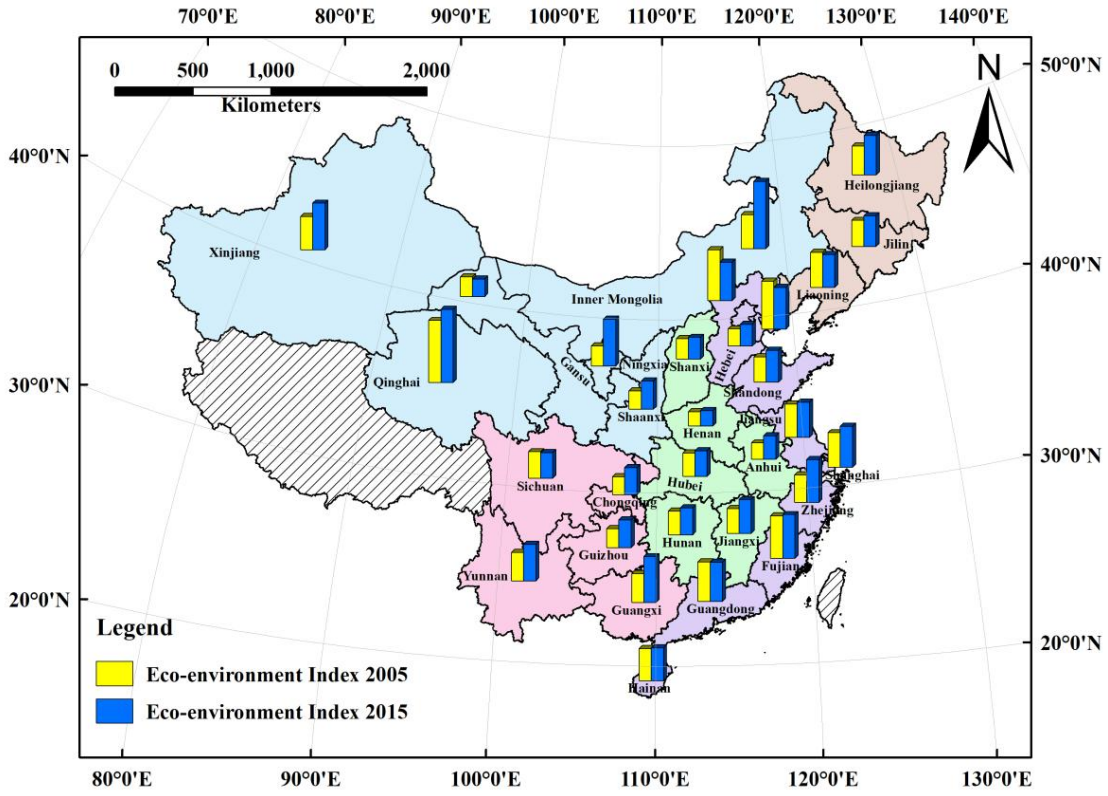

Figure 3-14 Result of comparison analysis of the eco-environment index

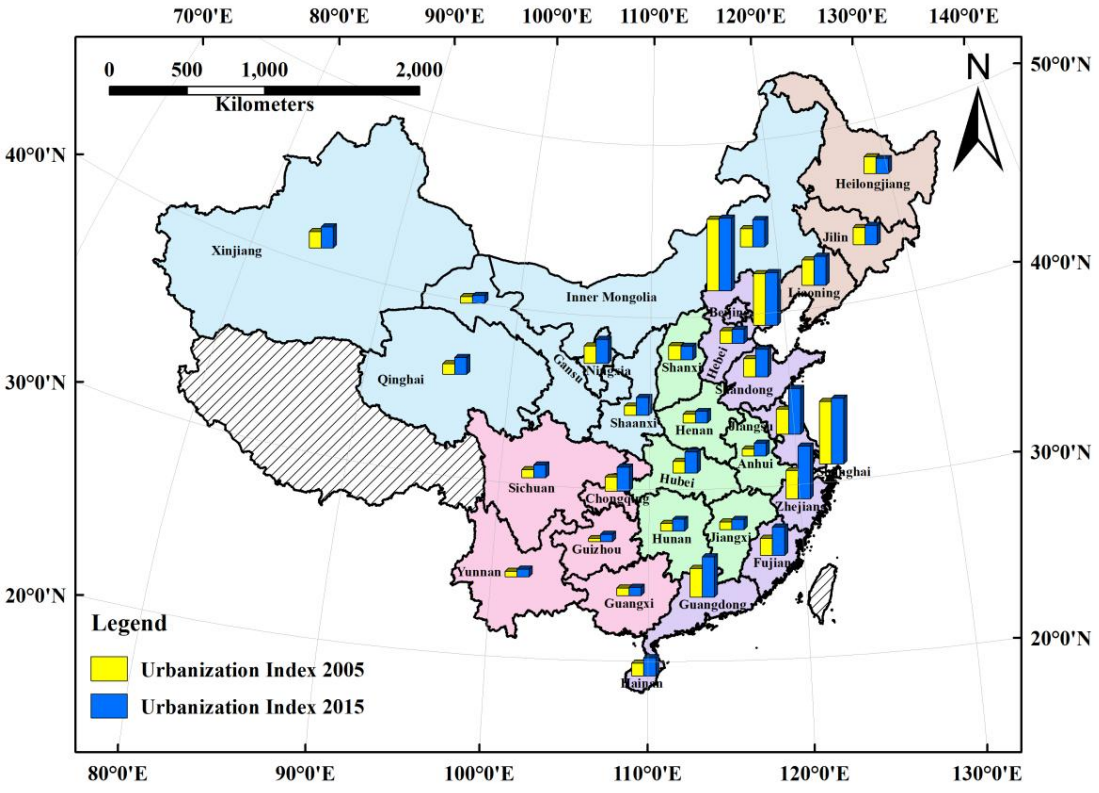

Figure 3-15 Result of comparison analysis of the urbanization index

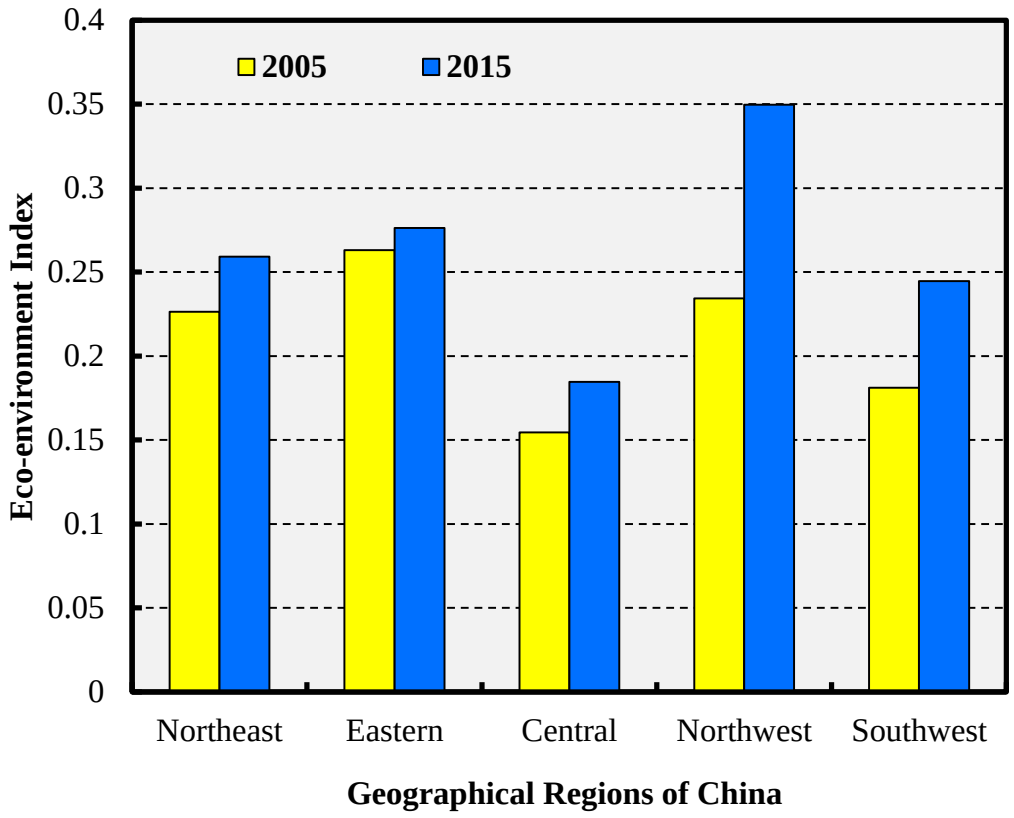

Figure 3-16 Regional comparison of eco-environment index in different year

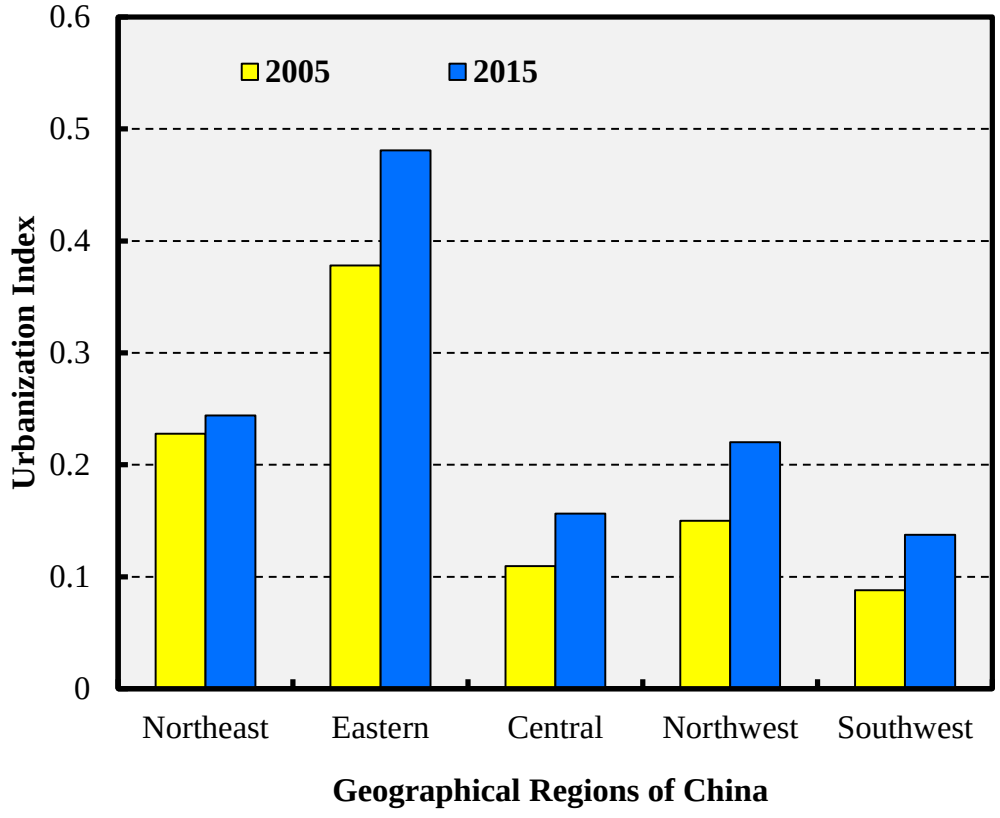

Figure 3-17 Regional comparison of urbanization index in different year

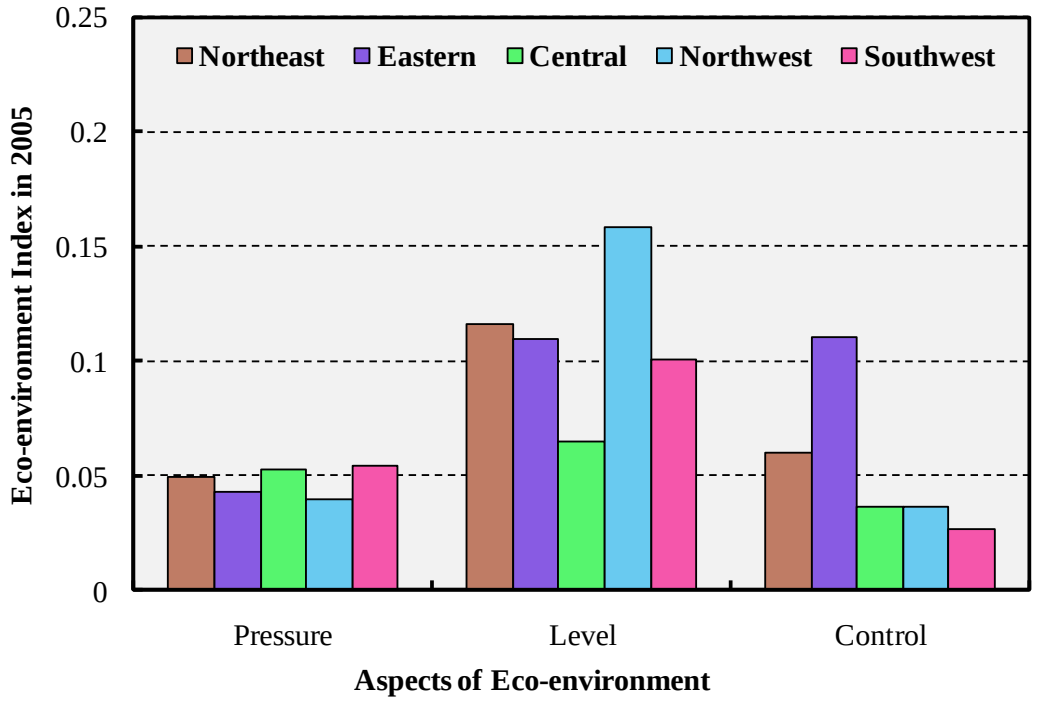

Figure 3-18 Regional comparison of eco-environment aspects in 2005

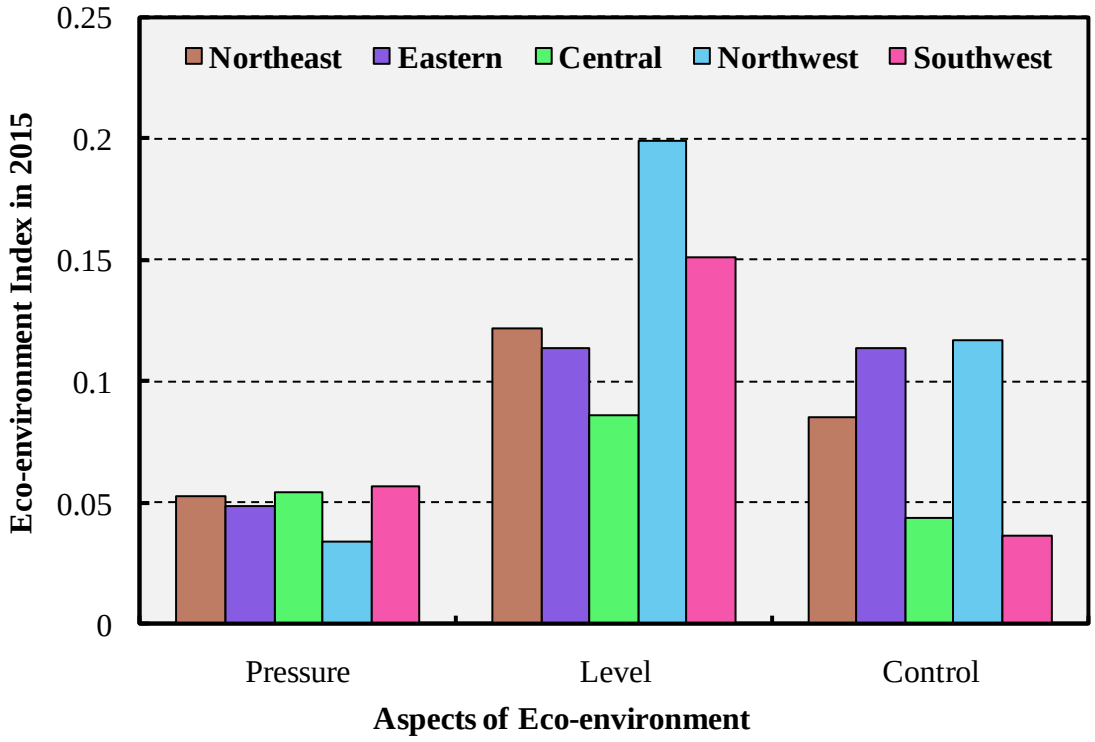

Figure 3-19 Regional comparison of eco-environment aspects in 2015

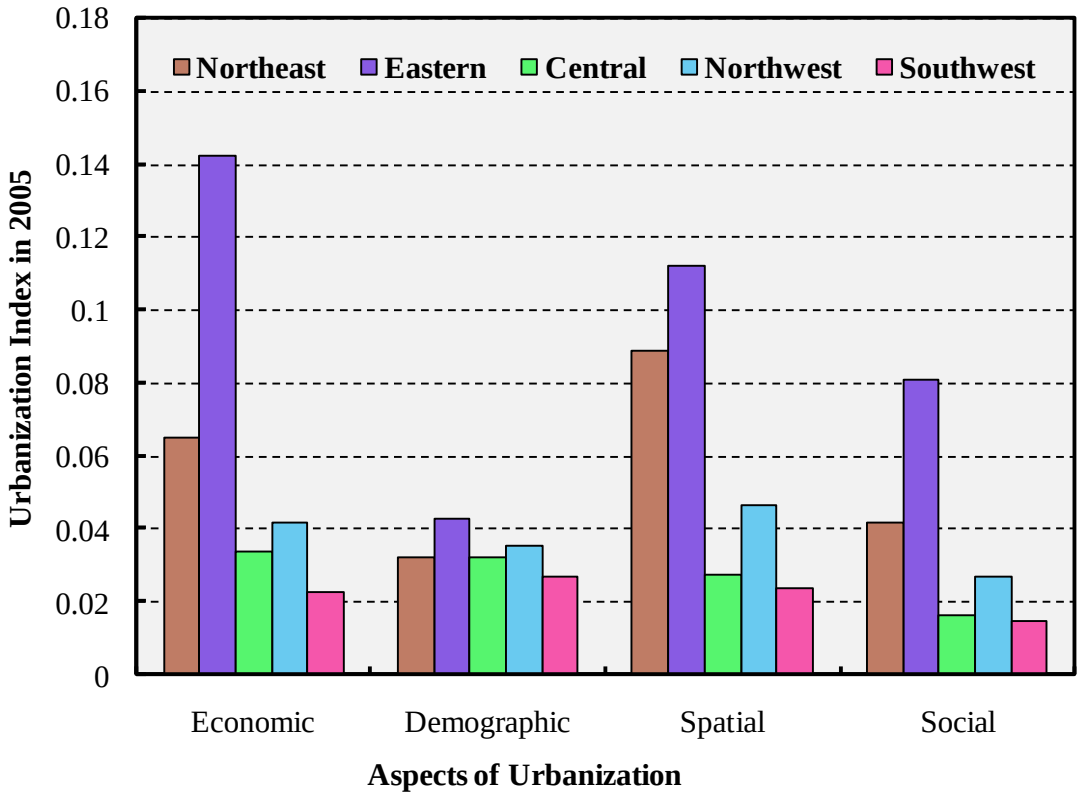

Figure 3-20 Regional comparison of eco-environment aspects in 2005

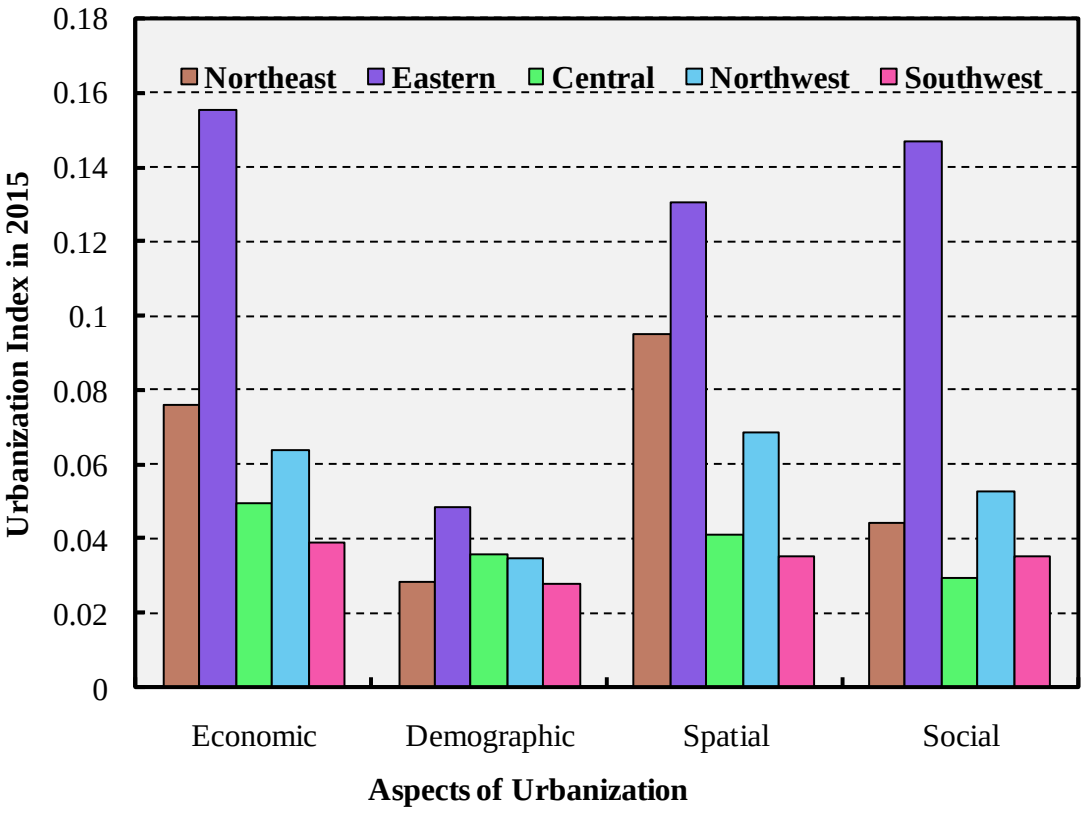

Figure 3-21 Regional comparison of eco-environment aspects in 2015

3.3.4. Results of comprehensive assessment

Comprehensive evaluation on eco-environment and urbanization index was then carried out to estimate the balance degree and health degree of the city development.

Figure 3-22 shows the results of quadrant scatter in 2005 and Figure 3-23 shows the distribution map of the comprehensive evaluation. In 2005, there were 6 provinces located in senior coordination zone: Beijing, Jiangsu, Liaoning, Shanghai, Tianjin and Guangdong province. Only one province located in excessive urbanization zone: Zhejiang province, showed an over urbanization and lack of eco-environment development.17 provinces located in low level coordination zone and 6 provinces located in lag of urbanization zone. Lag of urbanization provinces mainly located in north China (1 in Northeast and 3 in Northwest), the result give evidence that urbanization was unbalanced and actions are required to get better coordination of development. A large proportion of provinces in China were in low level coordination zones. Although it doesn't mean bad coordination, however, both of the urbanization level and eco-environment level have promotion space in the future.

Figure 3-24 shows the results of quadrant scatter in 2015 and the distribution map of comprehensive evaluation was shown in Figure 3-25. Number of province located in senior coordination zone increased to 7 according to the results. Beijing, Shanghai, Guangzhou and Tianjin remain in senior coordination zone while the Liaoning and Jiangsu province were located in excessive urbanization zone, which indicated that the urbanization level increase faster than that of eco-environment, thus these two provinces should pay more attention on its eco-environment to get a better coordination development. On another hand, coordination development in Zhejiang, Inner Mongolia and Fujian province became much better and located in senior coordination zone in 2015. In addition, Heilongjiang, Xinjiang and Qinghai remained lag of urbanization in 2015, Ningxia, Guangxi and Yunnan also located in lag of urbanization zone in 2015. The results also indicated that provinces in Eastern China pay more attention on their eco-environment development with a relative high level of urbanization. In 2015, Shandong, Liaoning and Jiangsu province located in excessive urbanization zone, in which Liaoning and Jiangsu was senior coordination in 2005 and Shandong was low level of coordination in 2005. The result showed that these three provinces focus more on the urbanization development rather than the eco-environment development.

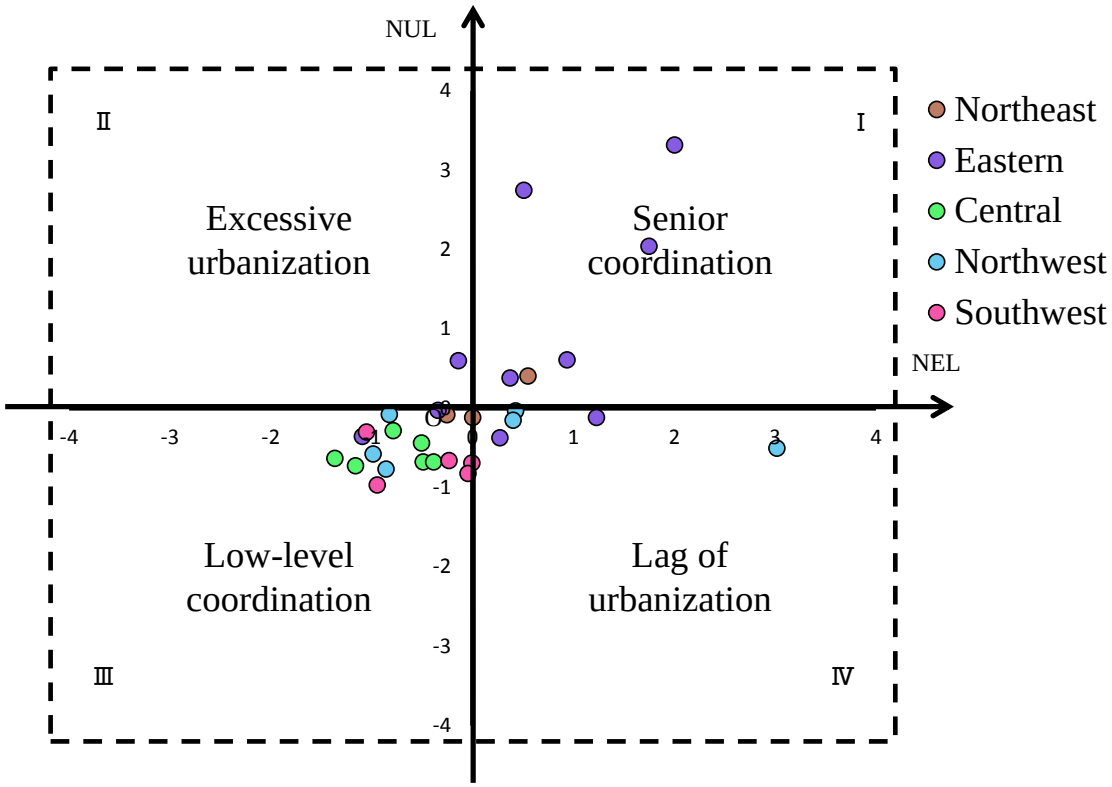

Figure 3-22 Results of quadrant scatter in 2005

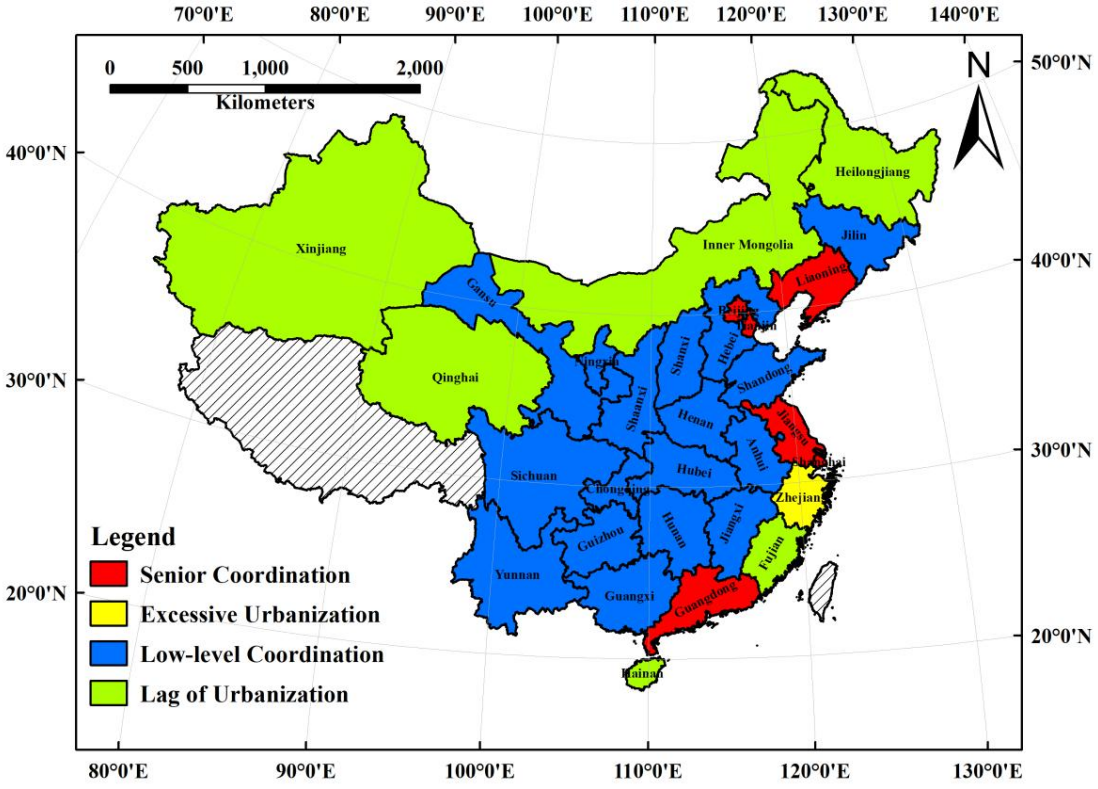

Figure 3-23 Distribution of comprehensive assessment in 2005

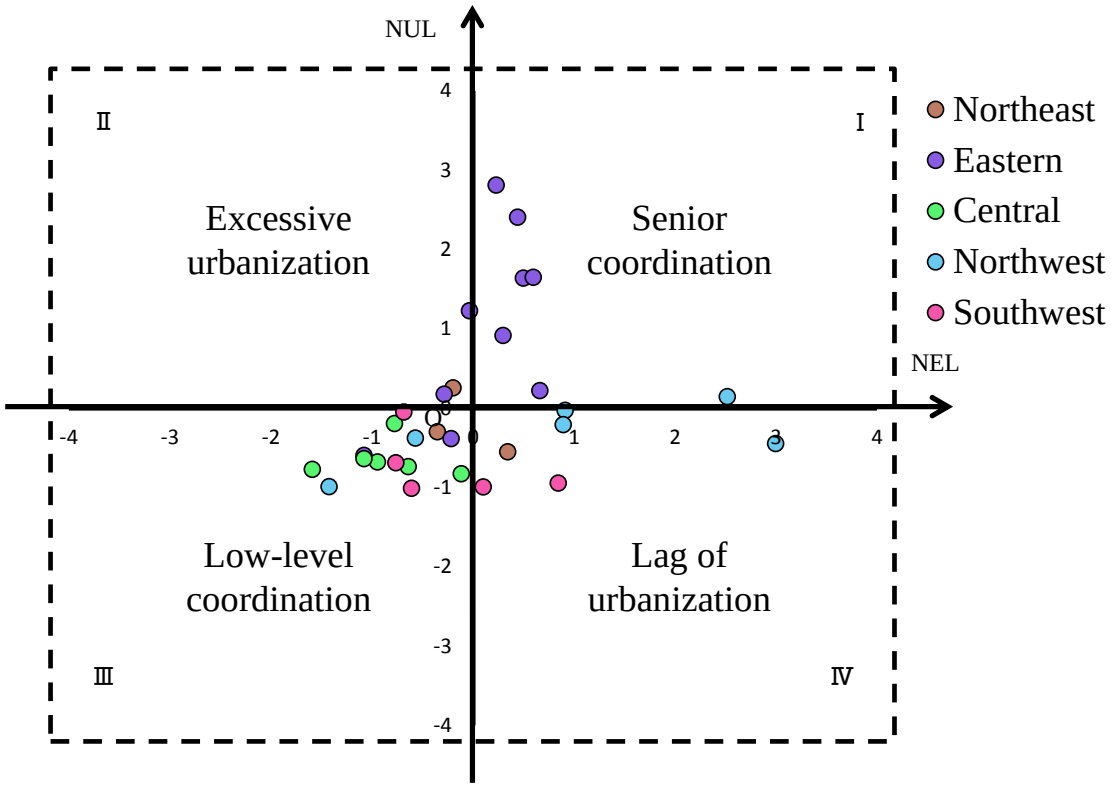

Figure 3-24 Results of quadrant scatter in 2015

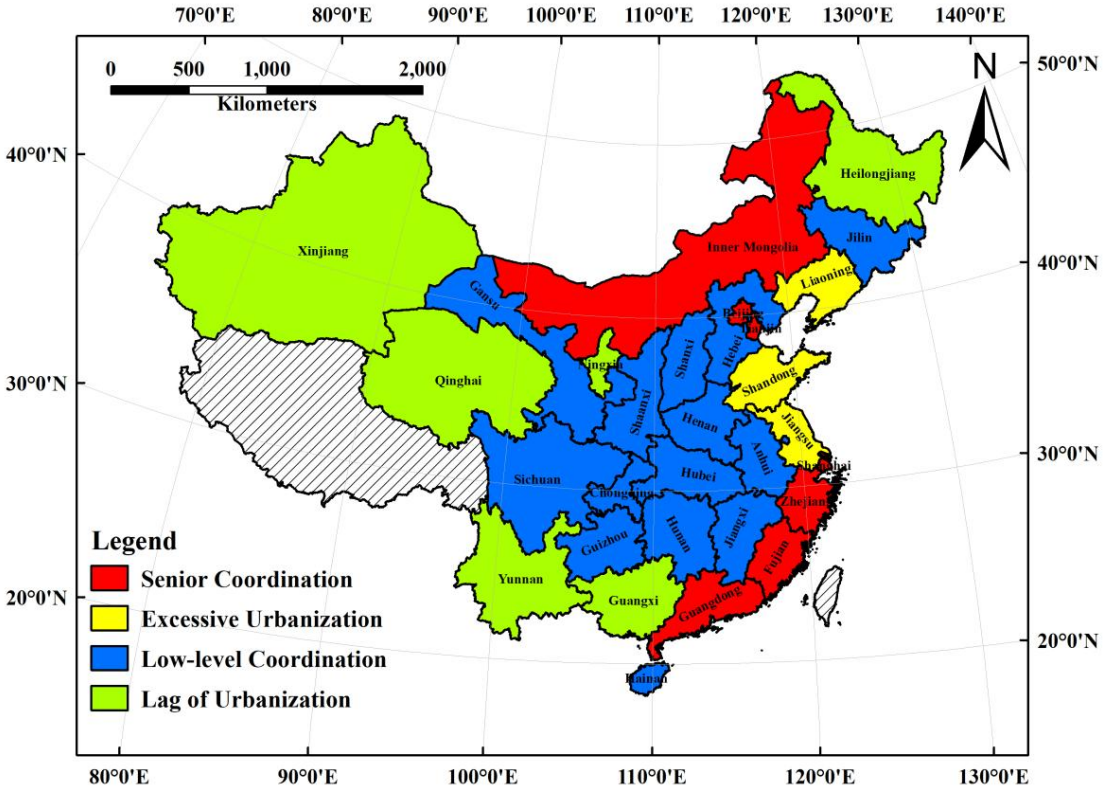

Figure 3-25 Distribution of comprehensive assessment in 2015

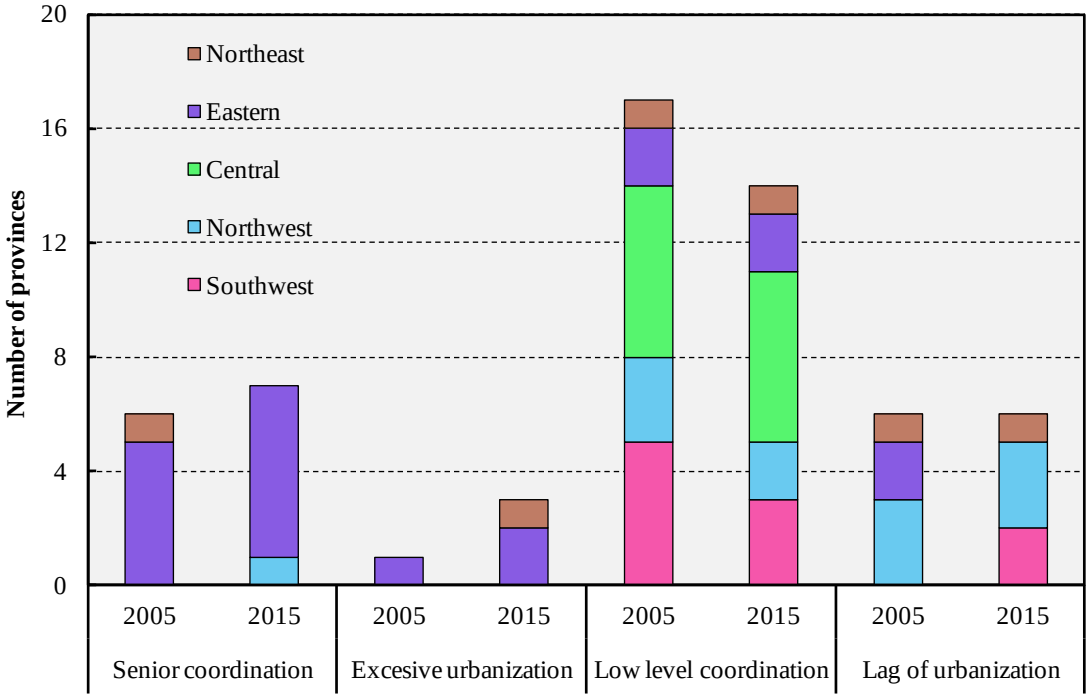

Figure 3-26 Regional comparison of comprehensive assessment

Figure 3-26 shows the regional comparison of comprehensive assessment which shows the comparative result of the coordination over two years. According to the results, it turned out that number of provinces in senior coordination increased from six to seven provinces, in both 2005 and 2015, Eastern China account for a vast majority of senior coordination. Excessive urbanization region increased from 1 province into 3 provinces. All of the provinces in Northwest, Southwest and Central China located in the low level coordination and lag of urbanization in both 2005 and 2015.

3.4. Summary

As the urbanization processing draws more and more attention, it is meaningful and useful to have an investigation of the urbanization processing in China in recent decades. In addition, environmental issues arose along with the urbanization, it is essential to do more in-depth study to explore the relationship between the urbanization and eco-environment to provide guidance for sustainable development. Integrated assessment of urbanization and eco-environment was conducted in this chapter and main results can be summarized as follows:

a) Based on the principal component analysis and maximum entropy method, the indicator system of eco-environment and urbanization was generated. Eco-environment indicator system was composed of 5 negative indices and 11 positive indices. The weights of eco-environment pressure, eco-environment level, and eco-environment control are 6.57%, 64.75%, and 28.67% respectively. Urbanization indices system was composed of 2 negative indices and 20 positive indices. Economic urbanization, demographic urbanization, spatial urbanization, and social urbanization account for 30.33%, 8.85%, 27.38%, and 33.44% respectively.

b) In both 2005 and 2015, the most urbanized province in China was Beijing. The highest value of eco-environment index was Qinghai which holds a highest value of eco-environment level indexes in both years.

c) Among the 30 provinces, there are 6 provinces have a decrease in eco-environment value: Beijing, Tianjin, Gansu, Liaoning, Sichuan and Guangzhou province. The fastest growing province was Inner Mongolia which increased from 0.25 in 2005 to 0.50 in 2015rbanization index of Zhejiang province increased from 0.33 in 2005 to 0.61 in 2015, the fastest increased aspect of urbanization was social urbanizations.

d) The results provided strong evidence that the urbanization level in China is unbalanced, Northwest, Southwest and Central China should pay attention to the urbanization development to catch up with the urbanization level in Eastern China.

e) Results of quadrant scatter in 2005 showed that there were 6 provinces located in senior coordination zone, 17 provinces located in low level coordination zone and 6 provinces located in lag of urbanization zone. In 2015, Number of province located in senior

coordination zone increased to 7 according to the results. The results also indicated that provinces in Eastern China pay more attention on their eco-environment development with a relative high level of urbanization. All of the provinces in Northwest, Southwest and Central China located in the low level coordination and lag of urbanization in both 2005 and 2015.

Reference

[1] Liyin Shen, Jingyang Zhou, Martin Skitmore, Bo Xia, Application of a hybrid Entropy–McKinsey Matrix method in evaluating sustainable urbanization: A China case study, Cities, 42 (2015) 186-194.

[2] Adnan Kasman, Yavuz Selman Duman, CO2 emissions, economic growth, energy consumption, trade and urbanization in new EU member and candidate countries: A panel data analysis, Economic Modelling, 44 (2015) 97-103.

[3] Hengzhou Xu, Wenjing Zhang, The causal relationship between carbon emissions and land urbanization quality: A panel data analysis for Chinese provinces, Journal of Cleaner Production, 137 (2016) 241-248.

[4] De Zhou, Jianchun Xu, Li Wang, Zhulu Lin, Assessing urbanization quality using structure and function analyses: A case study of the urban agglomeration around Hangzhou Bay (UAHB), China, Habitat International, 49 (2015) 165-176.

Chapter Four: Measurement and Assessment of Urban Sprawl in Major Cities in China

4.1. Introduction

Urbanization and economic growth cause remarkable changes of landscape patterns which are indentified by the mosaics of built- up land, cropland, forests, and so forth (Deng, et al.2017). Many metrics and statistics have been used to quantify the sprawl. Spatial or landscape metrics, in general, can be defined as quantitative indices to describe structures and patterns of a landscape (O'Neill, et al.1988). To get the spatial pattern and development of the built-up area, DMSP/OLS nighttime stable light dataset was applied in this chapter. DMSP/OLS is widely applied in urban research in recent years, one of the hottest topic is the extraction of urban built-up area and monitoring the urban sprawl. By applied the empirical thresholds method in this research, urban built-up areas were extracted from the DMSP/OLS NTL. Beijing, Shanghai and Guangzhou city was selected as the study area to carry out the measurement and assessment of urban sprawl.

As the chart of research flow shows (Figure 4-1), the mainly used dataset in this chapter is the time series nighttime stable light dataset from DMSP/OLS. The preprocessing of the original data then conducted which including: boundary masking, inter-calibration, intra-calibration and inter-annual series correction to improve the continuity and comparability of nighttime light data. Next step was to conduct a Log-liner regression analysis with the social-economic statistics to explore the correlation between the urbanization processing assessment by remote sensing and social statistics. Then an empirical threshold method was applied and thresholds were set into each city to define the separation boundary to extract the urban built-up area from the nighttime light data. Then the acquired data was processing by software of Fragstats to get the changing of the urban sprawl by landscape metrics. In this research, we selected three landscape metrics at class level and five landscape metrics at landscape level.

The log-liner regression showed that there is a closely correlation between the remote sensing derived urbanization with the social-statistics from several aspects such as economic, demographic, energy consumption etc. The correlation analysis results provided strong evidence that the DMSP/OLS stable nighttime light data could be considered as the data source to monitor the urbanization and urban sprawl. From the result of the landscape metrics

analysis on the three cities, a general understanding of the urban sprawl and distribution pattern characteristics could be got from the selected landscape metrics.

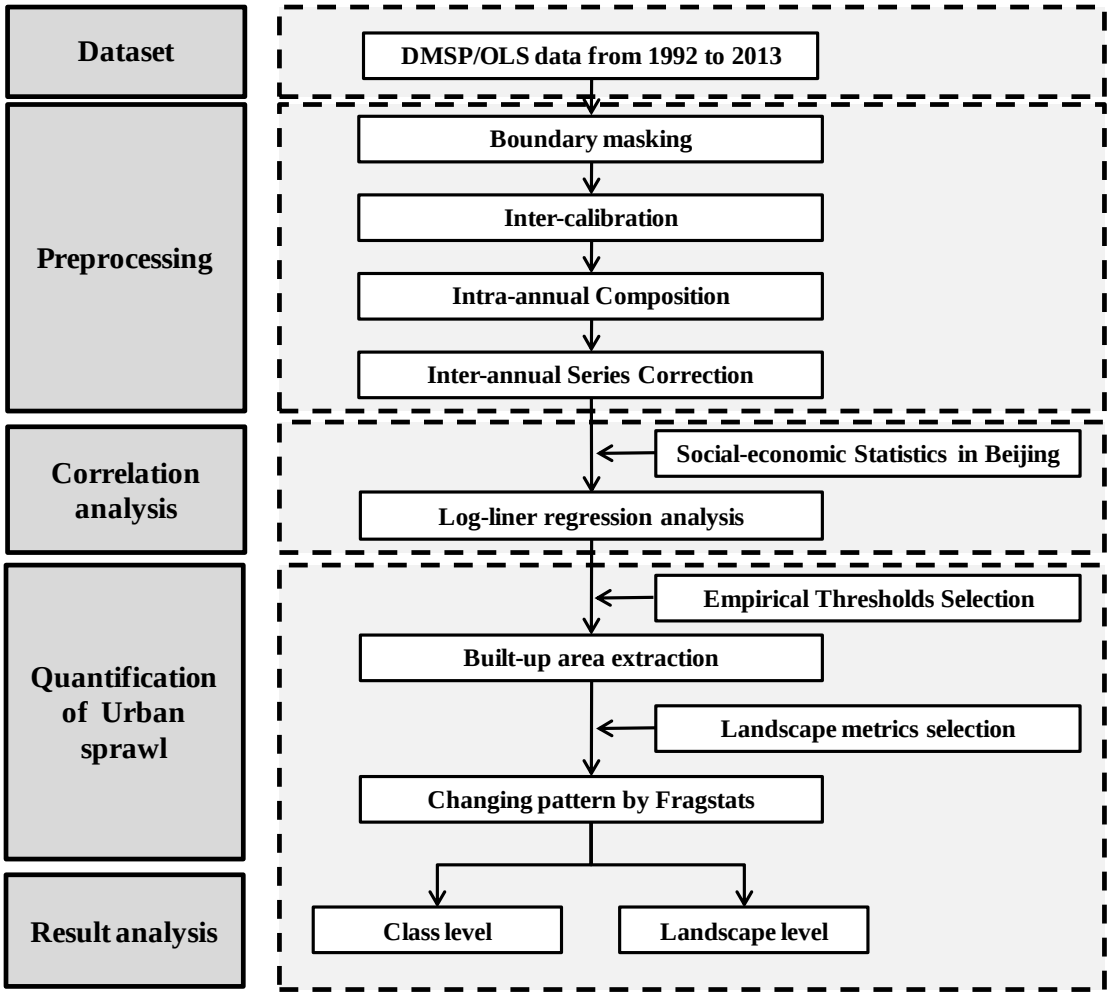

Figure 4-1 Research Flow

4.2. Introduction of DMSP/OLS nighttime images

4.2.1. History of DMSP/OLS

In recent years, satellite observations have been widely used in urban studies across the world, one of which is the Defense Meteorological Satellite Program's Operational Line Scanner System (DMSP/OLS). The DMSP/OLS dataset, which was originally used to monitor the global distribution of clouds and cloud top temperatures in the 1970s, was not widely noticed until 1992. DMSP has been promoted by the Department of Defense of United States, it is a meteorological satellite program which is only being used for military affairs across the world. The program is managed by the Air Force Space Command with onboard operations provided by the National Oceanic and Atmospheric Administration (Fan, et al.2014). The Defense Meteorological Satellite Program provides global visible and infrared cloud data and other specialized meteorological, oceanographic, and solar-geophysical data in support of worldwide Department of Defense, Department of Commerce, and National Aeronautics and Spacing for the military Administration operations.

There are multiple kinds of sensors that mounted on the satellite, among the sensors, OLS (Operational Linescan System), whose initial purpose was to provide users visible and infrared imagery which are used to monitor the global distribution of clouds and cloud top temperature twice eatch day, but actrually, the DMSP/OLS was widely used in urban studies and energy or population research (Liu, et al.2015). The OLS is an oscillating scan radiometer with two broad spectral bands: the Visible Near-Infrared (VNIR, 580~910 nm Full Width at Half Maximum (FWHM)) and Thermal Infrared (TIR, 1030~1290 nm FWHM). The current OLS system has been operated by the USA Air Force DMSP since 1976. Nighttime images are collected using the VNIR band, which is intensified by a photomultiplier tube to detect radiance emission down to the $5E^{-1}$ watts/cm^2/sr range. There are two spatial resolutions of nighttime images: "fine" resolution data have a nominal spatial resolution of 0.56 km, while "smooth" data have a nominal spatial resolution of 2.7 km with 5 × 5 block averaging(Huang, et al.2014).

The archive data set consists of low resolution global and high resolution regional, imagery recorded along a 3000 km scan, satellite ephemeris and solar and lunar information. Infrared pixel value corresponds to a temperature range of 190 to 310 Kelvins in 256 equally spaced

steps. Onboard calibration is performed during each scan. Visible pixels are relative values ranging from 0 to 63 rather than absolute values in Watts per m^2. Instrumental gain levels are adjusted to maintain constant cloud reference value under varying conditions of solar and lunar illumination.

Version 4 of global DMSP/OLS nighttime light series of 1992 to 2013 provide annual global composites of stable nighttime light derived from the visible band. These images are composed of grid-based annual visible band digital number range from 0 to 63 with spatial resolution of 30 arc-second (approximately 1 km at the equator). Table 4-1 shows the time series of DMSP/OLS nighttime lights for the period of 1992 to 2013. The sensor cluster was consisted of six individual sensors: F10 (1992-1994); F12 (1994-1999); F14 (1997-2003); F15 (2000-2007); F16 (2004-2009) and F18 (2010-2012).

Table 4-1 DMSP-OLS sensor cluster collection years

Year	**Series of Satellite**					
	F10	**F12**	**F14**	**F15**	**F16**	**F18**
1992	F101992					
1993	F101993					
1994	F101994	F121994				
1995		F121995				
1996		F121996				
1997		F121997	F141997			
1998		F121998	F141998			
1999		F121999	F141999			
2000			F142000	F152000		
2001			F142001	F152001		
2002			F142002	F152002		
2003			F142003	F152003		
2004				F152004	F162004	
2005				F152005	F162005	
2006				F152006	F162006	
2007				F152007	F162007	
2008					F162008	
2009					F162009	
2010						F182010
2011						F182011
2012						F182012
2013						F182013

(Data source: Department of Defense of United States)

4.2.2. Application of DMSP/OLS in urban studies

Based on the characteristics of the different datasets derived from the DMSP/OLS database, researchers have applied each to a variety of research topics. Table 4-2 shows the detailed information of applications of DMSP/OLS nighttime images for different research topics. The major categories including: settlement dynamics and impacts on the environment; demographic and socioeconomic information; short-term light monitoring; short-term light monitoring and other applications.

The first category of application was the mapping of settlements, including urban areas, built-up areas, impervious surface areas and urban boundaries (Su, et al.2015). There are two subcategories in this topic: Urban land dynamic and impacts of urbanization on soil, net primary productivity, and urban surface temperature. The major challenge of these research topics is the determination of the distinguish method of urban area region from the nighttime light images. Most widely method now is the threshold method, which is originally proposed

Table 4-2 Applications of DMSP/OLS nighttime images for different research topics.

Major Categories	**Research Topics**
Settlement dynamics and impacts on the environment	Urban land dynamics (e.g., urban extent, urban boundary, impervious surface area, built-up area)
	Impacts of urbanization on soil, net primary productivity, urban surface temperature.
Demographic and socioeconomic information	Demographic information (e.g., population, urban population, population density)
	Socieconomic parameters (e.g., GDP, freight traffic, copper stock, poverty index, income index)
	Energy and electrity power consumption
Short-term light monitoring	Short-term lighting (e.g., gas flare, burining area and light flash)
	Fishing vessel monitoring
Other applications	Anthropogenic gas emission
	Nighttime sky brightness and light pollution
	Other applications (e.g., human helth, water footprint, wars and conflicts, earthquake damage, climate station

(Data source: National Geophysical Data Center Earth Observation Group.)

by Imhoff (Imhoff, et al.2010), which compared changes in polygon perimeter along the increase in threshold. To the situation in China, due to its vast territory, the different regional thresholds are required to obtain the urban area in different areas.

The second category of application is on the inferring socioeconomic development from the DMSP/OLS database. Nighttime light images showed closely related with the intensity of human activity. Among this category, there are three subcategories which are: demographic information, socioeconomic parameters and energy and electricity power consumption. The two most common parameters extracted from the DMSP/OLS database were population, GDP and energy consumption, other parameters such as income, copper stock and freight traffic also attracted researchers' attention. DMSP/OLS nighttime images can be used as an ancillary proxy to assess the degree of development at different scales. For example, a global poverty map was produced by combining DMSP/OLS data with the world population distribution from LandScan 2004. A provincial level poverty assessment was also carried out by comparing the integrated poverty index from statistical censuses with the average light index from DMSP/OLS data in China (Zhang and Seto.2011).

The third category of the application is the using in the field of short-term light monitoring. Studies on short-term light phenomena may focus on spatial and temporal dynamics of some unstable light, and even instantaneous lighting phenomena. Recent studies have included monitoring forest fires and their impacts on aerosol properties and burned areas, monitoring gas flares, detecting fishing vessels and identifying lighting flashes.

Final category of applications contained miscellaneous interdisciplinary research. For example, By comparing the nighttime light loss after a major disaster such as earthquake, scholars developed a system that provides timely information on the spatial distribution of the impacted urban area. Several other studies combined CO2 emission from point sources like power plants with nighttime lights data, which was in agreement with existing inventory dataset. Another example is that by comparing the nighttime lights intensity before and after certain military actions in Bagdad, assessed the impact of the military actions on the cities.

4.2.3. Disadvantages of DMSP/OLS data

Although the advantages of nighttime DMSP/OLS data are commonly recognized, several disadvantages in using the sensor to observe nighttime emissions have been identified. These disadvantages including:

a) Relatively low spatial resolution;

b) Absence of onboard calibration;

c) Lack of inter-satellite calibration, Inter-annual series correction;

d) Lack of records of in-flight gain changes;

e) Limited 6-bit quantization of digital numbers;

f) Light saturation in highly developed urban area because of the standard operation at the high gain setting;

g) The blooming effect such as overestimation of lit area due to the coarse spatial resolution of data and reflectance of light from adjacent areas;

h) Limited accessibility to high quality daily OLS data.

However, the strategies were developed to overcome some of these shortages. For instance, to overcome the lack of onboard calibration, scholars have assembled a radiance calibrated nighttime image of the United States acquired at reduced gain setting between March 1996 and February 1997 (Elvidge, et al.2009). Empirical studies have proved that the radiance-calibrated data is a useful spatial indicator for energy related human activity such as electricity consumption and greenhouse gas emission (Hsu, et al.2015).

To overcome the lack of inter satellite calibration, several methods were proposed during the past several decades. These methods include the invariant region and the quadratic regression method proposed by Elvidge et al (Elvidge, et al.2009). the second- order regression and optimal threshold method proposed by Liu et al (Liu, et al.2015). Although studies based on these calibration methods showed performance improvement after the rectification the assumption that the nighttime light remains stable over time in a particular area requires a careful choice of the invariant region manually.

Another example of the overcome of shortcoming is the application of the different algorithms in these studies. For instance, Li developed a three-dimensional model to extract light volume using the triangulated irregular network functionality in Arcgis (Li and

Zhou.2017). Zhang et al proposed a method for combining nighttime data with MODIS NDVI data to reduce saturation effects in urban cores (Zhang and Seto.2011). All of the above studies showed that using the saturation-calibrated data could improve the estimation of human activity and human impacts on the environment.

4.3. Preprocessing of DMSP/OLS NTL images

Due to the lack of on-board calibration, the original DMSP/OLS images were not comparable, so they can't be used directly to extract the dynamics of urban expansion in China (Liu, et al.2012). In addition, Digital Number (DN) values of nighttime images were influenced by differences between sensors, differences in crossing time between satellites and degradation of sensors. These factors caused discrepancies in DN values between two satellites for the same year and abnormal fluctuations in DN values from the same satellite for different years. Therefore, DN values of nighttime light data can't be used directly to represent the absolute radiance of light. Thus, preprocessing of DMSP/OLS images is necessary to deal with these problems. The purpose of our preprocessing of DMSP/OLS nighttime data is to solve four problems:

a) Discrepancies appeared between DN values derived from different satellites for the same year.
b) Abnormal fluctuations appeared in DN values for different years derived from the same satellite.
c) The number of lit pixels differed between two satellites for the same year.
d) The number of lit pixels derived from the same satellite decreased abnormally between different years.

To improve the continuity and comparability of nighttime light data, a new method to correct the data systematically was applied in this research. The preprocessing of the DMSP/OLS images including three aspects: Inter-calibration; Intra-annual Composition and Inter-annual series correction.

4.3.1. Inter-calibration

The objective of inter-calibration is to improve the comparability of nighttime stable light data in the study area during the whole research period from 1992 to 2013. Inter-calibration of nighttime stable light was performed by Elvidge et al (Elvidge, et al.2009). Discrepancies in DN value within the nighttime stable light dataset were effectively reduced after inter-calibration. In this study, we performed an inter-calibration of nighttime stable light data for the selected area according to the method developed by Elvidge et al and the actual

Table 4-3 Coefficients of the second-order regression model for DMSP/OLS data

Satellite	Year	a	b	c	R^2
F10	1992	-0.005	1.383	0.006	0.871
	1993	-0.004	1.353	0.002	0.901
	1994	-0.008	1.300	0.007	0.881
F12	1994	-0.002	1.259	0.004	0.867
	1995	-0.005	1.247	0.013	0.890
	1996	-0.002	1.189	0.018	0.896
	1997	-0.002	1.183	0.006	0.910
	1998	0.002	0.926	0.007	0.955
	1999	0.000	1.000	0.000	1.000
F14	1997	-0.010	1.660	0.003	0.921
	1998	-0.002	1.225	-0.004	0.982
	1999	-0.006	1.437	0.001	0.979
	2000	-0.005	1.245	0.013	0.949
	2001	-0.004	1.096	0.019	0.946
	2002	-0.006	1.023	0.048	0.877
	2003	-0.007	1.178	0.022	0.942
F15	2000	-0.003	1.076	0.010	0.910
	2001	-0.001	0.989	0.004	0.922
	2002	-0.001	0.903	0.018	0.953
	2003	-0.010	1.416	0.021	0.914
	2004	-0.009	1.300	0.033	0.924
	2005	-0.007	1.129	0.053	0.880
	2006	-0.008	1.066	0.058	0.874
	2007	-0.010	1.209	0.049	0.865
F16	2004	-0.004	0.995	0.031	0.893
	2005	-0.006	1.108	0.031	0.916
	2006	-0.007	1.020	0.030	0.870
	2007	-0.004	0.947	0.031	0.911
	2008	-0.001	0.761	0.054	0.900
	2009	0.000	0.607	0.057	0.870
F18	2010	0.001	0.535	0.034	0.844
	2011	-0.002	0.684	0.048	0.862
	2012	0.000	0.652	0.029	0.899
	2013	0.001	0.541	0.039	0.886

situation of urban development in China (Elvidge, et al.2009). The method was based on a second order regression model to match the composite of F12 in 1999 to minimize the effects of variation among sensors, on this basis, the nighttime light data series can be adjusted to the same radiometric baseline (Elvidge, et al.2009). As the model was empirically developed using the region with little nighttime light change as the reference data, by analyzing the

socio-economic characteristics based on GDP and built-up area data for Chinese cities from 1992 to 2013, Yichun city in Heilongjiang Province, China was selected as the reference region. Then we developed a second-order regression model for each satellite using the equation below and a set of annual composites were compared with F12-1999 for the city of Yichun using the regression for each satellite using the equation:

$$\mathrm{DN}_{\mathrm{calibrated}} = \mathrm{a} \times \mathrm{DN}^2 + \mathrm{b} \times \mathrm{DN} + \mathrm{c} \qquad (4-1)$$

Where

DN is the original digital value of the nighttime light data;

$\mathrm{DN}_{\mathrm{calibrated}}$ is the inter-calibrated DN value;

a, b *and* c are coefficients.

Table 4-3 shows the result of inter-calibration. The average value of the correlation coefficient of the regression model of all satellites over all years equals 0.908, the highest correlation coefficient was 0.982 while the lowest was 0.844. By the inter-correlation, the difference between the different satellite on various year decreased relatively.

4.3.2. Intra-annual composition

The DMSP/OLS time series was available from 1992, during this period, several years have two datasets on one year such as 1994, 1997 etc. The objectives of the intra-annual composition were to make full use of the information derived from to two satellites for the same years and to remove any intra-annual unstable lit pixels. We obtained two nighttime stable light annual composites from two dataset during the period from 1992 to 2013. To get full use of the nighttime stable light data, we performed an intra-annual composition for the dataset from these years using averaged DN value of two nighttime light images.

Firstly, all lit pixels were examined to identify whether the pixels were intra-annuall unstable lit pixels. A lit pixel was defined as an intra-annual unstable lit pixel if it was detected by only one satellite (Liu, et al.2012). Then, in intra-annual composites, DN value of intra-annual composites, DN values of intra-annual unstable lit pixels were replaced with value of zero, and the DN value of each intra-annual stable lit pixel was replaced by the average DN value of two nighttime stable light images from the same year. The processing produced one intra-annual composite for each year which could be expressed as the equation below:

$$DN_{(n,i)} = \begin{cases} 0 & DN^{a}_{(n,i)} = 0 \; or \; DN^{b}_{(n,i)} = 0 \\ \left(DN^{a}_{(n,i)} + DN^{b}_{(n,i)}\right) & Ot\square erwise \end{cases} \quad (4-2)$$

Where:

$DN^{a}_{(n,i)}$ and $DN^{b}_{(n,i)}$ are the digital number value of the lit pixel from the two nighttime light data in the *n*th year respectively, $DN_{(n,i)}$ is the digital number value of the *i*th lit pixel of intra-annual composite in the *n*th year.

4.3.3. Inter-annual series correlation

In addition, to make sure the nighttime stable light image based urban dynamics matched the actual process and to remove the discrepancies in the multi-year dataset, the inter-annual correlation was applied to each nighttime light image. The objective of the inter-annual series correction were to remove inconsistencies in the multi-year dataset and to correct digital number values for consistently lit pixels so as to ensure that the dynamics of urban expansion obtained using the nighttime light data reflect the actual processing of urbanization in the study areas. Here, we assumed that the urban areas would grow continuously outward and that the lit pixels would become brighter over time. We also assumed that an urban patch detected in an early nighttime light image would not disappear at a later year (Zhou, et al.2014). Scholars have revealed that a lit pixel with a higher DN value had a higher probability of extraction as an urban patch. Therefore, we further assumed that the lit pixels detected in earlier nighttime stable light images should be maintained in the results of later images and that the DN value of lit pixels detected in an earlier nighttime light images should not be greater than their value in a later image, considering the unprecedented urbanization in China during the past several decades. Based on these assumptions, we performed the inter-annual series correlations.

Firstly, all lit pixels were examined for consistency in the multi-year dataset. A pixel was considered to be an inter-annual unstable lit if it was detected in an earlier nighttime stable light image but disappeared in a later nighttime stable light image. Secondly, digital number value of the inter-annual unstable lit pixels were replaced with values of zero, and the DN value of each inter-annual stable lit pixel was corrected to ensure that its value in an early

nighttime stable light image did not exceed its digital value in a later image. The inter-annual correlation could be expressed as the equation below:

$$DN_{(n,i)} = \begin{cases} 0 & DN_{(n+1,i)} = 0 \\ DN_{(n-1,i)} & DN_{(n+1,i)} > 0 \ and \ DN_{(n-1,i)} > DN_{(n,i)} \\ DN_{(n,i)} & Otherwise \end{cases} \quad (4-3)$$

Where:

$DN^{a}_{(n-1,i)}$, $DN^{a}_{(n,i)}$ and $DN^{a}_{(n+1,i)}$ are the digital number values of the *i*th lit pixel of the nighttime light data in the *n-1*th, the *n*th and *n+1*th years respectively.

4.4. Correlation analysis of the DMSP/OLS data

In order to verify the correlation between the DMSP/OLS nighttime stable light datasets with the urbanization process and make sure that the data of nighttime images could present the urbanization level during the period from 1992 to 2013, we carried out a correlation analysis of the DMSP/OLS data with the social-statistics. In this research, we selected Beijing city as the example to explore the correlation between the satellite observing urbanization and government statistics on the development of the city.

4.4.1. Calculation of DMSP/OLS nighttime light images indicators

Our method for correlation analysis of the DMSP/OLS nighttime stable light images with the dynamics of urbanization process including three main steps: calculating the annual average DN value during the period from 1992 to 2013; counting the total number of lit number of lit pixels; calculating the urban area proportion.

a) Calculation of the annual average DN

In this study, we used the annual average DN as one of the three indicators to estimate the annual degree of urbanization in Beijing. The annual average DN is defined as the annual average DN value of all pixels that are located in the administrative districts, taking the pixels that located at the boundaries into consideration, the DN value of each pixel was multiplied by the area that it located. In addition, the calculation was proceeded after the preprocessing of the DMSP/OLS NTL imagery, it can be illustrated by the equation below:

$$\text{Annual average DN} = \frac{\sum DN_{pixel} \times Area_{pixel}}{Area_{sum}} \qquad (4-4)$$

Where

DN_{pixel} and $Area_{pixel}$ are the DN value and the trapezoid area of each pixel;

$Area_{sum}$ is the sum of the area within the administrative boundary.

b) Counting the total number of lit pixels

Total number of lit pixels explains the overall level that how many pixels were lit within the scope of study region. The total number of pixels derived from the satellite within Beijing city was 24991, then after the inter-annual correlation, the total number of pixels

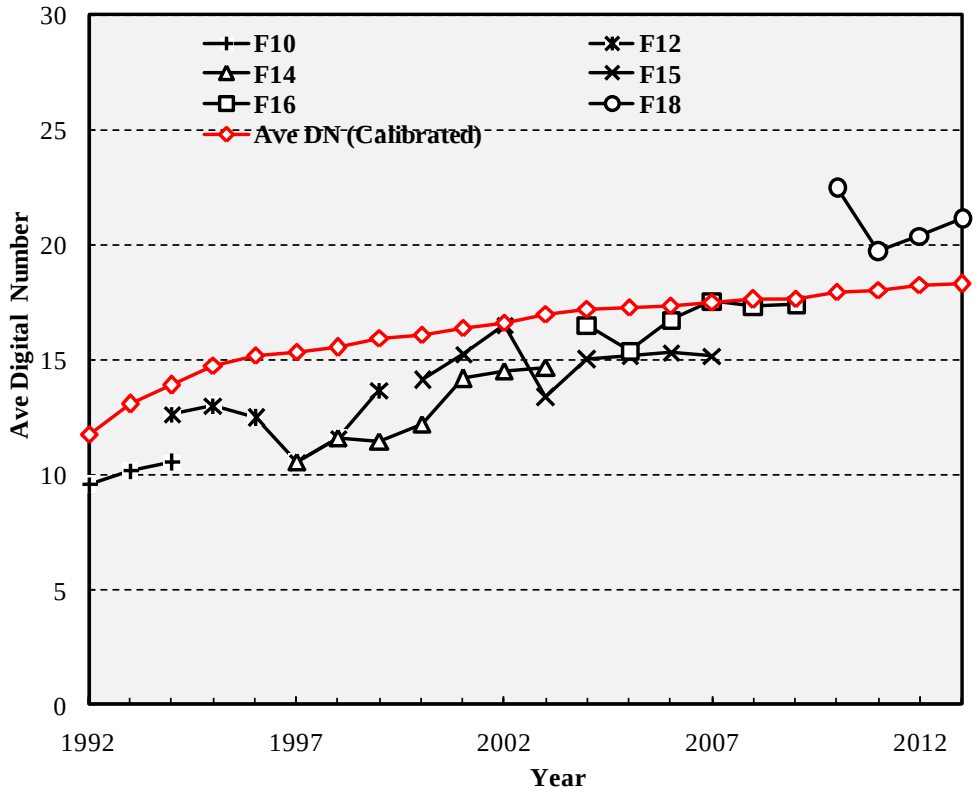

Figure 4-2 Change of annual average DN in Beijing before and after calibration

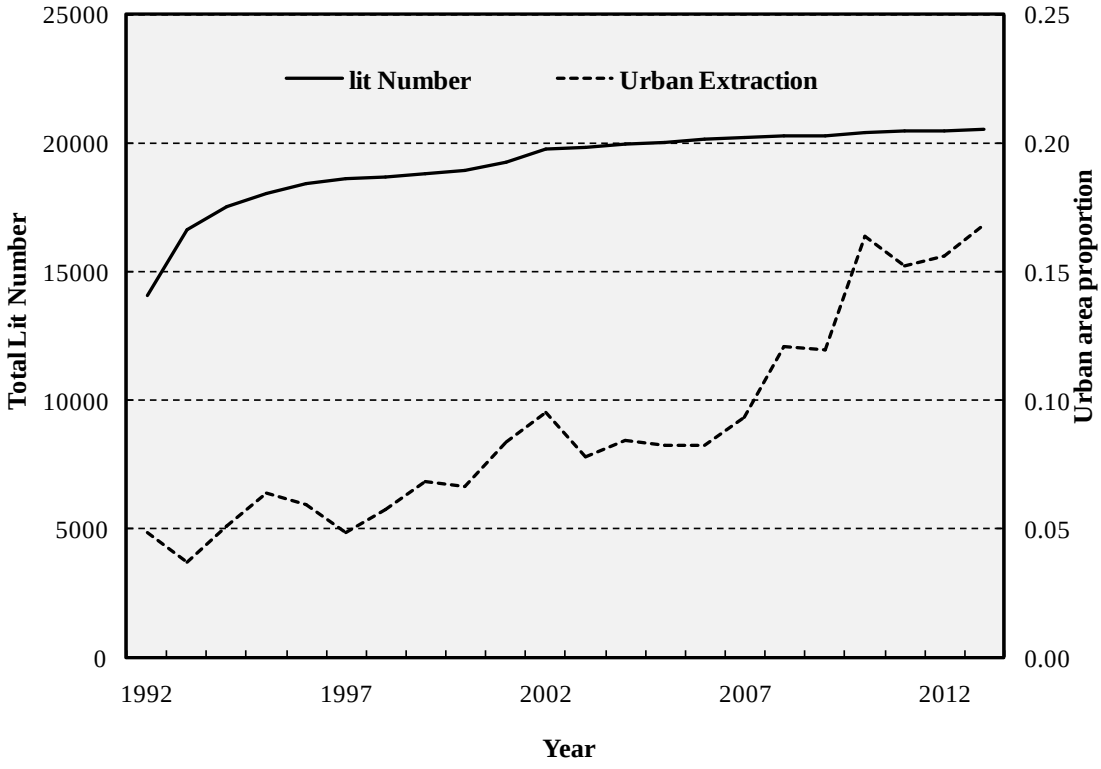

Figure 4-3 Change of total lit number and urban area proportion in Beijing

greater than 0 in each year from each satellite was counted. For the year which has two satellites dataset, the pixel was counted if only it was lit in either of its dataset.

c) Urban area proportion

For the extraction of lit urban area, we adopted the threshold technique which developed by Henderson et al (Henderson, et al.2003). Furthermore, the optimal thresholds for extraction were determined based on the method provided by Gao et al (Gao, et al.2015). Beijing is located in Northern Coastal China (NCC) region, the thresholds of NCC was exploited for the extraction.

4.4.2. Urbanization dynamics process assessment by DMSP/OLS in Beijing

In this study, the annual average DN value under Beijing's boundary was calculated as illustrated by equation 4-4. The dynamics of urbanization which estimated by DMSP/OLS nighttime light data was shown in Figure 4-2. By preprocessing of the imageries, the calibrated annual average DN value was calculated and displayed in red. The average DN increased 1.56 times, from 11.73 in 1992 to 18.28 in 2013; with an average annual growth rate of 2.16%. by calibration, we had got a smooth result of average DN trend which may seem more reasonable than the initial nighttime light data. In addition, the total lit number and urban area proportion trend are calculated and shown in Figure 4-3 for the Beijing city. Respectively, the lit number increased 1.46 times from 14081 in 1992 to 20526 in 2013, the urban area proportion enhanced from 4.86% in 1992 to 16.83% in 2013 by 3.46 times. The lit number increased quickly in the first decade than the next decade of the period from 1992 to 2013. However, the trend of the urban area proportion shows an opposite trend which the later decade increased faster than before. The lit number increased quickly in the few years from 1992 which could be considered as a fast period of urban sprawl, then it slowed down and the urbanization level in the expanded area developed fast instead of continuous expansion outward. The entire three indicators trend showed that Beijing has experienced continued and rapid urbanization during the period from 1992 to 2013.

4.4.3. Correlation analysis of DMSP/OLS indicators with social-economic variables

4.4.3.1. Social-economic statistics collection

To judge whether the DMSP/OLS nighttime light images are keeping with the actual urbanization processing during the period from 1992 to 2013, the correlation analysis with

social-economic statistics was carried out to verify the feasibility of the datasets. Social-economic statistics of Beijing were obtained from the China Statistical Yearbook, the Beijing Statistical Yearbook and the National Bureau of Statistics of the People's Republic of China (NBSPRC.2016). The indicators were primarily selected according to the following general selection criterion: (1) choose the most cited indicators; (2) cover the components of urbanization processing and (3) choose the simplest indicators to facilitate indicators. Permanent population and gross domestic product (GDP) were selected as representative indicators of demographic and economic, in addition, these two indicators were the most widely used socio-economic indexes to establish the relationship with the urbanization processes based on DMSP/OLS NTL, which have been estimated by previous researchers (Fan, et al.2014, Stathakis, et al.2015). Besides, popularization and promotion of natural gas in some ways could reflect the development of energy industry structure in the city, there is also little research on establishing relationship with DMSP/OLS NTL, as a result, total consumption of natural gas was selected. Freight traffic plays an important role during the development of a city, length of highways and the total number of civil motor vehicles were chose to reflect the freight traffic development in Beijing. Therefore, the data collection includes seven annual indexes: GDP; permanent population; total energy consumption; total consumption of natural gas; the total electricity consumption; length of highways; and the total number of civil motor vehicles (Huang, et al.2014, Ma, et al.2014). Therefore, the data collection including 7 annual indexes: GDP, permanent population; total energy consumption; total consumption of nature gas; total electricity consumption, length of highways, total number of civil motor vehicles.

4.4.3.2. Log-liner regression analysis

The relationship between the NTL indicators and social-economic variables was initially examined through a log-linear regression analysis. Representatively, the Average DN-Ln(GDP), Total Lit Number-Ln(GDP) and Urban Area proportion-Ln(GDP) showed in Figure 4-4. From the regression analysis, it is easy to determine that the DMSP/OLS based indicators is closely related to the GDP of Beijing during the period from 1992 to 2013. In particular, The correlation coefficient of determination of Ln(GDP) with average NTL-DN value, total lit number and urban area proportion were 0.924, 0.807 and 0.815, respectively,

with both showing a close positive correlation. In-depth analysis, comparing the correlation of GDP with NTL indicators, we found that the urban area proportion have a better correlation than the other two indexes, which was arisen from the approximate increase trends of GDP and urban area proportion.

Linear regression was then applied between the NTL indicators and all collected social-economic parameters from 1992 to 1993 to estimate the correlation between them. Table 4-4 showed the correlation results, both of annual average DN value, total lit number and urban area proportion are closely correlated with the social-economic variable. The correlation coefficients of annual average DN value are all above 0.646 with an average value of 0.736. In particular, the correlation of Ave DN with total consumption of natural gas is among the best, with a coefficient of 0.841. On the other hand, the best correlation of total lit number with social-economics parameters was total consumption of nature gas with a coefficient of 0.764, while the average correlation coefficient was 0.607. For the correlation analysis with urban area proportion, the correlation coefficients were all above 0.788, held an average value of 0.890 while the maximum was 0.939 that derived from the population. The result illustrates that DMSP/OLS NTL based urbanization indicators are effective ways to evaluate and monitor the development at city level.

Table 4-4 Correlation result between NTL indicators and social-economic statistics.

Parameter (P)	Unit	Increase Rate	Ave DN	TLN	UAP
			Coefficient of Determination R^2 with Ln(P)		
GDP	Billion	27.92	0.924	0.807	0.815
Population	Million	1.92	0.805	0.665	0.916
Total energy consumption	Million tce	2.40	0.841	0.724	0.810
Total consumption of natural gas	Billion m^3	85.30	0.966	0.954	0.674
Total electricity consumption	Billion kWh	4.97	0.926	0.810	0.789
Length of highways	Thousand km	2.01	0.752	0.633	0.785
Total number of civil motor vehicles	Million	15.16	0.895	0.771	0.840
Average	-	19.96	0.873	0.766	0.804

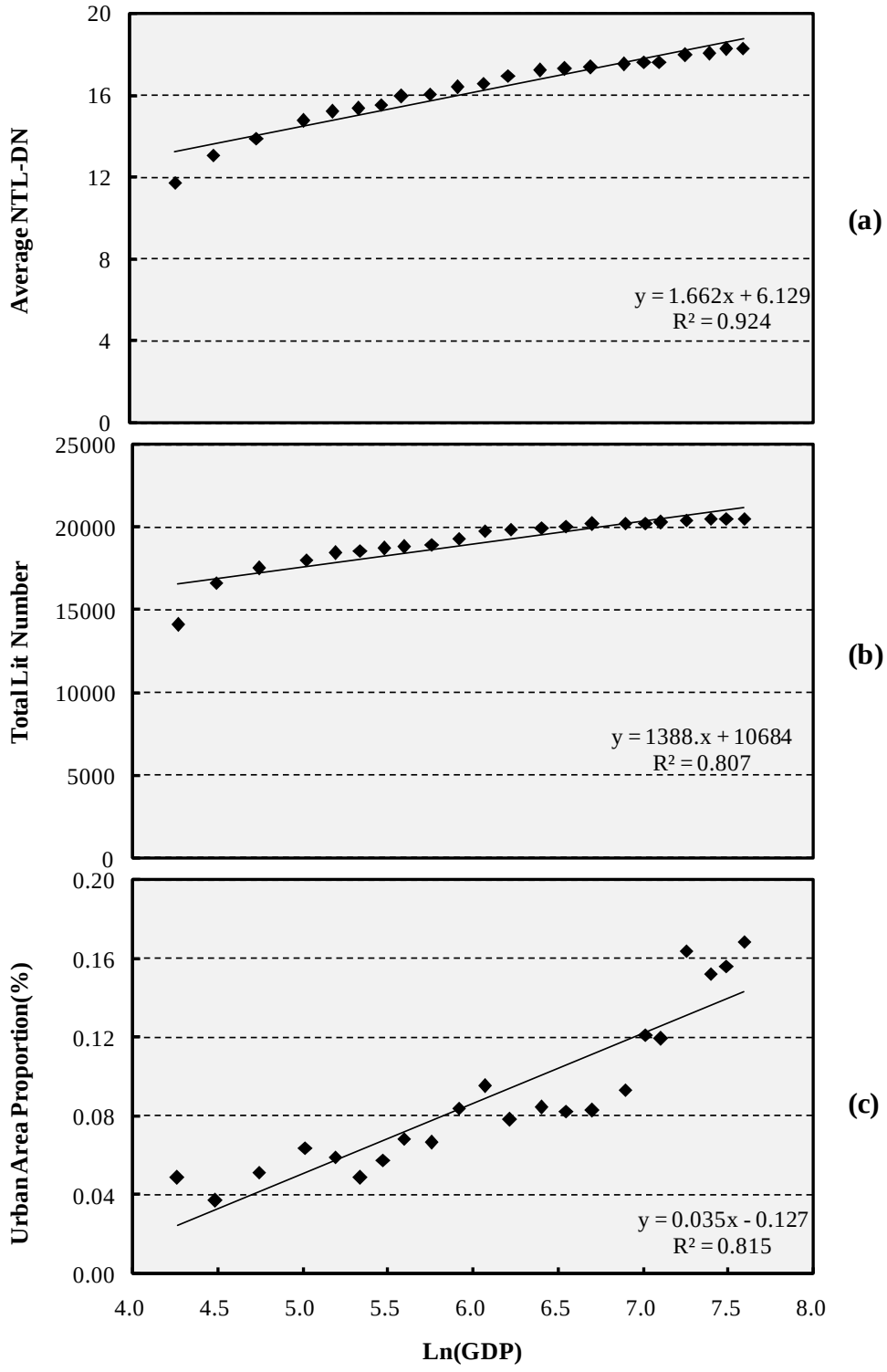

Figure 4-4 Scatter plots between the Ln(GDP) and DMSP/OLS/NTL indicators from 1992–2013.

(a) Scatter plot between Ln(GDP) and Ave NTL-DN value; (b) Scatter plot between Ln(GDP) and Total Lit Number; and(c) Scatter plot between Ln(GDP) and UrbanArea Proportion.

.

4.5. Extraction of urban area in major cities of China

4.5.1. Study area and research period selection

In this study, we selected three most urbanized and populated city as the study area which is: Beijing, Shanghai and Guangzhou city. The representativeness of these three cities could represent the highest level of urbanization process in China and provide referential meaning for the develop and sprawl of the other cities in China.

As the capital city of China, Beijing is well know world wide as a famous ancient city and international metropolis, which is located at 39°56’ N and 116°20’ E. As the political, cultural and economic center of the People’s Republic of China, Beijing city covers an area of 16,808 km^2. In terms of topography, two-thirds of Beijing are mountainous areas where the city is surrounded by mountains from all sides, except for the southeast of the city, where a plain slopes slightly to the Bohai Rim. Beijing city is characterized by a warm temperature zone and has a typical continental monsoon climate with four distinct seasons, including a hot and rainy summer and a cold and dry winter.

Shanghai is located on China’s central eastern coast, at the mouth of the Yangtze River, with latitude of 31°14’ N and longitude of 121°29 E. Shanghai is administered as a municipality with province-level status. It is also one of the largest cities in China in terms of population and one of the most developed urban areas in the world. For more than 150 years, since about 1850, Shanghai has been China’s biggest economic centre. In 2013, it had a total population of 24.15 million, a total GDP of 2160.21 billion Yuan, and an urbanization level of 89.60%, which is the highest city of all China. The municipality’s socioeconomic plan expects Shanghai to maintain continues growth with respect to its nonagricultural population in coming decades. Shanghai administers 16 municipal districts covering a total area of 6340.5 square kilometers. Shanghai, which has a subtropical humid monsoon climate, exhibits the characteristics of four distinct seasons, full sunshine and abundant rainfall. Shanghai is China’s economic, transportation, technological, industrial, finance, trade, exhibition and shipping center.

Guangzhou city is located in southern China between 22°26’ N to 23°56’ N and 112°57’ E 114°03’ E, in the central part of the Pearl River Delta. It lies in the southern part of Guangdong province. Guangzhou is one of the most rapidly growing regions in China,, with a

huge economy and dense population. Guangzhou is the capital city of Guangdong province, which is an important political, economic, cultural, and scientific centering southern China. The total area of the Guangzhou city is 7434.4 km^2, consists of 10 administrative districts and two country-level cities. Guangzhou is the largest city in south China, it is also the busiest port city in China after Shanghai. At the end of 2012, the population was 12.83 million, 85.02% of this population resides in urban areas.

Nighttime stable light data from 1992 to 2013 were obtained and the start time of the research period was selected from 1992, in addition, the landscape assessment of built-area was based on the remote sensing extraction from DMSP/OLS night stable light data which was extracted by threshold methods. The time interval of the research period was set by three years based on the threshold value selection used in this research. Thus, the research period was set from 1992 to 2013, the assessment was carried out from Beijing, Shanghai and Guangzhou city every three years.

4.5.2. Selection of the thresholds for urban area extraction

A few methods are avalible to extract urban information from NSL imagery, including an empirical threshloding technique (Elvidge, et al.2009), a thresholding technique based on mutation detection (Imhoff, et al.2010) and an image-classification method (Cao, et al.2009). Of these methods, the thresholding technique with ancillary data has been widely used because of its simplicity and relatively high accuracy and reliability. Thresholding techniques have been extensively used to map urban extents from NTL images at multiple scales (from local to global scales) owing to their simplicity, especially when an optimal threshold was available (Henderson, et al.2003, Zhou, et al.2015). However, it was very difficult to extract a

Table 4-5 Optimal thresholds for lighted urban area extraction in study area.

City	Optimal Threshold				
	1992	1993-1997	1998-2002	2003-2007	2008-2012
Beijing	51	56	57	61	59
Shanghai	50	54	58	59	59
Guangzhou	61	62	63	61	61

Note: The thresholds were based on the method providedby Liu *et al.* (Liu, et al.2012)

single threshold for urban information in China due to the great regional variation in physical environment and social-economic development status.

With the thresholding method, pixels with NTL intensity larger than a predefined value were determined as “urban areas”. However, optimal thresholds were often difficult to select, both locally and regionally, let alone the optimal values at global scale. Moreover, optimal thresholds derived for different DMSP/OLS images were incompatible because of the inconsistency of DN among NTL images. Thus, it remained a challenge to map urban extents and to detect urban dynamics from DMSP/OLS NTL images by using the thresholding techniques, the reliability and accuracy of ancillary data were key factors to ensure that this technique was successful. Therefore, we used the thresholding technique developed by Henderson et al along with ancillary data to extract the urban information in Beijing, after the systematically correcting NST data from 1992 to 2013 (Henderson, et al.2003). Due to the great regional variation of the three cities of the study areas, in this study, we adopted the threshold technique developed by Liu et al. to determine the optimal thresholds for extracting lighted urban areas in the three cities of the study area. For each city, optimal thresholds were determined for each period when the urban areas extracted using nighttime stable light data matched the ancillary data best (Liu, et al.2012).

4.5.3. Quantifying the spatiotemporal pattern of urban area

After mapping the urban area of the three cities during the period from 1992 to 2013, we then carried out the urban area proportion to quantify the patterns of urban area of the three cities with the following formula:

$$UAP = \frac{UAA}{TA} \times 100\% \qquad (4-5)$$

Where:

UAP is the urban built-up area percentage (%);

UAA is the total urban area in a specific zone (km^2);

TA is the total area under the city boundary (km^2).

Then we characterized the changes of urban area from 1992 to 2013 in the three cities using the index of relative urban area expansion index, with the equation below:

$$UAEI = \frac{UAA_j - UAA_i}{TA} \times \frac{1}{T} \times 100\% \qquad (4-6)$$

Where:

UAEI is the relative urban built-up area expansion index (%);

UAA_j is the total urban built-up area in the *j*th year (km^2);

UAA_i is the total urban built-uo area in the *i*th year (km^2);

TA is the total area under the city boundary (km^2).

T is the time step

4.5.4. Dynamics of DMSP/OLS NTL extraction of urbanization

Figure 4-5 shows the DMSP NTL extracted urban dynamics in Beijing city every three year from 1992 to 2013. By visual observation, all of the three cities showed an obvious expansion during the period. As to Beijing city, due to that the northwest part of the city is covered by mountains, the built-up area in Beijing mainly sprawled towards the other directions, especially the south and east directions. The situation in Shanghai is considerably differ from the Beijing city (Figure 4-6), the administrative area in Shanghai is less than that of Beijing, after 20 years development, NTL extraction in Shanghai also showed an obviously increasing in both DN and built-up area. The situation in Guangzhou is very similar with the situation in

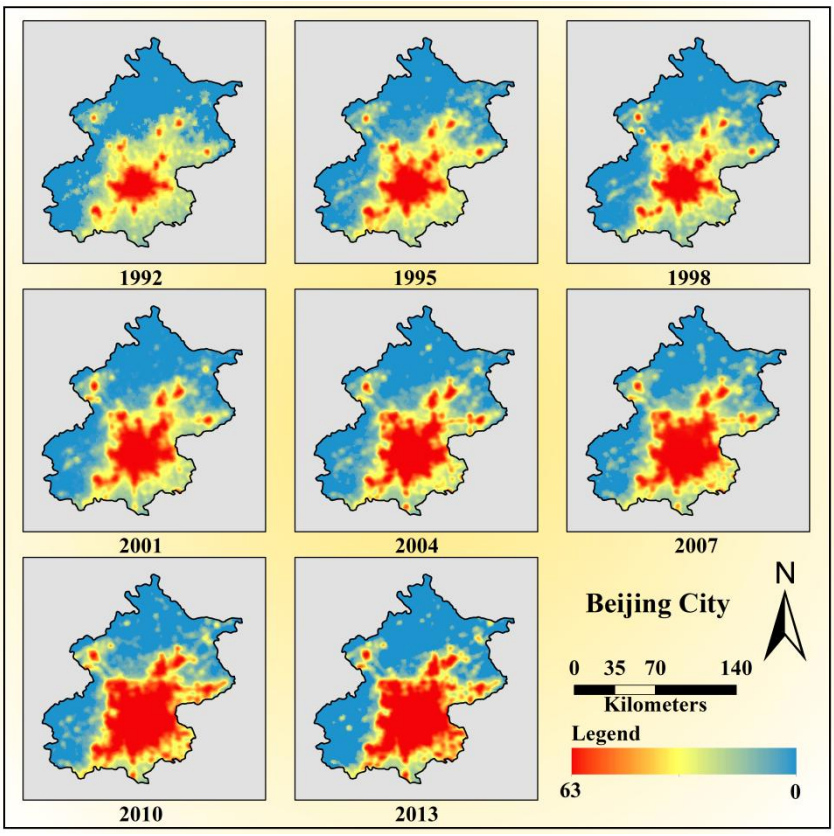

Figure 4-5 Urban dynamics of Beijing city from DMSP/OLS NTL

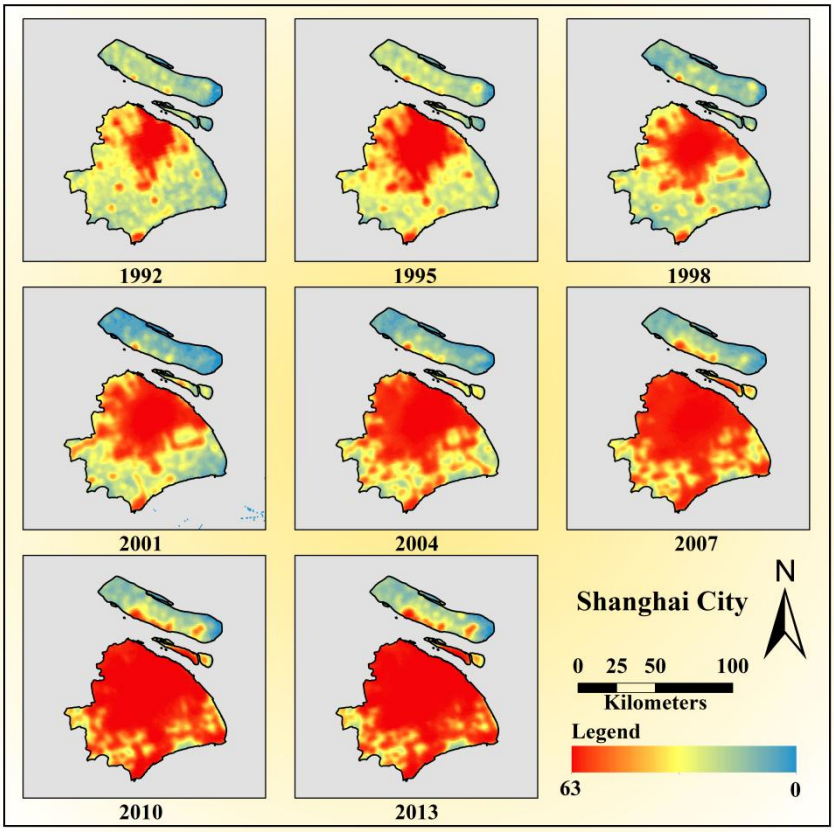

Figure 4-6 Urban dynamics of Shanghai city from DMSP/OLS NTL

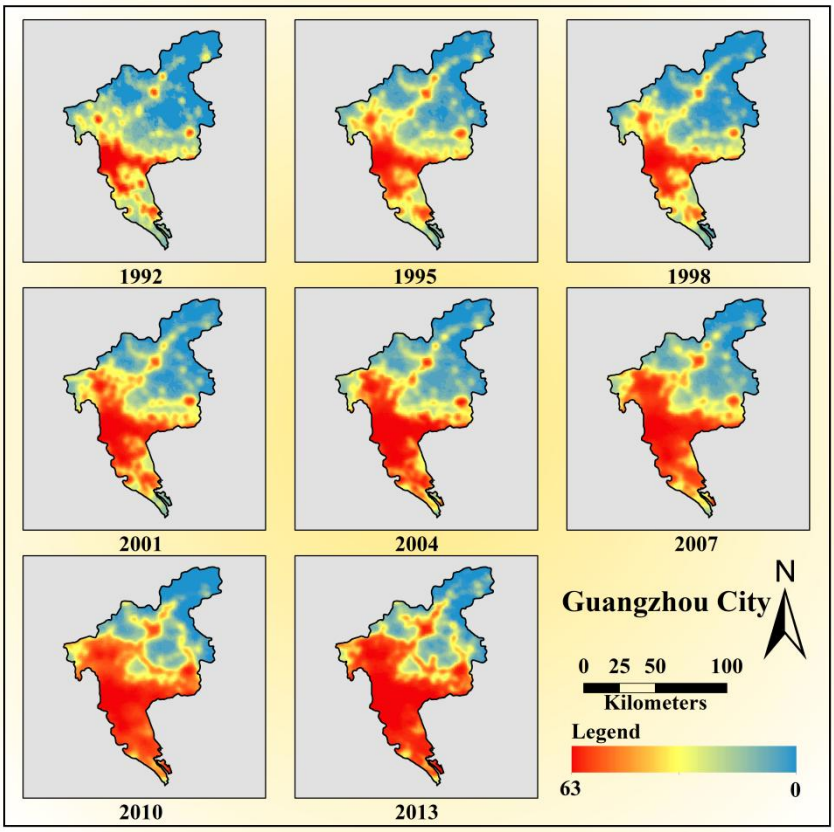

Figure 4-7 Urban dynamics of Guangzhou city from DMSP/OLS NTL

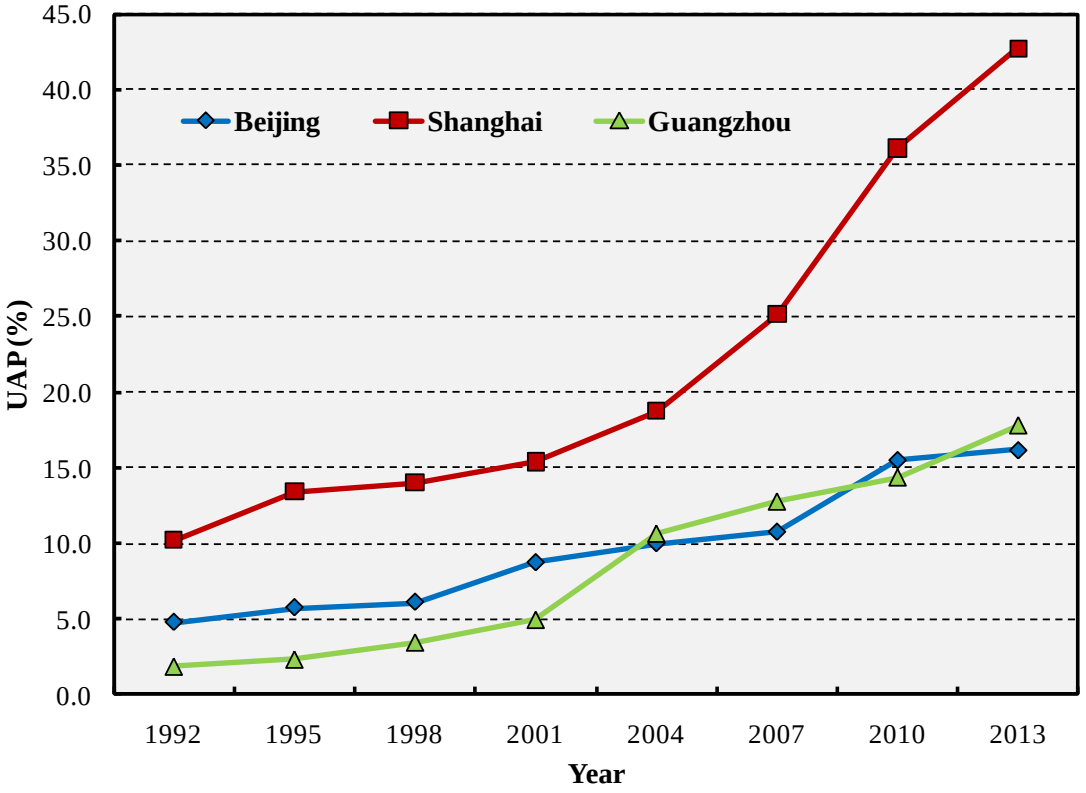

Figure 4-8 UAP change in the study area from 1992 to 2013

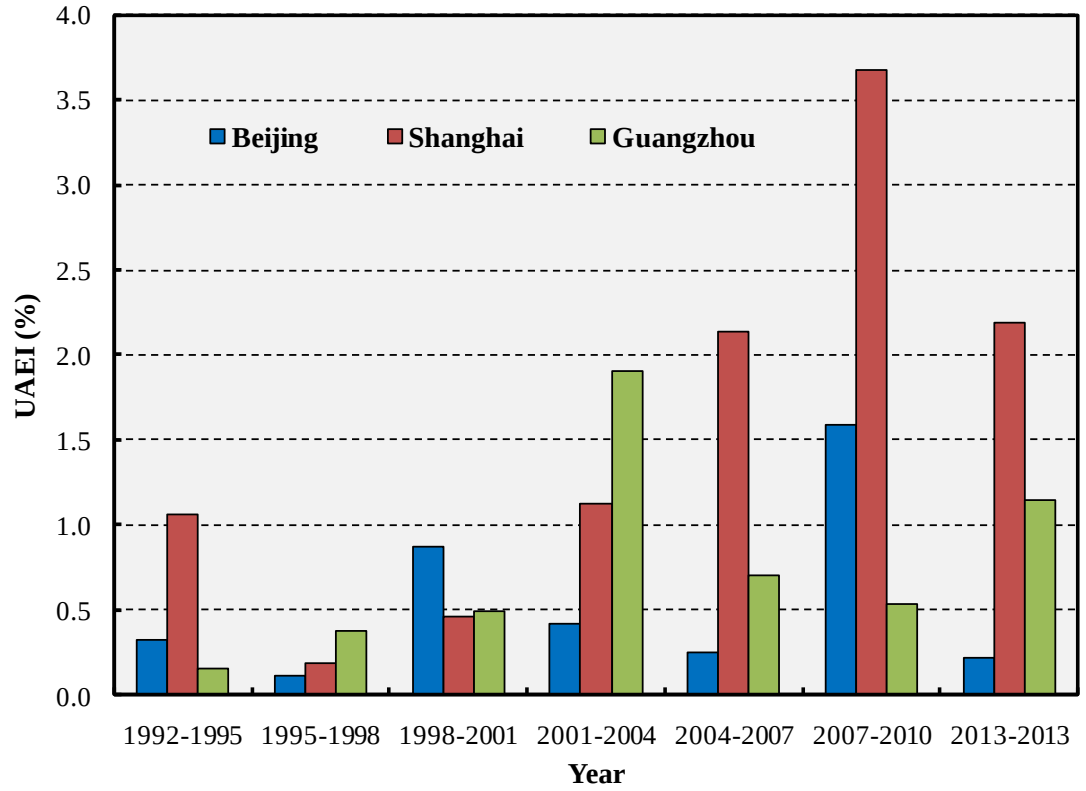

Figure 4-9 UAEI change in the study area during the period from 1992 to 2013

Beijing due to the vast territory (Figure 4-7), the built-up area in the city in 1992 only occupy very few parts of the city, the DN value in most area was low, the DN value increased after two decades high value of DN which displayed in red occupy a large part of the city.

Figure 4-8 shows the statistic result of the UAP. Looking deeply in the UAP change, all of the three cities showed an increase trend during 1992 to 2013. The urban built-up proportion in Beijing increased from 4.75% in 1992 into 16.17% in 2013 by 3.4 times. The proportion in Shanghai increased from 10.17% in 1992 into 42.74% in 2013, increased by 4.2 times. To the situation in Guangzhou, the proportion increased from 1.806 % in 1992 to 17.77% in 2013, the increased rate reached 9.9 times which is the highest of the three cities. The proportion of urban built-up area in Beijing and Guangzhou is lower than the value in Shanghai, mainly because that in these two cities, there were a large proportion that covered by the mountain and forest.

Figure 4-9 shows the information of UAEI change in the study area from 1992 to 2013. There is a significant difference in different cities and in different period. As to Beijing city, the average urban expansion index every three years was 0.54%, the most quickly expanded period was from 1998 to 2001. Shanghai showed a relative higher expansion rate compared with the other two cities. The average expansion rate index was 1.55% every three year, the fastest expansion occurred in the period from 2007 to 2010. To the situation of Guangzhou city, the average UAEI was 0.76%, 2001 to 2004 holds the highest expansion rate.

4.6. Changing pattern of built-up areas

4.6.1. Selection of landscape metrics

Landscape metrics are numeric measurements that quantify spatial patterning of land cover patches, land cover classes or entire landscape mosaics of a geographic area (Dupras, et al.2016). The analysis on the landscape metrics has become a trend in urban change studies. Landscape metrics provided a comprehensive view of the overall landscape structure, including area, density, boundary, shape, core area, isolation, closeness, difference, connection and diversity. Urban compactness is one of the major indicators of sustainable urban development that has been widely used to measure urban forms. Meanwhile, fractal

Table 4-6 Selected Landscape metrics

Indices	**Calculation formulars**	**Level**	**Units**
Number of patches (NP)	Number of patches is a measure for the extent of subdivision or fragmentation of patch type	Class	None
Percentage of landscape(PLAND)	Percentage of landscape quantifies the proportional abundance of each patch in he landscacpe	Class	Percetage
Largest patch index(LPI)	Largest patch index quantifies the percentage of total landscape area comprised of the largest patch. It is the percent measure of dominance.	Class	Prrcentage
Landscape division (DIVISION)	Division is based on the cumulative patch areadistribution and is interpreted as probability that two randomly chosen pixels in the landscape are not situated in the same patch	Landscape	Proportion
Landscape Shape Index (LSI)	Landscape shape index provides a standardized measure of total edge or edge density that adjusts for the size of the landscape.	Landscape	None
Contagion Index (CONTAG)	Contagion is inversely related to edge density. When edge density is very low, for example, when a single class occupies a very large percentage of the landscape, contagion is high, and vice versa.	Landscape	Proportion
Shannon's diversity index (SHDI)	Shannon's diversity index is used to describe the degree of abundance and uniformity of landscape type synthetically	Landscape	Information
Shannon's evenness index (SHEI)	Shannon's evenness index measures the evenness of proportional distribution of patch type area.	Landscape	None

dimension can measure the degree of irregularity of urban land uses.

Dynamic change model of land use is an important approach to study the land use change, through which researchers can analyze speed, process and development tendency of land use change in the future. The objective of the landscape ecology was fixed on the land mosaic body. As far as a region was concerned, landscape ecological development was mainly restricted by natural environment condition and natural source. In addition, spatial structure of different land use was achieved by overall land use shape which was synthetically reflected by interaction influence of socio-economic factors. By analyzing the change condition of landscape patches from the landscape ecology indices, we could summarize the rules of the urban development and predict change tendency of land use in future, and spatial measure object of landscape ecology might be applied in the spatial analysis of land use vicissitude. By using the Fragstats software, this paper selected 8 landscape indices to reflect the effects of land use change on ecology issues.

4.3.1 Calculation of the landscape metrics

a) Calculation formulas of number of patches

$$NP = number\ of\ patc\square es\ in\ t\square e\ landscape \qquad (4-7)$$

b) Calculation formulas of percentage of landscape

$$PLAND = \sum_{j=1}^{n} \frac{a_{ij}}{A} \times 100\% \qquad (4-8)$$

c) Calculation formulas of largest patch index

$$LPI = \frac{MAX_{(a_{ij})}}{A} \times 100\% \qquad (4-9)$$

d) Calculation formulas of landscape division index

$$DIVISION = 1 - \sum_{j=1}^{n} (\frac{a_{ij}}{A})^2 \qquad (4-9)$$

e) Calculation formulas of landscape shape index

$$LSI = \frac{0.25E^*}{\sqrt{A}} \qquad (4-10)$$

f) Calculation formulas of contagion index

$$CONTAG = 1 + \frac{\sum_{i=1}^{m}\sum_{j=1}^{m}\left[(P_i)\left(\frac{a_{ij}}{\sum_{j=1}^{m} a_{ij}}\right)\right][\ln (P_i)(\frac{a_{ij}}{\sum_{j=1}^{m} a_{ij}})]}{2ln_m} \quad (4-11)$$

g) Calculation formulas of shannon's diversity index

$$SHDI = -\sum_{i=1}^{m}(p_i \times ln_{p_i}) \quad (4-12)$$

h) Calculation formulas of Shannon's evenness index

$$SHEI = \frac{-\sum_{i=1}^{m}(p_i \times \ln p_i)}{ln_m} \quad (4-13)$$

Where

i＝ith patch;

j＝jth patch number

a_{ij}＝area(m^2) of patch ij;

A＝total landscape area (m^2);

n＝total number of patches in the landscape;

n_i＝number of patches in the landscape of patch type;

p_{ij}＝perimeter (m) of patch ij;

m＝total number of landscape types;

p_i＝proportion of the landscape occupied by patch type i;

Hmax＝ln(m) the largest diversity.

4.7. Dynamic change analysis and landscape assessment

4.7.1. Dynamic change of class level

During the process of landscape analysis, influence of landscape scale effect upon study results should be paid particular attention. Many proposed indices (such as, the number of patch, fragmentation, border density, patches abundance degree, and so on.) were easily influenced by landscape size and researchers' subjectivity, so that research results often lacked of a certain standard and logical contrast. To conquer these shortages, each of typical characteristic in respect of landscape ecology was synthetically analyzed by applying multiple indices for achieving more scientific and reasonable research results.

This study carried out four landscape metrics at the class level: number of patch (NP), percentage of landscape (PLAND), largest patch index (LPI), LPI-Built-up ratio. Landscape ecology characteristics were analyzed by using these four indices. At the scale of landscape, five landscape metrics were selected to analyze the dynamic change characteristics of land use in the study areas: Landscape division (DIVISION); Landscape Shape Index (LSI); Contagion Index (CONTAG); Shannon's diversity index (SHDI) and Shannon's evenness index (SHEI). The results were showed as follow:

Figure 4-10 shows the number of patch of the three cities during the period from 1992 to 2013. The number of patches of a particular patch type is a simple measure of the extent of subdivision or fragmentation of the patch type. Although the number of patches in a class may be fundamentally important to a number of ecological processes, often it has limited interpretive value by itself because it conveys no information about area, distribution, or density of patches. Change of the number of patch is quite different between the three cities. In Beijing city, the number of patch increased from 9 in 1992 to 18 in 2013. Number of patch kept unchanged from 1992 to 1998, which showed an edge-expansion of the built-up area rather than outlying. The number of patch increased sharply from 2010 to 2013. To the situation in Shanghai, the number of patch in 1992 was 6 which increased into 12 in 2013. The increase rate is higher from 2004 to 2013 than the period before. On the other hand, the number of patch in Guangzhou city is relative lower than the other two cities, this could be explained as that the compactness of built-up area in Guangzhou city is better than Beijing and Shanghai.

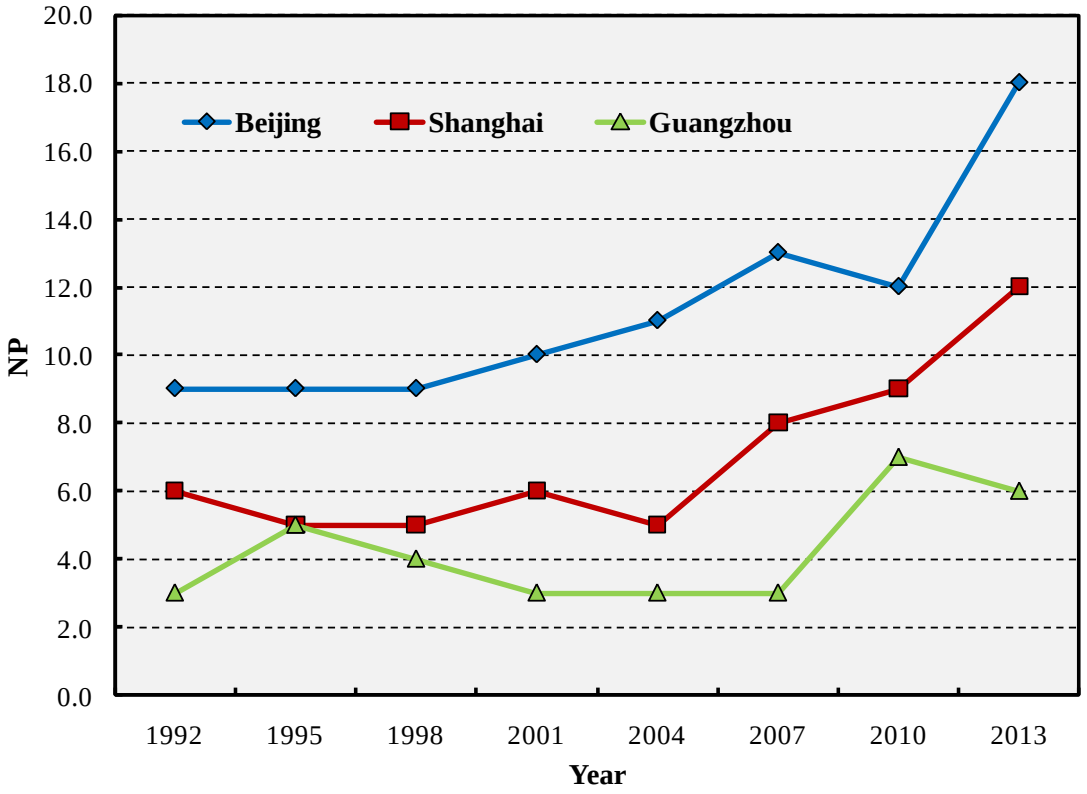

Figure 4-10 Number of Patch of the three cities during the period from 1992 to 2013

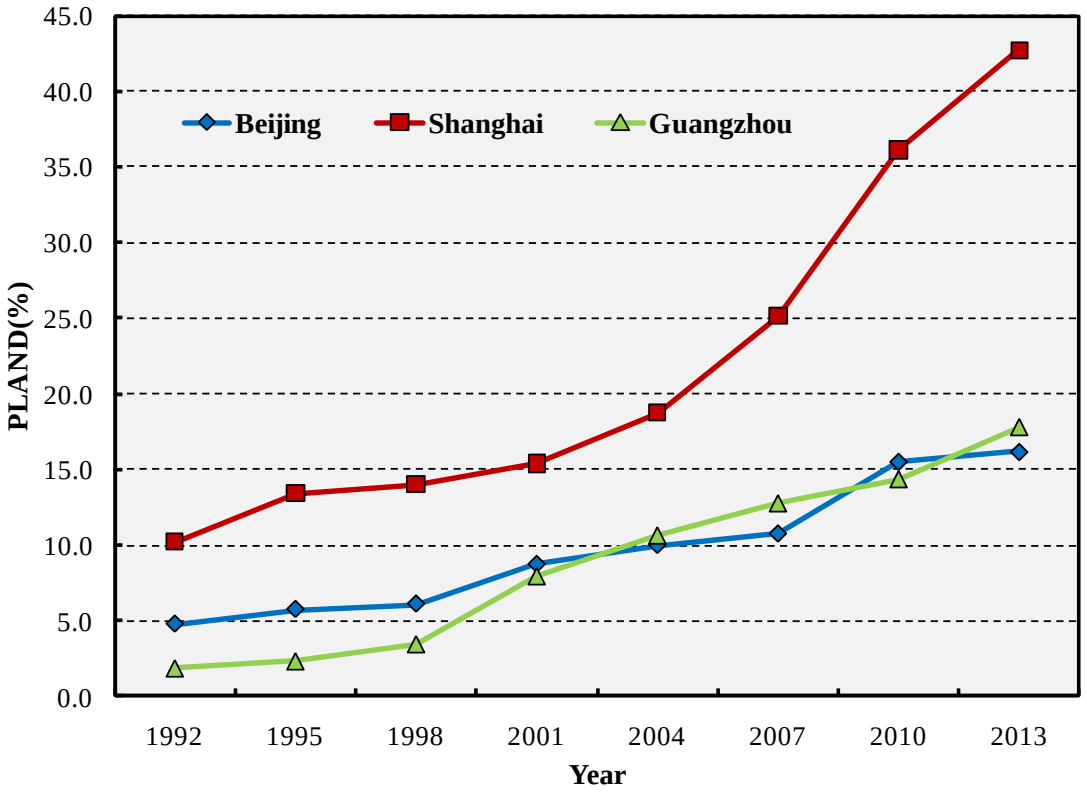

Figure 4-11 Percentage of landscape of the three cities during the period from 1992 to 2013

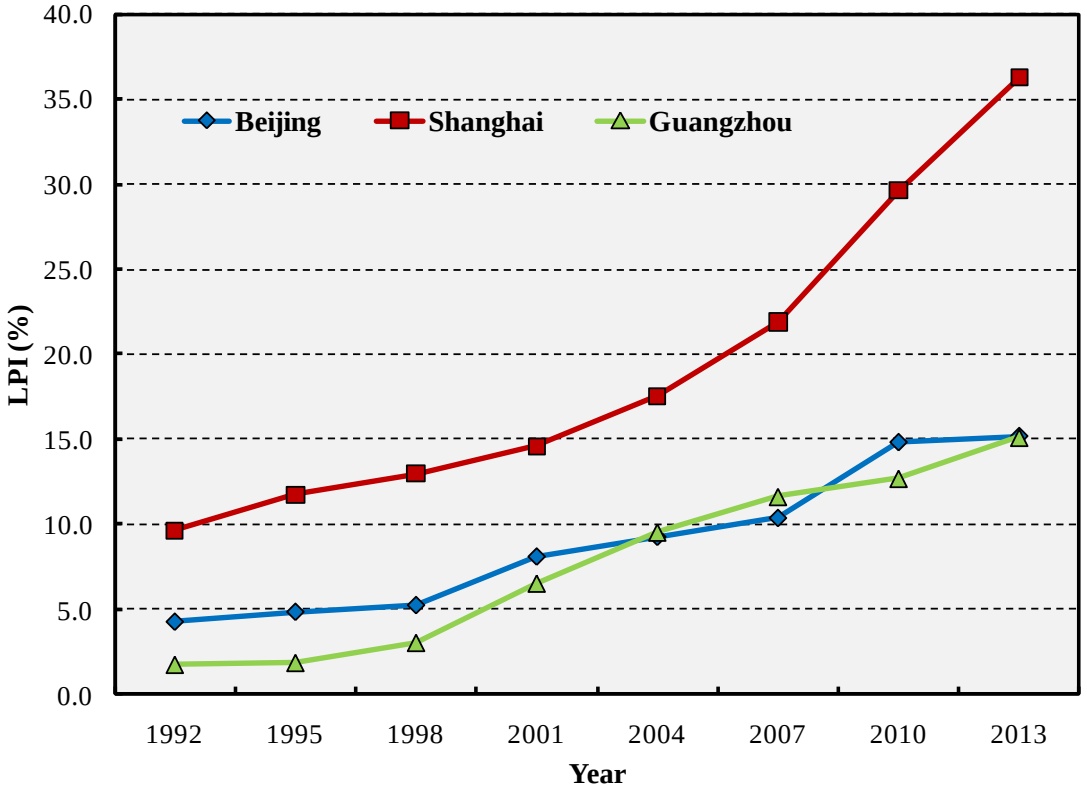

Figure 4-12 Largest patch index of the three cities during the period from 1992 to 2013

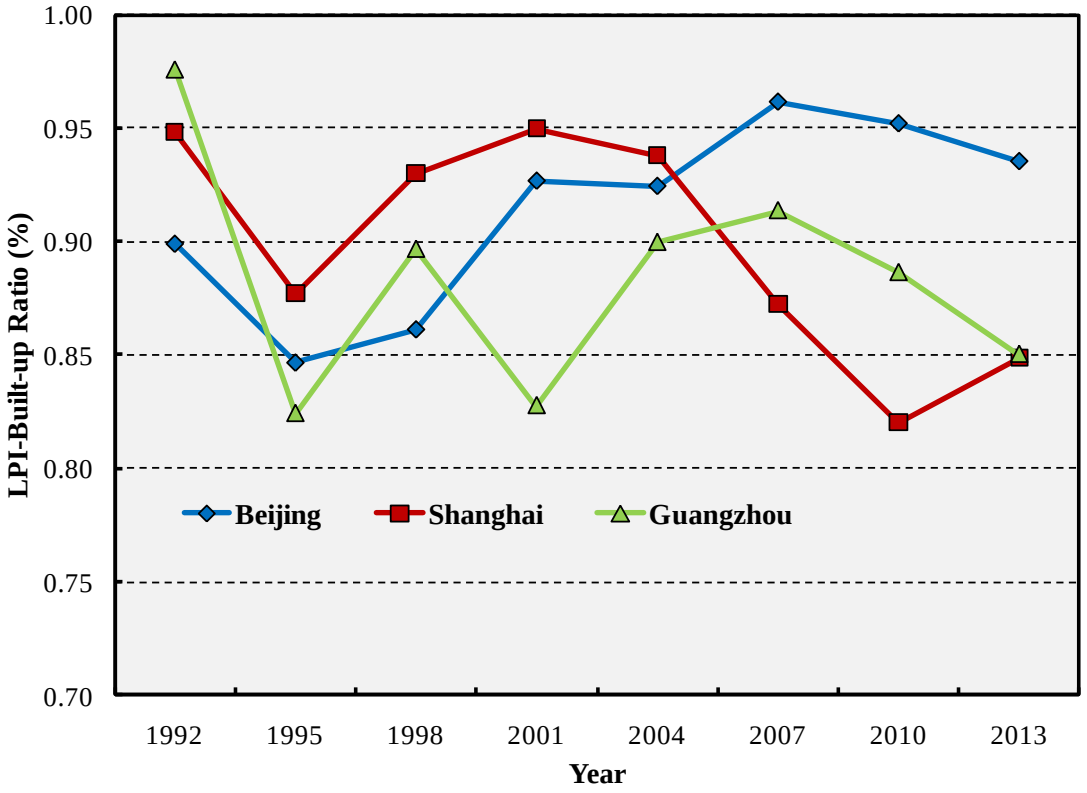

Figure 4-13 LPI-Built up Ratio of the three cities during the period from 1992 to 2013

Figure 4-11 and Figure 4-12 shows the change of percentage of landscape and the largest patch index of the three cities. Percentage of landscape quantifies the proportional abundance of each patch type in the landscape; moreover, largest patch index at the class level quantifies the percentage of total landscape area comprised by the largest patch. As such, it is a simple measure of dominance. To explore the relationship between the largest patch with the total built-up area, we carried another index which named LPI-Built-up ratio to show the change of largest patch development (Figure 4-13). The results indicated the built-up area in the three cities increased obviously in the period from 1992 to 2013. Go depth into the situation in Beijing, both of the percentage of landscape and the largest patch index showed an increasing trend. The largest patch in 1992 occupy for 4.2% percentage of the total area which increased to 15.1% in 2013. However, the LPI-Built-up ratio of Beijing decreased first then increased from about 1998, this tendency is quite differ from the other two cities. The largest patch index in Shanghai increased from 9.6% in1992 to 36.3% in 2013, which is the fastest among the three cities. On the contrary, the LPI-Built-up ratio in Shanghai decreased even though the built-up area increased by a large percentage. The largest patch occupied 0.95% in 1992 and this rate decreased into 0.85% in 2013, the change indicated that there were more and more built-up areas occurred rather than continuous expanding of the largest patch. The situation in Guangzhou is similar with the condition of Beijing. Large patch index increased during the period from 1992 to 2013 which from 1.8% to 17.8% in 1992 and 2013.

4.7.2. Dynamic change of landscape level

At the landscape level, five landscape metrics were selected to analyze the dynamic change characteristics of total land use in the study area: landscape division (DIVISION); landscape shape index (LSI); contagion index (CONTAG), Shannon's diversity index (SHDI) and Shannon's evenness index (SHEI). The result was shown as follows:

Figure 4-14 shows the change of landscape division of the three cities during the period from 1992 to 2013. Division is based on the cumulative patch area distribution and is interpreted as the probability that two randomly chosen pixels in the landscape are not situated in the same patch. The landscape division ranges from 0 to 1, DIVISION = 0 when the landscape consists of single patch. DIVISION is achieves its maximum value when the landscape is maximally subdivided; that is, when every cell is a separate patch. The result

showed that all of the three cities had an increased trend of landscape division. Shanghai City held the highest value of landscape division all through the period from 1992 to 2013. The value of landscape division index increased from 0.50 in 1992 into 0.76 in 2013. The change of value indicated that the division of land use in Shanghai city rose along with the city development. The landscape division index in Beijing city and Guangzhou city also had an obvious increase during the period from 1992 to 2013. Beijing city increased from 0.09 to 0.27 and Guangzhou city increased from 0.04 to 0.52 in 1992 and 2013 respectively.

Figure 4-15 shows the contagion index of the three cities during the period from 1992 to 2013. Contagion is inversely related to edge density. When edge density is very low, for example, when a single class occupies a very large percentage of the landscape, contagion is high, and vice versa. Contagion range from 0 to100%, CONTAG approaches 0 when the patch types are maximally disaggregated and interspersed, such as every cell is a different patch type CONTAG = 100 when all patch types are maximally aggregated. Low levels of patch type dispersion and low levels of patch type interspersion results in high contagion. Contagion index in the three cities showed a decreasing trend as time goes on. The reduce amplitude in Shanghai city and Guangzhou city is bigger than that of Beijing city. Shanghai city decreased from 71.37 percentage of 1992 to 33.54 percentage in 2013. In addition, the reduce rate of contagion index decreased faster from the year of 1998, which proved an evidence that the land use situation in Shanghai city became much more disaggregated and interspersed. As to the Guangzhou city, the division index in 1992 was 91.9 percent, which showed a much aggregated urban form the city held. The division index decreased with the development, the division index decreased into 52.24 percent in 2013. The contagion index in Beijing during the period from 1992 to 2013 also showed a decreased tendency, the value of contagion in 1992 was 83.5 percent, which is greater than Shanghai city but less than Guangzhou city, that means the land use in Beijing city is aggregated than the land use in Shanghai but disaggregated than Guangzhou city. The value of contagion index kept decreased while the vast decreasing occurred in the period of 2007 to 2010.

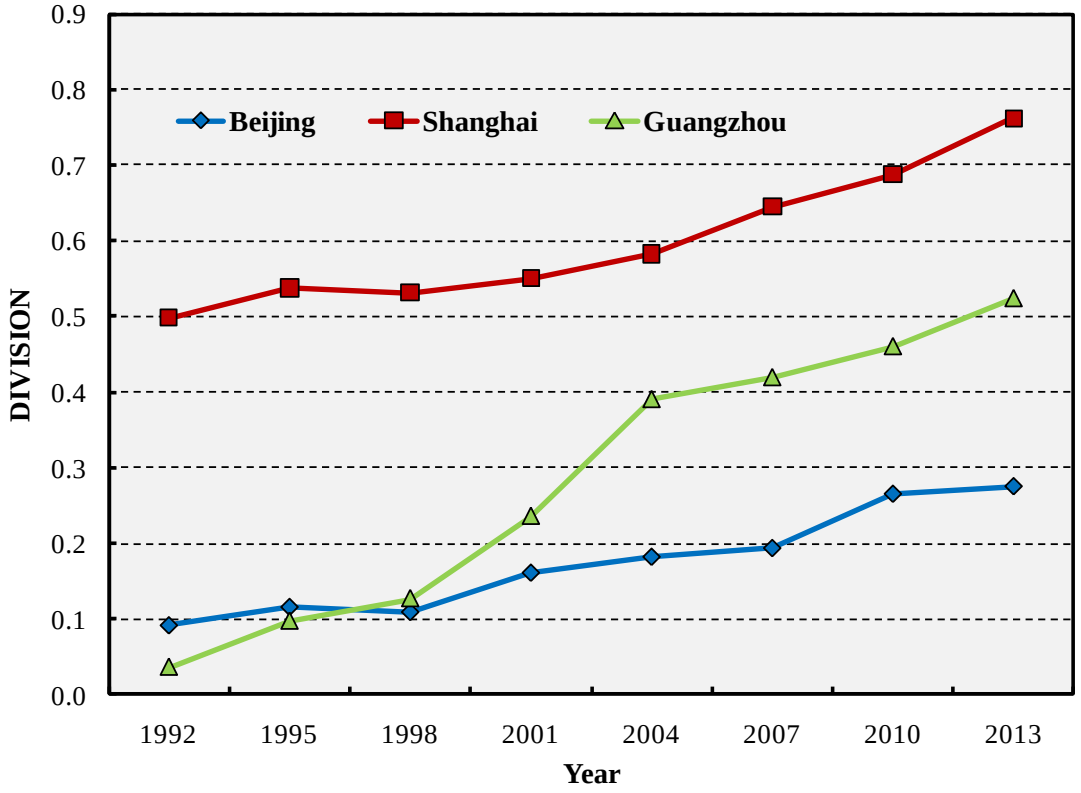

Figure 4-14 Landscape division of the three cities during the period from 1992 to 2013

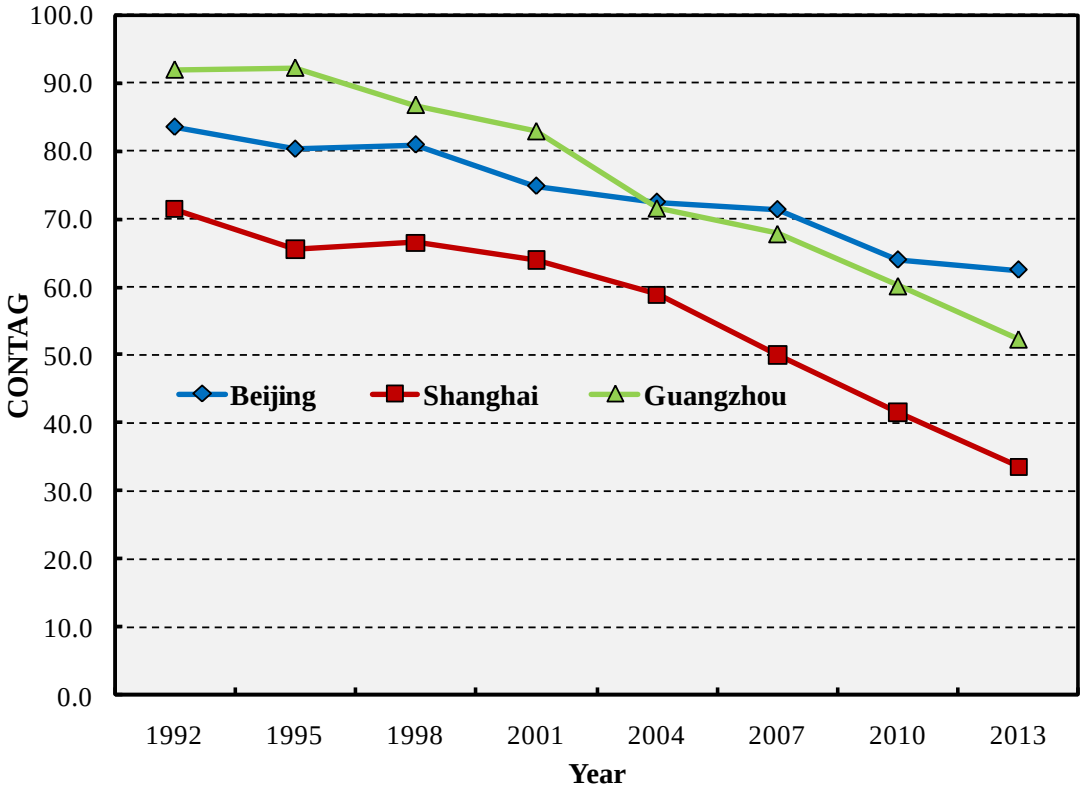

Figure 4-15 Contagion index of the three cities during the period from 1992 to 2013

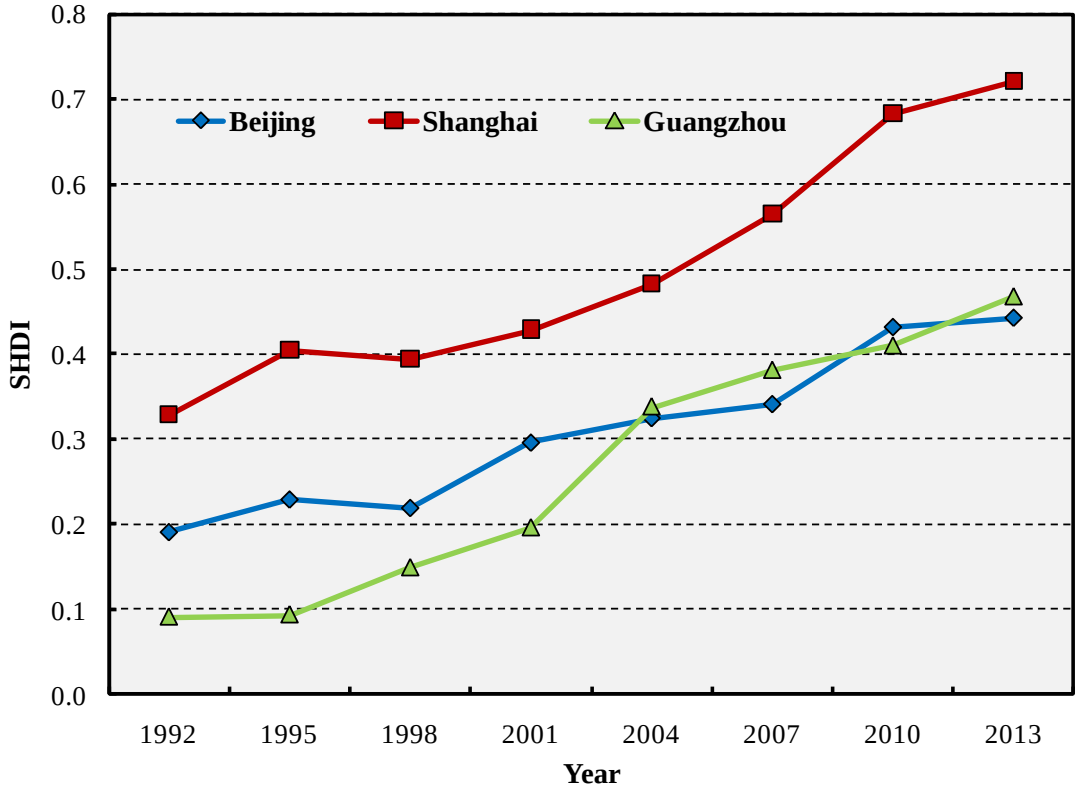

Figure 4-16 Shannon's diversity index of the three cities during the period from 1992 to 2013

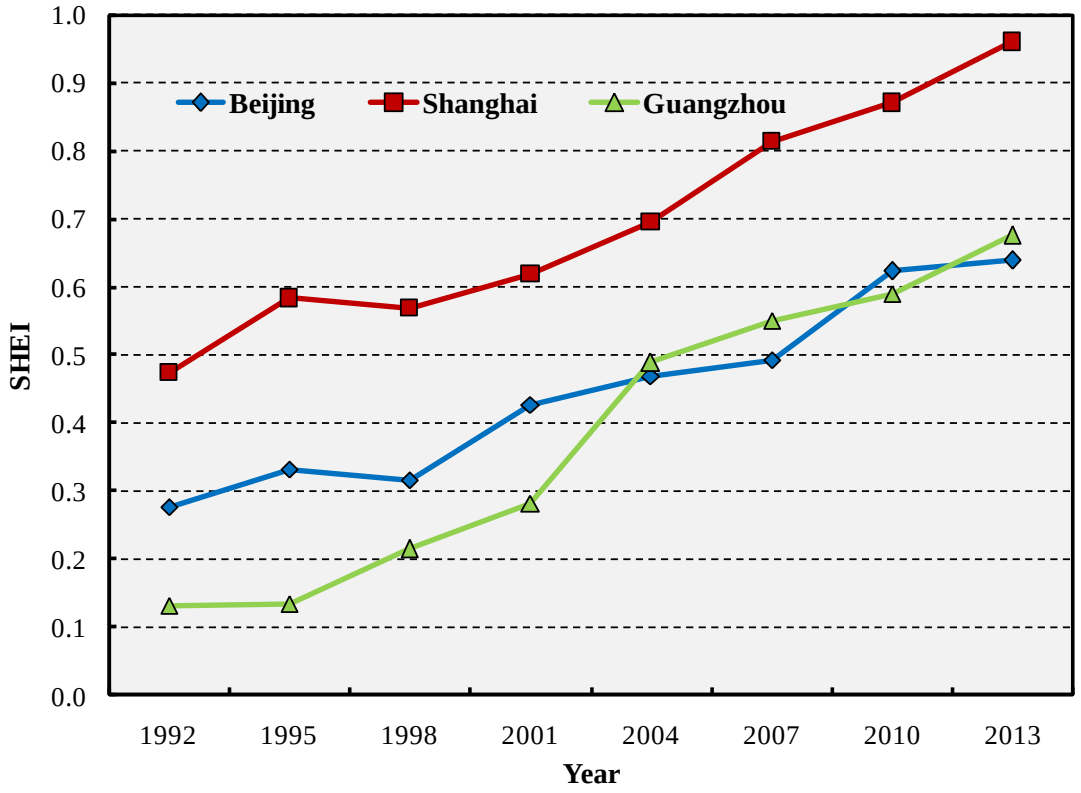

Figure 4-17 Shannon's evenness index of the three cities during the period from 1992 to 2013

Figure 4-16 showed the Shannon's diversity index in the three cities during the period from 1992 to 2013. Landscape diversity metrics are designed to capture richness and evenness, where richness refers to the number of different landscape types in an area; more diverse areas have more landscape types. Shannon's diversity index is a popular measure of diversity in community landscape, in addition, Shannon's diversity index is more sensitive to rare patch types. All of the three cities showed an increase tendency of Shannon's diversity index value. The value in Beijing increased from 0.19 in 1992 to 0.44 in 2013 by an increasing rate of 2.32. Shanghai city increased from 0.33 in 1992 to 0.72 in 2013, by an increasing rate of 2.19. Value of Shannon's diversity index in Guangzhou city increased from 0.09 in 1992 to 0.47 in 2013, by and increasing rate of 5.17 times. Increasing Shannon's diversity index indicated heterogeneity degree of landscape rose, landscape type has developing tendency towards complication or equalizing direction, which directly reflected that built-up land increased while the non-urban area were massively reduced.

The value of Shannon's evenness index in the three cities were calculated and showed in Figure 4-17. Landscape evenness reflects the percentage (of total area) distribution amongst different landscape types and it would be higher when there is a more balanced distribution. The result showed that all of the three cities developed toward a more balance type of land use. The value of Shannon's evenness index in Beijing increased from 0.28 in 1992 to 0.64 in 2013 by an increasing ratio of 2.32 times. Shanghai city also showed an increased tendency of Shannon's evenness index value during the period from 1992 to 2013, which increased from 0.47 in 1992 to 0.96 in 2013, which represents a quite high level of balance development of land use. To the situation in Guangzhou city, the Shannon's evenness index increased from 0.13 in 1992 to 0.68 in 2013, increased by 5.2 times after 20 years development.

4.8. Summary

In this chapter, we carried out measurement and assessment of urban ecological environment by DMSP/OLS stable nighttime light data. Main results can be summarized as follows:

a) The relationship between the NTL indicators and social-economic variables was initially examined through a log-linear regression analysis. The average value of correlation coefficients of annual average DN value with the social-economic indicators is 0.736. On the other hand, the average correlation coefficient of total lit number with social-economics parameters 0.607. For the correlation analysis with urban area proportion, the correlation coefficients were all above 0.788, held an average value of 0.890 The result illustrates that DMSP/OLS NTL based urbanization indicators are effective ways to evaluate and monitor the development at city level.

b) The result of the built-up area extraction of all the three cities showed an obvious expansion during the period from 1992 to 2013. The urban built-up proportion in Beijing increased from 4.75% in 1992 into 16.17% in 2013 by 3.4 times. The proportion in Shanghai increased from 10.17% in 1992 into 42.74% in 2013, increased by 4.2 times. To the situation in Guangzhou, the proportion increased from 1.806 % in 1992 to 17.77% in 2013.

c) To the built-up area expansion index. The average urban expansion index in Beijing city every three years was 0.54% Average expansion rate index in Shanghai was 1.55% every three year. To the situation of Guangzhou city, the average built-up area expansion index was 0.76%, 2001 to 2004 holds the highest expansion rate.

d) From the landscape metrics on class level, all of the three selected metrics Number of patches (NP); Percentage of landscape (PLAND); Largest patch index (LPI) showed an increased tendency in the three cities. The result give a general scene on the scale and speed on the built-up area expansion.

e) The study on the regional landscape pattern change was meaningful to understand dynamic change causes, transformation mechanisms and tendency of land use patterns. The dynamic changes of regional landscape indices can indicate the transformation of regional ecological functions; meanwhile, these characteristics of transformation changes

among various landscape types are beneficial to reveal sustainability of land use. The DIVISION of the three cities increased during the period from 1992 to 2013 which showed an enrichment of land use after 20 years development. Meanwhile, the decrease value of CONTAG also gives reason to the disaggregating and interspersing of the urban built-up area in the three cities. Shanghai Shannon's division index and Shannon's evenness index showed that the landscape of the study region developed toward more diverse and more balanced distribution during the period from 1992 to 2013.

Reference

[1] Xiangzheng Deng, John Gibson, Pei Wang, Relationship between landscape diversity and crop production: a case study in the Hebei Province of China based on multi-source data integration, Journal of Cleaner Production, 142 (2017) 985-992.

[2] R. V. O'Neill, J. R. Krummel, R. H. Gardner, G. Sugihara, B. Jackson, D. L. DeAngelis, B. T. Milne, M. G. Turner, B. Zygmunt, S. W. Christensen, V. H. Dale, R. L. Graham, Indices of landscape pattern, Landscape Ecology, 1 (1988) 153-162.

[3] Junfu Fan, Ting Ma, Chenghu Zhou, Yuke Zhou, Tao Xu, Comparative Estimation of Urban Development in China's Cities Using Socioeconomic and DMSP/OLS Night Light Data, Remote Sensing, 6 (2014) 7840-7856.

[4] Yanxu Liu, Yanglin Wang, Jian Peng, Yueyue Du, Xianfeng Liu, Shuangshuang Li, Donghai Zhang, Correlations between Urbanization and Vegetation Degradation across the World's Metropolises Using DMSP/OLS Nighttime Light Data, Remote Sensing, 7 (2015) 2067-2088.

[5] Qingxu Huang, Xi Yang, Bin Gao, Yang Yang, Yuanyuan Zhao, Application of DMSP/OLS Nighttime Light Images: A Meta-Analysis and a Systematic Literature Review, Remote Sensing, 6 (2014) 6844-6866.

[6] Yongxian Su, Xiuzhi Chen, Chongyang Wang, Hongou Zhang, Jishan Liao, Yuyao Ye, Changjian Wang, A new method for extracting built-up urban areas using DMSP-OLS nighttime stable lights: a case study in the Pearl River Delta, southern China, GIScience & Remote Sensing, 52 (2015) 218-238.

[7] Marc L. Imhoff, Ping Zhang, Robert E. Wolfe, Lahouari Bounoua, Remote sensing of the urban heat island effect across biomes in the continental USA, Remote Sensing of Environment, 114 (2010) 504-513.

[8] Qingling Zhang, Karen C. Seto, Mapping urbanization dynamics at regional and global scales using multi-temporal DMSP/OLS nighttime light data, Remote Sensing of Environment, 115 (2011) 2320-2329.

[9] Christopher D. Elvidge, Daniel Ziskin, Kimberly E. Baugh, Benjamin T. Tuttle, Tilottama Ghosh, Dee W. Pack, Edward H. Erwin, Mikhail Zhizhin, A Fifteen Year Record of Global Natural Gas Flaring Derived from Satellite Data, Energies, 2 (2009) 595-622.

[10] Feng-Chi Hsu, Kimberly Baugh, Tilottama Ghosh, Mikhail Zhizhin, Christopher Elvidge, DMSP-OLS Radiance Calibrated Nighttime Lights Time Series with Intercalibration, Remote Sensing, 7 (2015) 1855-1876.

[11] Xuecao Li, Yuyu Zhou, Urban mapping using DMSP/OLS stable night-time light: a review, International Journal of Remote Sensing, (2017) 1-17.

[12] Zhifeng Liu, Chunyang He, Qiaofeng Zhang, Qingxu Huang, Yang Yang, Extracting the dynamics of urban expansion in China using DMSP-OLS nighttime light data from 1992 to 2008, Landscape and Urban Planning, 106 (2012) 62-72.

[13] Yuyu Zhou, Steven J. Smith, Christopher D. Elvidge, Kaiguang Zhao, Allison Thomson, Marc Imhoff, A cluster-based method to map urban area from DMSP/OLS nightlights, Remote Sensing of Environment, 147 (2014) 173-185.

[14] M. Henderson, E. T. Yeh, P. Gong, C. Elvidge, K. Baugh, Validation of urban boundaries derived from global night-time satellite imagery, International Journal of Remote Sensing, 24 (2003) 595-609.

[15] Bin Gao, Qingxu Huang, Chunyang He, Qun Ma, Dynamics of Urbanization Levels in China from 1992 to 2012: Perspective from DMSP/OLS Nighttime Light Data, Remote Sensing, 7 (2015) 1721-1735.

[16] NBSPRC, National Bureau of Statistics of the People's Republic of China. Avalible online: http://www.stats.gov.cn/ (2016).

[17] Demetris Stathakis, Vassilis Tselios, Ioannis Faraslis, Urbanization in European regions based on night lights, Remote Sensing Applications: Society and Environment, 2 (2015) 26-34.

[18] Lin Ma, Jiansheng Wu, Weifeng Li, Jian Peng, Hao Liu, Evaluating Saturation Correction Methods for DMSP/OLS Nighttime Light Data: A Case Study from China's Cities, Remote Sensing, 6 (2014) 9853-9872.

[19] Xin Cao, Jin Chen, Hidefumi Imura, Osamu Higashi, A SVM-based method to extract urban areas from DMSP-OLS and SPOT VGT data, Remote Sensing of Environment,[20] Jerôme Dupras, Joan Marull, Lluís Parcerisas, Francesc Coll, Andrew Gonzalez, Marc Girard, Enric Tello, The impacts of urban sprawl on ecological connectivity in the Montreal Metropolitan Region, Environmental Science & Policy, 58 (2016) 61-73.

Chapter Five: Macro-Scale Analysis on Climate Change and Urban Heat Island Effects

5.1. Introduction

Urbanization is nowadays a rising trend globally, especially in an alarming rate in developing countries. Urban growth is characterized by the transformation of natural land covers into built up areas (Dewan and Yamaguchi.2009). The modification of land surface will result in urban climate change. Numerous studies have focused on the impact of the urban form on urban environment. Urban form, which is a term that broadly refers to the layout and design of a city, affects ecological and environmental quality through the composition and fragmentation of land pattern, the water and energy consumption, and air movement (Qiao, et al.2014). The traditional method for analyzing UHI is based on LST data, measured at local observation points. However, since 1960, with the advent of high-resolution earth monitoring satellites, remote sensing technology has been widely used for LST measurements and obtainment of another UHI basic data (Weng, et al.2004).

Satellite observation provides a quantitative measurement of urban sprawl and UHI. Advanced Very High Resolution Radiometer (AVHRR) data from the National Oceanic and Atmospheric Administration (NOAA), Thermal infrared (TIR) data from the Thematic Mapper (TM) and Enhanced Tematic Mapper Plus (ETM+), Moderate-Resolution Imaging Spectro radiometer (MODIS) LST products have been successively utilized to study the UHI effect(Amiri, et al.2009). Land Surface Temperature (LST) is an important parameter in the UHI phenomenon, which manifests high spatial and temporal inhomogeneity especially in urban areas (Fu and Weng.2016).

This chapter details the study area, required dataset with the methodology adopted to achieve the aim of this research. Firstly, Beijing was selected as the study area to carry out the UHI observations by retrieval the land surface temperature. The used dataset and the methodology were then adopted to achieve the aim of the research. The dataset collected for this study which is composed of satellite images (i.e. Landsat TM and OLI), geographic data (i.e. City boundary, main road). Then, the spatial correlation and relationship between land surface temperature (LST), normalized difference vegetation index (NDVI) associated with the DMSP/OLS. The result showed a strong negative linear relationship between the urbanization level and NDVI and LST, however, in contrast, a strong positive linear relationship existed between the NTL-DN value and LST. By conducting a spatial comparison

analysis of 1995 and 2009, the vegetation coverage change and surface temperature difference were calculated and compared with the NTL-DN difference. Our result revealed that the regions of fast urbanization resulted in a decrease of NDVI and increase of LST. By conducting a spatial comparison analysis of 1995 and 2009, the vegetation coverage change and surface temperature difference were calculated and compared with the NTL-DN difference. Our result revealed that the regions of fast urbanization resulted in a decrease of NDVI and increase of LST.

As Figure 5-1 shows, the remote sensing data used in this chapter was consisted of two parts: DMSP/OLS NTL and Landsat TM imageries; after necessary preprocessing, the DMSP NTL DN maps and Landsat derived NDVI maps and LST maps in 1995 and 2009 were got to explore the inter-correlation between the urbanization level, surface heat island and vegetation coverage. In addition, the NDVI, LST and NTL-DN difference in 1995 and 2009 were compared to get the change situation of the three indexes in Beijing city. The analysis method in this chapter was composed of three parts: spatial relationship analysis, temporal comparison analysis and urban heat island analysis, respectively.

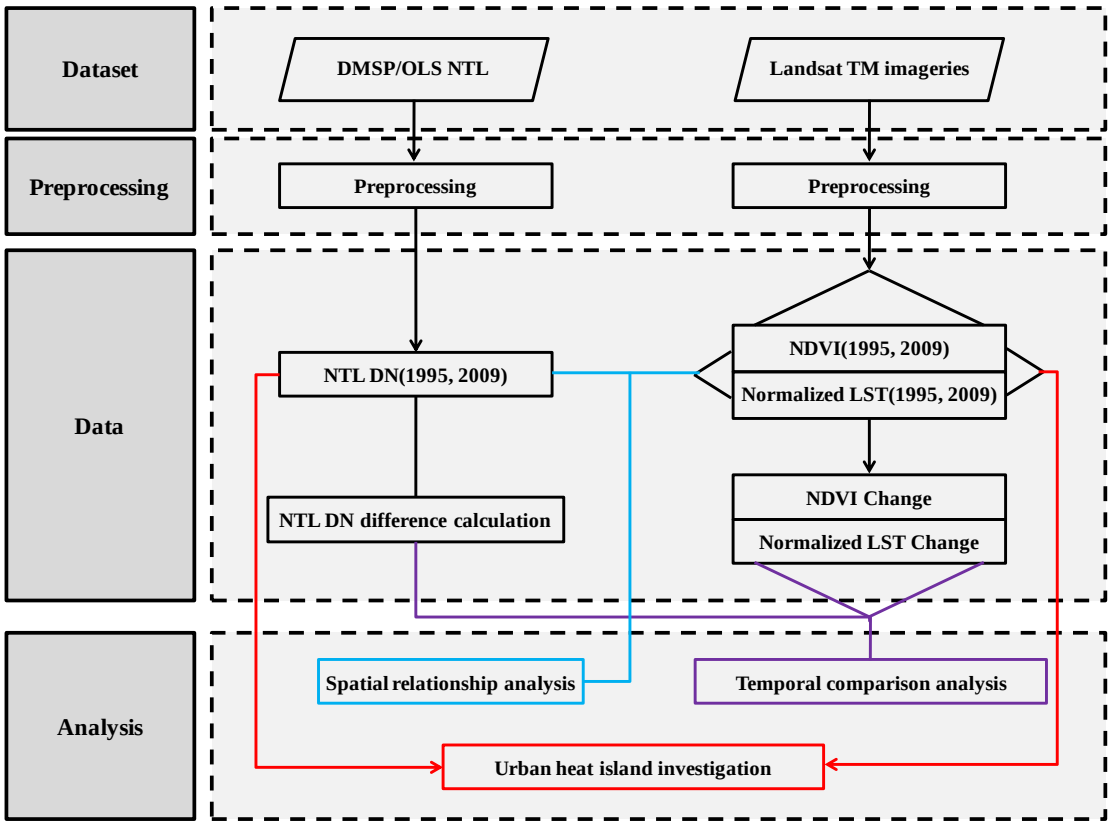

Figure 5-1 Research flow chart

5.2. Satellite imagery introduction

5.2.1. Landsat series images

Landsat TM and OLI images are the key datasets used for this study. This section hence presents a review of the history of the remote sensing industry in conjunction with the characteristics of these satellites. These Landsat data can be freely accessed from the USGS portal, and is processed by NASA to generate radiometric calibration and atmospheric correction algorithms to the Level-1 products.

The first operational space program for scheduled monitoring of land and oceans, namely Landsat 1, was launched on July 23, 1972. The idea of Landsat was proposed in 1965 by the director of the US Geological Survey, William Pecora, for gathering facts about the Earth's resources. The incomparable specifications of satellite images offer an exceptional opportunity for scientists to monitor vast areas at frequent optional periods. Further, the availability of satellite images has led to better simulations of LULC and UHI. This is because future simulation of LULC and UHI is strongly associated with the frequent availability of past patterns of LULC. In this study, the data used in the paper spanned 30 years, which divided into the year nodes of 1985, 1995, 2005, 2009, 2015 originated from Landsat 5, Landsat 7 and Landsat 8 series images.

The Landsat Program is the longest running exercise in the collection of multispectral,

Table 5-1 Information of the Landsat program

Platform	**Launch**	**Decommissioned**	**Operator**	**Sensor**
Landsat 1	1972.06.23	1978.01.06	NASA	MSS, RBV
Landsat 2	1975.01.22	1983.07.27	NASA/NOAA	MSS, RBV
Landsat 3	1978.03.05	1983.09.07	NASA	MSS, RBV
Landsat 4	1982.07.16	2001.06.15	NASA/NOAA	TM, MSS
Landsat 5	1984.03.01	2013.06.05	NASA/NOAA	TM, MSS
Landsat 6	1993.10.05	Didn't achieve orbit	NASA/NOAA	ETM
Landsat 7	1999.04.15	Operational	NASA/USGS	ETM+
Landsat 8	2013.02.11	Operational	NASA/USGS	OLI, TIRS

digital data of the earth's surface from space. The program is managed by the U.S. Geological Survey (USGS) and the National Aeronautics and Space Administration (NASA). The Landsat program offers the longest continuous global record of the Earth‟s surface. It continues to deliver visually stunning and scientifically valuable images of our planet.

Landsat represents the world's longest continuously acquired collection of space-based land remote sensing data. It is considered as the unique national assets. The first Landsat was launched in 1972; the most recent, Landsat 8, was launched on February 11, 2013. The information of each satellite was shown in the Table 5-1 in detail. Here is some explanation of the abbreviations in the table: NASA(National Aeronautics and Space Administration); NOAA(National Oceanic and Atmospheric Administration); USGS(U.S. Geological Survey); MSS(Multispectral Scanner); RBV(Return Beam Vidicon); TM(Thematic Mapper); ETM(Enhanced Thematic Mapper); ETM+(Enhanced Thematic Mapper Plus); OLI(Operational Land Imager); TIRS(Thermal Infrared Sensor).

5.2.1.1. Landsat 5 thematic mapper

On March 1, 1984, the Landsat 5 was launched to the space to collect imagery of the surface of Earth as a continuation of the Landsat Program. After 29 years in space, Landsat 5 was officially decommissioned on June 5, 2013(Sobrino, et al.2004). Recognized by the Guinness Book of Records as the longest-operating Earth-observing satellite mission in history, Landsat 5 orbited the planet more than 150,000 times while transmitting over 2.5 million images of land surface conditions around the world, greatly outliving its original three-year design life.

For more than a quarter of a century, Landsat 5 has observed our changing planet. It has recorded the impact of natural hazards, climate variability and change, land use practices, development and urbanization, ecosystem evolution, increasing demand for water and energy resources, and changing agricultural demand worldwide(Cristóbal, et al.2009). Vital observations of the Mount Saint Helens eruption, Antarctica, the Kuwaiti oil fires, the Chernobyl disaster, rainforest depletion, major wildfires and floods, urban growth, global crop production, and ice shelf expansion and retreat have helped increase our understanding and awareness of the impact of humans on the land.

Table 5-2 Characteristics and applications of TM sensor bands (USGS, 2015a)

Band No.	Spectral Responses	Wavelength interval	Spatial Resolution	Applications
1	Blue	0.45-0.52μm	30m	Coastal water mapping
2	Green	0.52-0.60μm	30m	Soil vegetation differentiation
3	Red	0.63-0.69μm	30m	Deciduous/coniferous differentiation
4	Near Infrared	0.76-0.90μm	30m	Green reflectance by healthy vegetation
5	Mid-Infrared	0.55-1.75μm	30m	Chlorophyll absorption for plant
6	Thermal Infrared	10.4-12.5μm	120m	Specifies differentiation
7	Mid-Infrared	2.08-2.35μm	30m	Biomass surveys

The TM sensor was mounted on Landsat 4, 5 and 6 platforms. Although Landsat 6 mission was unsuccessful, TM sensors on Landsat 4 and 5 have provided valuable information from July 1982. The TM sensor is a whisk broom across track scanner for passive remote sensing missions. In the whisk broom scanner, a mirror scans the ground track of satellites and the information of each pixel is collected by using a single detector. TM records energy in 7 bands of the electromagnetic spectrum, which includes visible, reflective infrared, middle infrared and thermal infrared regions. The TM sensor collects data in 30× 30m resolution in bands 1 through 5 and 7, while thermal band 6 captures images with spatial resolution of 120× 120 m. Table 5-2 shows the spatial and spectral resolution of the TM sensor in tandem with associated applications.

5.2.1.2. Landsat OLI

Landsat OLI is the newest and most advanced member of the Landsat constellation and was launched on February 11, 2013. It was located 705 km above Earth in a sun-synchronous orbit using an Atlas-V rocket. For the first time in Landsat history, it uses push broom sensors to scan Earth's surface. In such sensors "a line of detectors is arranged perpendicular to the flight direction of the spacecraft. As the spacecraft flies forward, the image is collected one line at a time, with all of the pixels in a line being measured simultaneously". The satellite covers the whole globe in 16 days, except for the highest polar latitudes. In line with its predecessors, it captures images with 30 × 30m resolution except in thermal bands. OLI

Table 5-3 Specifications of Landsat OLI spectral and thermal bands (USGS, 2015a)

Band No.	Spectral Responses	Wavelength interval	Spatial Resolution	Applications
1	Coastal aerosol	0.43-0.45μm	30m	Coastal and aerosol studies
2	Blue	0.45-0.51μm	30m	Bathymetric mapping
3	Green	0.53-0.59μm	30m	Emphasizes peak vegetation
4	Red	0.64-0.67μm	30m	Discriminates vegetation slopes
5	Near Infrared (NIR)	0.85-0.88μm	30m	Discriminates moisture of soil and vegetation
6	Short-wave Infrared	1.57-1.65μm	30m	Improved moisture content of soil and vegetation
7	Short-wave Infrared	2.11-2.29μm	30m	Biomass surveys
8	Panchromatic	0.50-0.68μm	15m	15 meter resolution, sharper image definition
9	Cirrus	1.36-1.38μm	30m	Improved detection of cirrus cloud contamination
10	Thermal Infrared 1	10.60-11.19μm	100m	100 meter resolution, thermal mapping and estimated soil moisture
11	Thermal Infrared 2	11.50-12.51μm	100m	100 meter resolution, Improved thermal mapping and estimated soil moisture

images cover an area of 170 km north-south by 183 km east-west. Landsat OLI records Earth's surface in 9 spectral and 2 thermal bands. Its spectral bands provide more information than Landsat TM and ETM. For example, bands 1 and 9 can be used for studying coastal aerosols and cirrus clouds respectively (USGS, 2015a). Table 5-3 presents the details of Landsat OLI bands with associated applications.

5.3. Retrieve of land surface temperature

5.3.1. Method to retrieve the LST

Land surface temperature (LST) is a key variable in climatologically and environmental studies, related to surface energy balance and the integrated thermal state of the atmosphere within the planetary boundary layer. Traditionally, LST was referred to standard surface-air temperature measured by a sheltered thermometer 1.5-3.5 meter above a flat grassy, well-ventilated surface. With satellite technology, another type of LST, satellite-based surface temperature is becoming available globally. Satellite LST products provide an estimate of the kinetic temperature of the earth's surface skin, the aggregate surface medium viewed by the sensor to a depth of about 12 μm. The skin temperature of the surface is inferred from the

thermal emission of the earth's surface and is generally some average effective radiative temperature of various canopy and soil surfaces.

As one of the most important parameters in the UHI phenomenon, land surface temperature, which manifests high spatial and temporal inhomogeneity especially in urban areas(Fu and Weng.2016). LST is actually the skin temperature of the land surface which differs from the land surface air temperature. Land surface temperature can be derived from freely available data sources such as Landsat, MODIS and ASTER (Zhou, et al.2014). The thermal band of these sensors enables data collection on thermal properties of the land surface based on the amount of emitted energy. Besides, such data can also be used to monitor LULC change over time. Thus these two prospects enabled researchers to explore the link between LULC change and LST change over time. In this way, monitoring UHI effect due to LULC change has become feasible (Cristóbal, et al.2009).

A lot of algorithms have been proposed such as Single Channel, Split window, Mono window, Radiative transfer equation etc. to obtain the land surface temperature from a original satellite dataset (Taleghani, et al.2014, Dos Santos, et al.2017). Among these methods, Split window relies on two spectrally adjacent thermal bands, but Landsat 4, 5 and even ETM+ possess only one thermal band. Thus this method is unsuitable for those images. Similarly the problem with the Radiative transfer equation method is that it requires in-situ radio sounding to be launched concurrently with satellite pass. Like Radiative transfer equation method, Mono window method also involves various parameters such as effective mean atmospheric temperature, emissivity and transmittance to be determined, which requires in-situ measurement. Single Channel method on the other hand requires high quality atmospheric transmittance code to estimate the atmospheric features involved in the model, and is complicated. Therefore, explicitly an image based approach utilizing surface emissivity representing the brightness temperature only, without requiring atmospheric profile parameters has been considered in this study.

According to the review above, in this paper, we adopted the method of the Single-Channel algorithm to obtain LST from the thermal band of Landsat TM sensor data.this algorithm provides a simple and highly effective method for obtaining LST, thus facilitating the study and analysis on UHI effects. This method can be used in order to process both Landsat TM

and OLI data. It consists of 3 separate steps, namely, NDVI Thresholds, Thermal Band to Brightness Temperature and Retrieve LST (Land Surface Temperature).

5.3.2. Pre-processing of the Landsat imageries

The Landsat images were collected from the United satates Geological Survey Earth Explore website. Pre-processing steps are necessary to prepare raw satellite images for processing. The general pre-processing steps include detection and restoration of bad lines, geometric correction, radiometric calibration (normalisation), atmospheric correction (AC) and topographic correction (Weng, et al.2004). Figure 5-2 shows the steps of the preprocessing required for imageries before the retrieve of the LST.

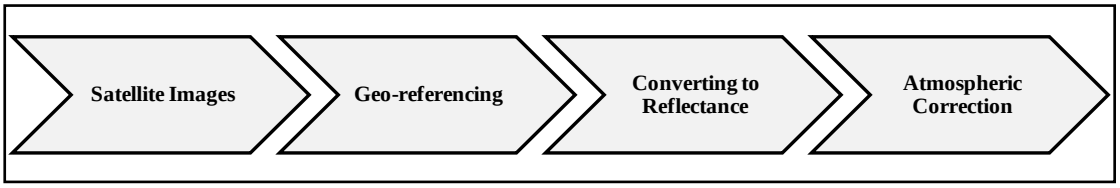

Figure 5-2 Pre-processing steps of Landsat TM and OLI iamges

5.3.2.1. Geo-referencing

The objective of the process of Geo-referencing is to remove geometric distortions of satellite images so that every pixel will be in its proper planimetric map location. In this study, the satellite images were acquired as level 1T processing with geometric accuracy less than 1 pixel, which is acceptable for a long-term monitoring of UHI, therefore, geo-referencing was not applied in this study.

5.3.2.2. Converting to reflectance

Reflectance is defined as “the proportion of the radiation striking a surface to the radiation reflected off of it” Reflectance values are classified into two types. Firstly, top-of-atmosphere (TOA) reflectance measured by devices above the atmosphere from the satellites. In the application of the remote sensing data for surface conditions, the atmospheric effects should be removed from TOA reflectance values before they can be used in further processing. The second kind of reflectance is named surface reflectance, whose values are ready for extracting quantitative information about the features on the earth(Chander, et al.2009).

Normalization is required when classification is conducted by using either multi-temporal images or different sensor types. Satellite thermal infrared (TIR) sensors measure top of the

atmosphere (TOA) radiance, from which brightness temperature can be derived using Plank's law (Dash, et al.2002). The TOA radiances are the mixing result of three fractions of energy:

a) Emitted radiance from the Earth's surface,

b) Upwelling radiance from the atmosphere,

c) Downwelling radiance from the sky.

Therefore, atmospheric effects, including absorption, upward emission, and downward irradiance reflected from the surface must be corrected before land surface brightness temperatures are obtained.

The conversion of reflectance for Landsat TM and Landsat OLI is different, detailed introduction is shown as following.

a) Landsat TM conversion

In this study, we employed all bands of TM images excluding the thermal band (band 6). The first step is calculation of at-sensor spectral radiance in converting image data into a physically meaningful common radiometric scale. The following equation was applied to convert the digital numbers for both reflective and thermal bands to at-sensor radiance

$$L_\lambda = \frac{LMAX_\lambda - LMIN_\lambda}{Q_{calmax} - Q_{calmin}} \times (Q_{cal} - Q_{calmin}) + LMIN_\lambda, \quad (5-1)$$

Where:

L_λ is the spectral radiance at the sensor's aperture in W/(m^2 sr μm);

Q_{cal} is the quantized calibrated pixel value in DN;

Q_{calmin} is the minimum quantized calibrated pixel value corresponding to $LMIN_\lambda$;

Q_{calmax} is the maximum quantized calibrated pixel value corresponding to $LMAX_\lambda$;

$LMIN_\lambda$ is the spectral radiance that is scaled to Q_{calmin} in W/(m^2 sr μm);

$LMAX_\lambda$ is the spectral radiance that is scaled to Q_{calmax} in W/(m^2 sr μm).

Then the TOA reflectance values of TM images were calculated by using the equation below, the processing was conducted by the software of ArcGIS. The following equation states the conversion the digital number of pixels to TOA value:

$$\rho_\lambda = \frac{\pi \cdot L_\lambda \cdot d^2}{ESUN_\lambda \cdot cos\theta_s} \quad (5-2)$$

Where:

ρ_λ is the unitless planetary reflectance;

L_λ is the spectral radiance at the sensor's aperture in W/(m^2 sr μm);

d is the earth-sun distance (in astronomical units);

$ESUN_\lambda$ is the mean solar exo-atmospheric irradiance in W/(m^2 μm);

θ_s is the solar zenith angle in degrees.

b) Landsat OLI conversion

Differ from Landsat TM and Landsat ETM, the Landsat OLI offers new bands which were not available in its predecessors. According to the USGS, the TOA reflectance of OLI bands of 2, 3, 4, 5, 6, and 7 were calculated based on the equation which proposed by Li et al. (Li, et al.2013):

$$\rho_\lambda{}' = M_P Q_{cal} + A_P \qquad (5-3)$$

Where:

$\rho_\lambda{}'$ is the TOA reflectance without correlation for solar angle;

M_P and A_P are rescaled factors available in the meta data file respectively;

Q_{cal} is the DN of pixels.

To correct the obtained TOA reflectance values for the solar angle, the following equation was then applied:

$$\rho_\lambda = \frac{\rho_\lambda{}'}{\sin(\theta_{SE})} \qquad (5-4)$$

Where:

ρ_λ is the corrected TOA reflectance for sun angle;

θ_{SE} refers to sun elevation angle in degree derived from the metadata file of Landsat OLI images.

5.3.2.3. Atmospheric correction

Although converting digital numbers of satellite images to TOA values provides more accurate information about the Earth's surface, TOA values contain anomalies due to atmosphere effects. It is thus critical to remove such anomalies and obtain surface reflectance values. The images with surface reflectance values then can be used to extract quantitative information about associated features.

5.3.3. Derivation of NDVI

The NDVI index is a measure of the amount and vigor of vegetation at the surface. As vegetation reflects well in the near infrared part of the spectrum, NDVI has become a simple graphical indicator to assess the vegetation coverage of the target. Numerous studies have focused on understanding the relationship between LST and NDVI, and concluded that a close relationship between them existed. he Normalized Difference Vegetation Index (NDVI) is a measure of the amount and vigour of vegetation at the surface. It is a simple graphical indicator that can be used to assess whether the target being observed contains green vegetation or not, as a result , the NDVI can be considered as the index which can reflect the situation of the vegetation of the target. The reason NDVI is related to vegetation is that healthy vegetation reflect very well in the near infrared part of the spectrum. Green leaves have a reflectance of 20% or less in the 0.5 to 0.7 μm range (green to red) and about 60% in the 0.7 to 1.3 μm range (near infrared). The NDVI can be calculated by the pixel value of band 3 and band 4 from the equation below.

For this study, to explore the relationship between vegetation coverage and LST and DMSP/OLS based urbanization level, the Landsat image based NDVI was calculated as the reflection of the vegetation coverage. Data supplied by Band 3 and Band 4 of Landsat TM, Band 4 and Band 5 of Landsat OLI can be used to construct this vegetation index according to the following equation:

$$NDVI = \frac{Band\ 4 - Band\ 3}{Band\ 4 + Band\ 3} \qquad (5-5)$$

Where:

Band 4 and Band 3 are Bands of Landsat TM images.

$$NDVI = \frac{Band\ 5 - Band\ 4}{Band\ 5 + Band\ 4} \qquad (5-6)$$

Where:

Band 5 and Band 4 are Bands from Landsat OLI images.

Theoretically, NDVI values are represented as a ratio ranging in value from -1 to 1 but inpractice extreme negative values represents water, values around zero represent bare soil or no green area and values close to 1 represent dense green vegetation possible. Researches related has shown that the NDVI is directly related to the photosynthetic capacity and hence

energy absorption of plant canopies, that is to say, the NDVI value stand for the vegetation rate directly.

5.3.4. Thermal band DN to brightness temperature

The procedure described by Weng et al. was adopted for retrieval of LST. The thermal infrared Bands (Band 6) of Landsat TM and (Weng, et al.2004) TM and ETM+ sensors have only one thermal band, while the Landsat 8 TIRS has two spectrally adjacent thermal bands (bands 10 and 11). However, as showed in the USGS Landsat Web site, there is calibration uncertainty associated with band 11. In addition, Tsou et al. have made a made a comparison and found that when using single band LST estimated from band 10 has a higher accuracy than band 11(Tsou, et al.2017). So in this research, we used band 10 of the Landsat 8 TIRS to retrieve the LST. The processing was composed of four parts:

a) Firstly, converting spectral radiance to at-sensor spectral which is a more physically useful variable, this step was calculated by equation (4-1);

b) Secondly, to converting the result of step one to at-sensor brightness temperature, this part was proceed under an assumption that the earth's surface is a black body and using the formula as below;

$$T_B = \frac{K_2}{\ln\left(\frac{K_1}{L_\lambda} + 1\right)} \qquad (5-7)$$

Where:

T_B is the effective at sensor brightness temperature in Kelvin;

L_λ is the spectral radiance at the sensor's aperture in W/(m^2 sr μm);

K_1 and K_2 are the calibration constant for Landsat TM; K_1 is 607.76 W/(m^2 sr μm); and K_2 is 1260.56 K.

c) Third, the obtained brightness temperatures were referenced to a black body, which differ from the properties of real objects. Correction for spectral emissivity (ε) is a must and the emissivity corrected surface temperature was computed as follows:

$$T_s = \frac{T_B}{1 + (\lambda \times T_B/\alpha)\ln\varepsilon} \qquad (5-8)$$

Where:

T_s is the surface radiant temperature in Kelvin;

T_B is the effective at sensor brightness temperature in Kelvin;

λ is the wavelength of emitted radiance, herein, $\lambda = 11.5\mu m$;

$\alpha = \square c/b$ $(1.438 \times 10^{-2}$m K);

b is the Bolzmann constant $(1.38 \times 10^{-23}$ J/K);

$\square$ is Plank's constant $(6.626 \times 10^{-34}$ Js);

c is the velocity of light $(2.998 \times 10^{8}$ m/s);

ε is the surface emissivity which can be calculated from NDVI, the estimation was shown in Table 5-4 below.

Table 5-4 Estimation of surface emissivity using NDVI

NDVI	**Land surface emissivity**
NDVI < -0.185	0.995
-0.185 ≤ NDVI < 0.157	0.970
0.157 ≤ NDVI ≤ 0.727	1.0094 + 0.047 Ln(NDVI)
NDVI > 0.727	0.990

As the surface radiant temperature is in Kelvin, which differs from the commonly used centigrade, the LST in Celsius was calculated by adding the absolute zero (approximately -273.15 □).

d) Finally, to ensure that the images from different years were comparable, normalized land surface temperature was put forward, which quantified the LST range from 0–1. The calculation required the equation below:

$$LST_{nor} = \frac{LST - LST_{min}}{LST_{man} - LST_{min}} \times 100\% \qquad (5-9)$$

Where:

LST_{nor} is the normalized land surface temperature;

LST_{min} and LST_{max} are the minimum and maximum value obtained within the study region, respectively.

5.4. Urban heat island in Beijing

5.4.1. Study area and period

In this research, the investigation of urban heat island effects in Beijing was carried out by two different scales: one is under the whole administration city boundary to explore the distribution and development of urban heat island; another one is under the Beijing 6th ring road boundary to analysis the situation in the urban core area of the city.

In order to investigate the phenomenon of urban heat island, ArcGIS have been put into use as an important tool to help getting the result of NDVI and LST and get the statistical data for further analysis. During the processing of theordinary data from remote sensing, several programs and tools in the ArcGIS was used as the image management measures.

For this part, Four Landsat 5 TM images were collected on 16 September 1995 (Landsat Scene ID: LT51230321995259HAJ00 and LT51230331995259HAJ00) and 22 September 2009 (Landsat Scene ID: LT51230322009265IKR00 and LT51230332009265IKR00) from the United States Geological Survey (USGS) Earth Explorer website (Table 5-5). The Landsat

Table 5-5 Detailed information of the collected data

Items	**Year**	
	1995	**2009**
Landsat scene ID	LT51230321995259HAJ00 LT51230331995259HAJ00	LT51230322009265IKR00 LT51230322009265IKR00
Station ID	HAJ	IKR
Data Type	L1T	L1T
Space Craft ID	Landsat 5	Landsat 5
Snesor ID	TM	TM
WRS-Path	123	123
WRS-Row	32	32
Data Acquired	1995.09.16	2009.09.22
Scene Center Time	1:55:25	2:43:41
Cloud Cover	0	0
Sun Azimuth	132.41	134.51
Sun Elevation	41.92	57.09
Map Projection	UTM-WGS84	UTM-WGS84

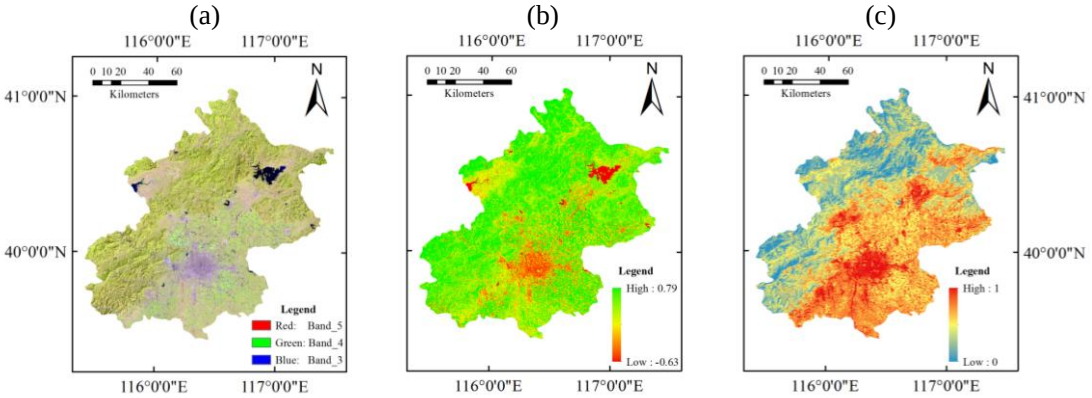

Figure 5-3 Distribution map of Landsat TM composite image, NDVI, and LST_{nor} in 1995

(**a**) Landsat TM composite image in 1995 (RGB = 432); (**b**) Distribution map of NDVI in 1995; (**c**) Distribution map of normalized LST in 1995;

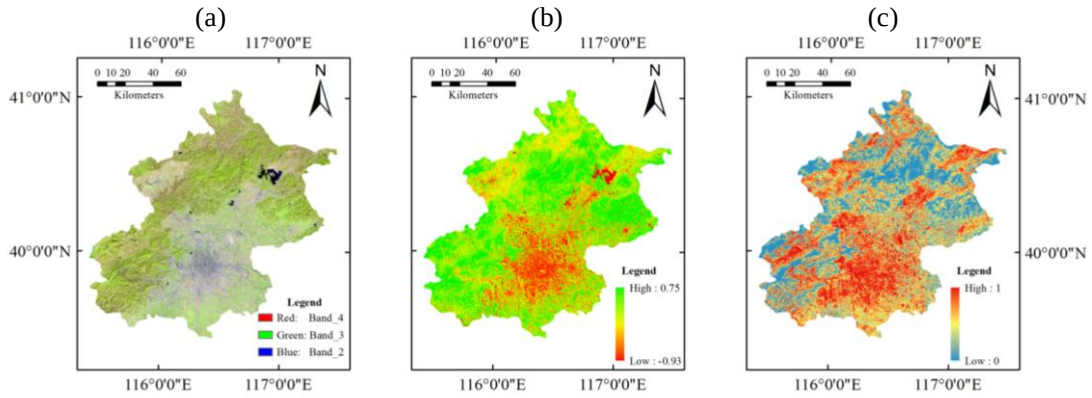

Figure 5-4 Distribution map of Landsat TM composite image, NDVI, and LST_{nor} in 2009

(**a**) Landsat TM composite image in 2009 (RGB = 432); (**b**) Distribution map of NDVI in 2009; (**c**) Distribution map of normalized LST in 2009;

TM images were all acquired under clear sky conditions. The images were further rectified to the Universal Transverse Mercator projection system (datum WGS84, UTM zone N50). Then the NDVI and LST were calculated by the method which introduced in the previous section.

Due to the Beijing city covers two neighbouring datasets, before the calculation, it is nesscessary to masaic the two datasets together and clip by the city bouondary. Figure 5-3 (a) and Figure 5-4 (a) showed the derived Landsat TM based composite images. Six reflective multispectral bands (Bands 1-5, Band 7) were used for compositing. Then the map was displayed by the rules below: Band 4 in Red, Band 3 in Green and Band 2 in Blue which also be called as the natural color.

5.4.2. Spatial distribution of NDVI and LST

Figure 5-3 (b) and Figure 5-3 (b) shows the spatial pattern of vegetation in 1995 and in 2009. An obvious horizontal gradient appeared between the urban area and its surroundings in both 1995 and 2009. The value of the NDVI ranges from –0.63 to 0.79 in 1995, and changes to –0.93 to 0.75 in 2009, and it can be seen that the NDVI changed significantly due to urban expansion during this period.

5.4.3. Spatial distribution of LST

Figure 5-3 (c) and Figure 5-3 (c) shows the spatial distribution of LST in 1995 and 2009.The normalized land surface temperature in the downtown area is obviously higher than that in the surroundings. Through a visual inspection, a surface urban heat island existed within the city.

5.4.4. Spatial relationship analysis of DMSP/OLS NTL and landsat images

An analysis based on the DN value was also conducted to explore the spatial correlation between the DMSP/OLS NTL-DN and Landsat based parameters. The calibrated NTL images are shown in Figure 5-5 (a) and Figure 5-6 (a) to represent the spatial distribution characteristics of NTL-DN in 1995, and 2009. Next, the average values of NDVI and LSTnor in each year were calculated using different NTL-DN values to adopt in the regression analysis with the NTL-DN value. To obtain the relationship between the NDVI and mean NTL-DN in 1995 and 2009, the results showed that as the value of NTL-DN increased, the trend of mean NDVI decreased, so the coefficient determination of each year reached 0.754 in 1995 (Figure 5-5 (b)) and 0.929 in 2009 (Figure 5-6 (b)), respectively, which suggests a close negative correlation between the NTL-DN and mean NDVI. The results revealed that in areas with a relatively higher NTL-DN value, the vegetation coverage would be less than in lower NTL-DN value areas. Meanwhile, the correlation between LST_{nor} and mean NTL-DN in 1995 (Figure 5-5 (c)) and 2009 (Figure 5-6 (c)) were established, and in contrast to the mean NDVI, the LST_{nor} showed a close positive correlation with determination coefficients reaching 0.651 in 1995 and 0.926 in 2009. In both years, the LST_{nor} showed an increasing trend along with the rise of the NTL-DN value, which can be used to draw conclusions on how the urbanization level impacts the temperature distribution. The results indicate that an area with a higher NTL-DN value (that is more urbanized), the mean LST_{nor} within it would be higher than the surroundings, which provides strong evidence that the surface urban heat island effects are influenced by urban development.

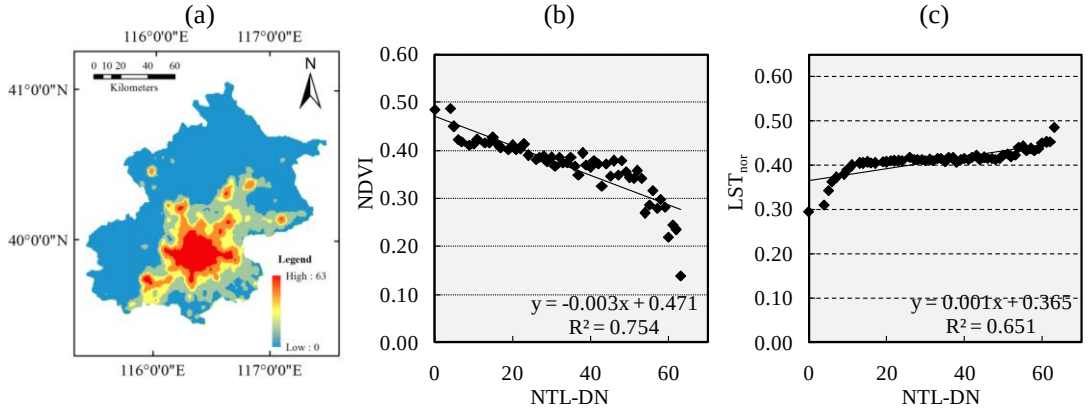

Figure 5-5 Spatial correlation analysis of NTL-DN and Landsat images in 1995: (**a**) Distribution map of NTL-DN in 1995; (**b**) Scatter plots between the NTL-DN and NDVI in 1995; (**c**) Scatter plots between the NTL-DN and LST_{nor} in 1995;

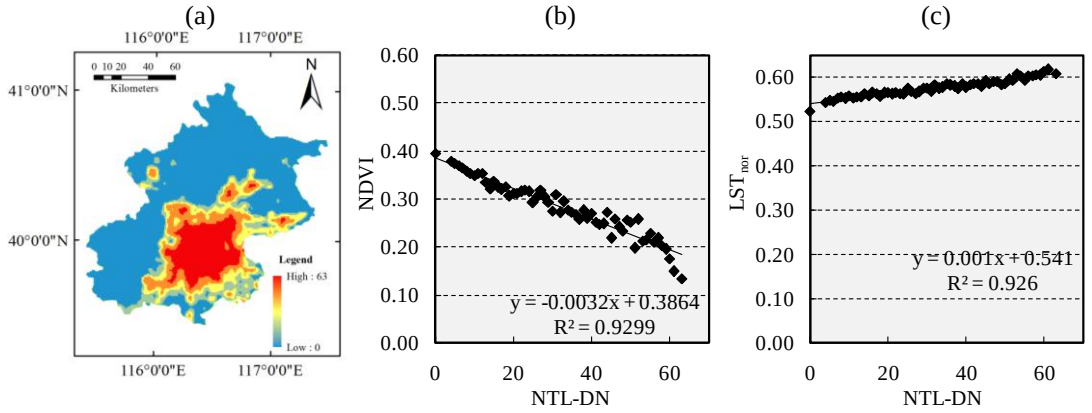

Figure 5-6 Spatial correlation analysis of NTL-DN and Landsat images in 2009: (**a**) Distribution map of NTL-DN in 2009; (**b**) Scatter plots between the NTL-DN and NDVI in 2009; (**c**) Scatter plots between the NTL-DN and LST_{nor} in 2009;

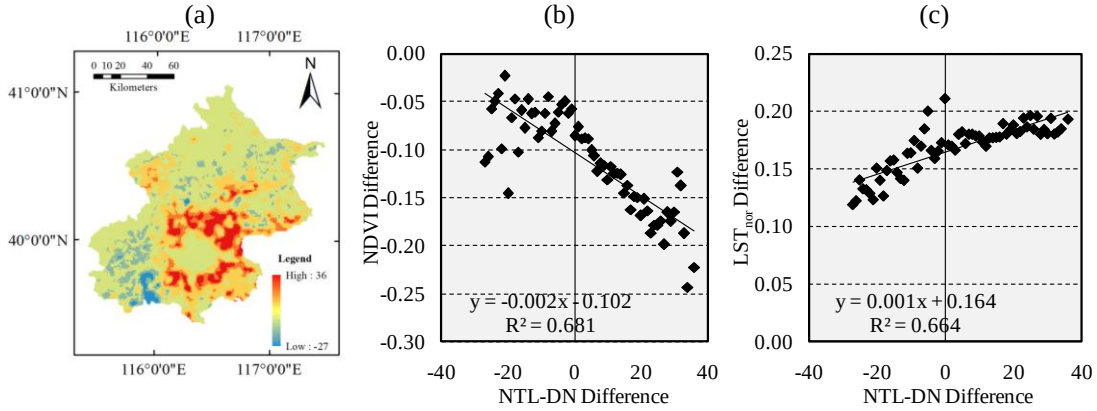

Figure 5-7 Spatial comparison analysis of NTL-DN and Landsat images: (**a**) Distribution map of the NTL-DN difference between 1995 and 2009; (**b**) Scatter plots between the NTL-DN difference and NDVI change between 1995 and 2009; and (**c**) Scatter plots between the NTL-DN difference and LST_{nor} change between 1995 and 2009.

5.4.5. Spatial-temporal comparison analysis in 1995 and 2009

To investigate the influence of SUHI driven by urban development, the images of NTL-DN, NDVI and LSTnor from two years was composited to obtain the difference between 1995 and 2009. Next, a spatial-temporal comparison analysis was carried out to explore the variation in vegetation coverage situation and the SUHI effects from the urbanization process revealed by NTL images. Figure 5-7 (a) shows the spatial pattern of the NTL-DN difference between the two years through visual assessment, with the NTL-DN of the previous downtown area remaining unchanged, whereas the surrounding areas had an obvious increase in NTL-DN value, which matched the urban sprawl and expansion in Beijing during this period. With the extraction of the NTL-DN difference, correlation analysis was then carried with using the NDVI difference during the research period (Figure 5-7(b)). The NDVI difference showed a negative correlation with the NTL-DN difference, where the determination coefficient reached 0.681, and the correlation was more obvious in the range where the NTL-DN difference had a positive value. The result suggested that the urbanization process would reduce vegetation coverage, given that urban sprawl changed the vegetation area into impervious surfaces. Another correlation analysis was conducted with the NTL-DN difference and LSTnor difference (Figure 5-7 (c)), where the result clearly demonstrated a positive correlation between the two parameters, where the coefficient of determination was 0.664. Areas with a higher value of NTL-DN difference, which represent faster urbanization zones, and the LSTnor difference showed a tendency to increase. The faster the development in the area, the higher the increase of LSTnor difference the area has. Additionally, the result further illustrated how urbanization affected the SUHI quantitatively over time in the city.

5.5. Spatial relationship between NTL-DN and UHI in Beijing

Figures 5-8 (a) and Figure 5-9 (a) showed the spatial pattern of urban heat island zones in 1995 and 2009, respectively. The average normalized LST was calculated within each NTL pixel to indicate the surface temperature distribution. Next, choropleth maps were produced based on the classification scheme of standard deviation, in which the first-class data values were greater than one standard deviation above the mean, and second-class values were between the mean and one standard deviation above the mean, and so on. Thus, the area was divided into four categories: heat island zone, sub-heat island zone, medium temperature zone, and low temperature zone. In both 1995 and 2009, the urban heat island zone was obviously assembling in the city center, and the heat island zone had a large expansion from all directions. Figures 5-8 (b) and Figure 5-9 (b) shows the area proportions and the average LST for the four categories, where the percentage of urban heat island zone increased from 9.3% in 1995 to 21.7% in 2009; the sub-heat island zone had no significant change from 29.3% to 28.6%; and both the medium temperature and low temperature zones had a decrease of area proportion, especially the low temperature area which decreased from 44.0 to 35.7%. These changes indicated an adverse effect on the thermal environment through the urbanization process from 1995–2009, and that the urban heat island zone occupied a higher proportion than before.

To better understand the relationship between the NTL-DN, NDVI and UHI zones, the statistics of average NTL-DN and NDVI in different UHI zones were obtained by super-imposing the heat island maps with images of NTL and NDVI. From Figures 5-8 (c) and Figure 5-9 (c), we obtained the characteristics of average NTL-DN and NDVI of each zone in 1995 and 2009. In both 1995 and 2009, the value of average NTL-DN presented a rising gradient from the low temperature zone to the heat island zone, whereas the NDVI showed a downward trend. The urban heat island zone held the highest average NTL-DN value of 58.26 in 1995, and the average values in the other three zones were 35.40, 25.73 and 10.03, respectively. In 2009, the average NTL-DN values in the four zones were 12.65, 24.95, 41.26 and 54.34, respectively, from the low temperature zone to the heat island zone. The results illustrated the spatial correlation between the surface temperature and the NTL images. The urban heat island zones located in more developed areas, the sub-heat island and medium

temperature zones took second and third place, and the low temperature zones were mainly located in the western and northern parts of the city where most of the area was covered with mountains and forests that have lower NTL-DN values than downtown. Furthermore, in both 1995 and 2009, the low temperature zones had the highest value of NDVI, whereas the urban heat island zones had the lowest. These results showed a positive correlation between the proportion of green space and their cooling effects.

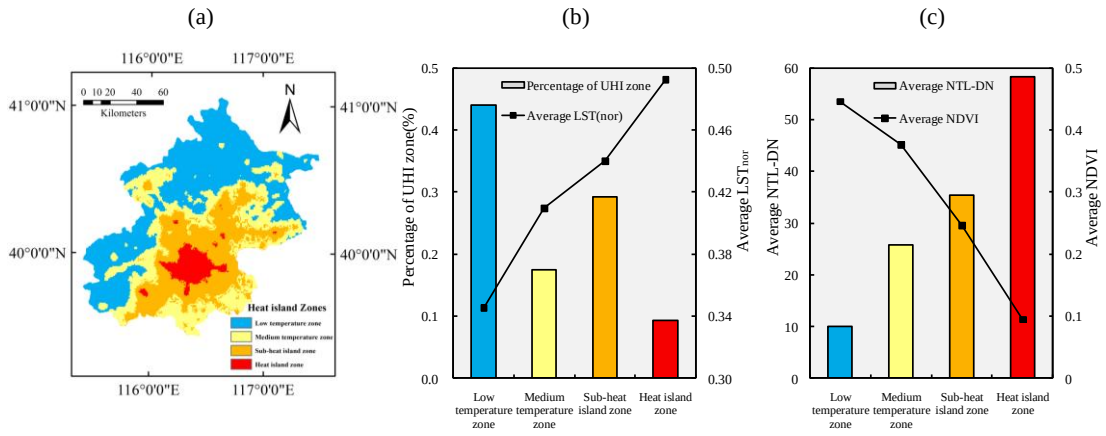

Figure 5-8 Heat island analysis results with NTL-DN and Landsat images in 1995: (**a**) Spatial pattern of heat island zones in 1995; (**b**) Proportions of UHI zones and average LST_{nor} in 1995; (**c**) Average NTL-DN and average NDVI of UHI zones in 1995;

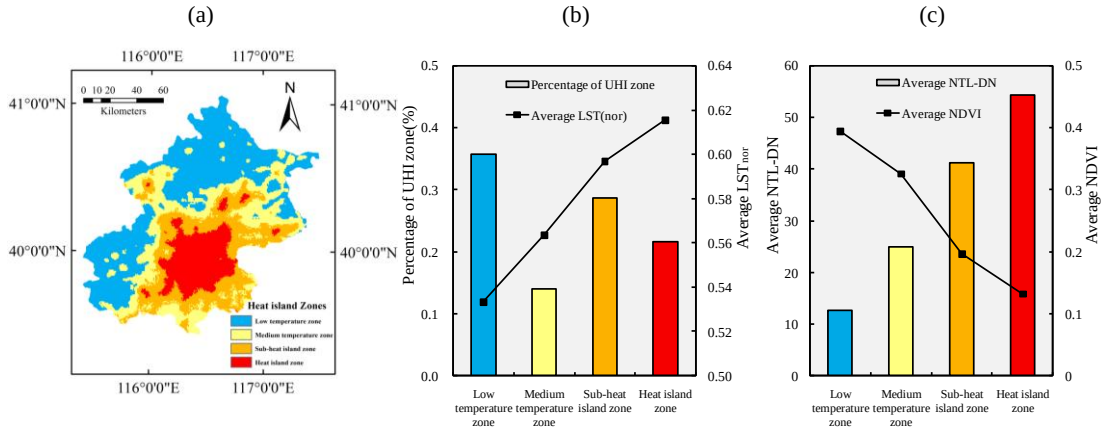

Figure 5-9 Heat island analysis results with NTL-DN and Landsat images in 2009: (**a**) Spatial pattern of heat island zones in 2009; (**b**) Proportions of UHI zones and average LST_{nor} in 2009; (**c**) Average NTL-DN and average NDVI of UHI zones in 2009;

5.6. Summary

In this chapter, we take Beijing city as case study to carry out urban heat island analysis and integrated assessment of the relationship between vegetation coverage and urbanization processing.

Two cloud free Landsat TM images in 1995 and 2009 were joint together to cover the total area of Beijing city. After necessary processing, the NDVI and LST map of Beijing city was got as the representative of the vegetation coverage and surface heat island situation. On the other hand, DMSP/OLS stable nighttime light data was carried out here to reflect the urbanization level on the specific year of 1995 and 2009. The results of this chapter were shown as below:

a) The value of the NDVI ranges from –0.63 to 0.79 in 1995, and changes to –0.93 to 0.75 in 2009, and NDVI changed significantly due to urban expansion during this period. Through a visual inspection in both 1995 and 2009, the normalized land surface temperature in the downtown area is obviously higher than that in the surroundings. Through a visual inspection, a surface urban heat island existed within the city.

b) Regression analysis was carried out between the NTL-DN with the NDVI and LST, the results showed that as the value of NTL-DN increased, the trend of mean NDVI decreased, high value of coefficient of determination (0.754 in 1995 and 0.929 in 2009) suggests a close negative correlation between the NTL-DN and mean NDVI. On the other hand, the LST showed a close positive correlation with determination coefficients reaching 0.651 in 1995 and 0.926 in 2009. The results indicate that an area with a higher NTL-DN value (more urbanized area), the mean LST within it would be higher than the surroundings, which provides strong evidence that the surface urban heat island effects are influenced by urban development.

c) Temporal comparison analysis between the difference of NTL-DN, NDVI and LST was carried out to investigate the SUHI driven by urban development. The NDVI difference showed a negative correlation with the NTL-DN difference, where the determination coefficient reached 0.681. Correlation analysis also has been conducted between the NTL-DN difference and LST difference. Result clearly demonstrated a positive

correlation between the two parameters, where the coefficient of determination was 0.664.

d) UHI zones were divided from the LST map in both 2005 and 2009 into four categories: heat island zone, sub-heat island zone, medium temperature zone, percentage of urban heat island zone increased from 9.3% in 1995 to 21.7% in 2009. Both the medium temperature and low temperature zones had a decrease of area proportion, especially the low temperature area which decreased from 44.0 to 35.7%. Changes of the proportions indicated an adverse effect on the thermal environment through the urbanization process from 1995–2009, and that the urban heat island zone occupied a higher proportion than before. In addition, in both 1995 and 2009, the value of average NTL-DN presented a rising gradient from the low temperature zone to the heat island zone, whereas the NDVI showed a downward trend.

Reference

[1] Ashraf M. Dewan, Yasushi Yamaguchi, Land use and land cover change in Greater Dhaka, Bangladesh: Using remote sensing to promote sustainable urbanization, Applied Geography, 29 (2009) 390-401.

[2] Zhi Qiao, Guangjin Tian, Lixiao Zhang, Xinliang Xu, Influences of Urban Expansion on Urban Heat Island in Beijing during 1989–2010, Advances in Meteorology, 2014 (2014) 1-11.

[3] Qihao Weng, Dengsheng Lu, Jacquelyn Schubring, Estimation of land surface temperature–vegetation abundance relationship for urban heat island studies, Remote Sensing of Environment, 89 (2004) 467-483.

[4] Reza Amiri, Qihao Weng, Abbas Alimohammadi, Seyed Kazem Alavipanah, Spatial–temporal dynamics of land surface temperature in relation to fractional vegetation cover and land use/cover in the Tabriz urban area, Iran, Remote Sensing of Environment, 113 (2009) 2606-2617.

[5] Peng Fu, Qihao Weng, A time series analysis of urbanization induced land use and land cover change and its impact on land surface temperature with Landsat imagery, Remote Sensing of Environment, 175 (2016) 205-214.

[6] José A. Sobrino, Juan C. Jiménez-Muñoz, Leonardo Paolini, Land surface temperature retrieval from LANDSAT TM 5, Remote Sensing of Environment, 90 (2004) 434-440.

[7] J. Cristóbal, J. C. Jiménez-Muñoz, J. A. Sobrino, M. Ninyerola, X. Pons, Improvements in land surface temperature retrieval from the Landsat series thermal band using water vapor and air temperature, Journal of Geophysical Research: Atmospheres, 114 (2009) n/a-n/a.

[8] Ji Zhou, Xu Zhang, Wenfeng Zhan, Huailan Zhang, Land Surface Temperature Retrieval from MODIS Data by Integrating Regression Models and the Genetic Algorithm in an Arid Region, Remote Sensing, 6 (2014) 5344-5367.

[9] Mohammad Taleghani, David J. Sailor, Martin Tenpierik, Andy van den Dobbelsteen, Thermal assessment of heat mitigation strategies: The case of Portland State University, Oregon, USA, Building and Environment, 73 (2014) 138-150.

[10] A. R. Dos Santos, F. S. de Oliveira, A. G. da Silva, J. M. Gleriani, W. Goncalves, G. L. Moreira, F. G. Silva, E. R. F. Branco, M. M. Moura, R. G. da Silva, R. S. Juvanhol, K. B. de Souza, Caas Ribeiro, V. T. de Queiroz, A. V. Costa, A. S. Lorenzon, G. F. Domingues, G. E.

Marcatti, N. L. M. de Castro, R. T. Resende, D. E. Gonzales, L. A. de Almeida Telles, T. R. Teixeira, Gmada Dos Santos, P. H. S. Mota, Spatial and temporal distribution of urban heat islands, Sci Total Environ, 605-606 (2017) 946-956.

[11] Gyanesh Chander, Brian L. Markham, Dennis L. Helder, Summary of current radiometric calibration coefficients for Landsat MSS, TM, ETM+, and EO-1 ALI sensors, Remote Sensing of Environment, 113 (2009) 893-903.

[12] P. Dash, F. M. Göttsche, F. S. Olesen, H. Fischer, Land surface temperature and emissivity estimation from passive sensor data: Theory and practice-current trends, International Journal of Remote Sensing, 23 (2002) 2563-2594.

[13] G. Li, D. Lu, E. Moran, S. Hetrick, Mapping impervious surface area in the Brazilian Amazon using Landsat Imagery, GIsci Remote Sens, 50 (2013) 172-183.

[14] Jinyeu Tsou, Jing Zhuang, Yu Li, Yuanzhi Zhang, Urban Heat Island Assessment Using the Landsat 8 Data: A Case Study in Shenzhen and Hong Kong, Urban Science, 1 (2017) 10.

Chapter Six: Conclusion

6.1. Conclusion

6.1. Conclusion

In the 21st century, urbanization is a very dynamic process worldwide which is forecasted by experts to increase even further in the future. As the urbanization and land sprawl had draw more and more attention, it is meaningful and useful to have an investigation of the urbanization processing in China in recent decades. The investigation of urbanization could help us to get a comprehensive understanding of what happened in the study region and promote better health and quality of life. The information it produces is helping urban residents and policymakers make informed decisions and take actions before the eco-environment get worse.

Land use and land cover change is one of the most important indicators in understanding the impact of human activities on the environment, which seem unprecedented despite profoundly affecting the earth's ecological systems. Global urban areas are rapid expanding nowadays, as ecosystems in urban areas are strongly influenced by anthropogenic activities, considerable attentions is currently directed towards monitoring changes in urban land use and land cover. As with the global warming and environment issues appeared, urban heat island had grown into prominent problem for the modern society. The urban heat island has so many bad influences such as energy consumption increasing, air pollution, water pollution, etc. Urban heat island is considered to be one of the major problems in the 21st century, it also be considered as one of the climatic disasters in urban areas and very harmful for citizens. Therefore monitoring the urban heat island effects is crucial for protecting the urban ecological and residential environment from being totally damaged.

This study focuses on the urbanization and eco-environment assessment, urban sprawl and urban expansion evaluation, urban heat island and its impact factors, urban structure and its effects on thermal comfort. Based on the previous study and theory analysis, the evaluation and simulation method is developed. The application research is executed for various considerations.

a) In Chapter one, research background and significance is investigated. In addition, previous study and current situation on the research fields was reviewed and discussed. The environmental issues caused by urbanization processing have become more and more serious, it is essential to do more in-depth study to explore the relationship between

the urbanization and eco-environment to provide guidance for sustainable development.

b) In Chapter two, an in-depth review of prior studies associated with the research topic was conducted. The literature review was carried out from three aspects: urbanization and eco-environment evaluation and coordination, urban sprawl assessment, urban heat island investigation.

f) In Chapter three, maximum entropy method was applied to help generate the evaluation system of eco-environment level and urbanization level at provincial scale in 2005 and 2015 in China. Comparison analysis and coordinate analysis was carried through to assess the development of urbanization and eco-environment as well as the balance and health degree of thee city develop. The weights of eco-environment pressure, eco-environment level, and eco-environment control are 6.57%, 64.75%, and 28.67% respectively. Urbanization indices system was composed of 2 negative indices and 20 positive indices. Economic urbanization, demographic urbanization, spatial urbanization, and social urbanization account for 30.33%, 8.85%, 27.38%, and 33.44% respectively. In both 2005 and 2015, the most urbanized province in China was Beijing. The highest value of eco-environment index was Qinghai which holds a highest value of eco-environment level indexes in both years.

c) In Chapter four, DMSP/OLS stable nighttime light dataset was used to measure and assess the urban dynamics from the extraction of built up area. Detailed information of data processing, method selection, dataset validation and evaluation system was introduced here. Urban sprawl was evaluated by analyzing the landscape metrics which provided general understanding of the urban sprawl and distribution pattern characteristics could be got from the evaluation. The result of the built-up area extraction of all the three cities showed an obvious expansion during the period from 1992 to 2013. The urban built-up proportion in Beijing increased from 4.75% in 1992 into 16.17% in 2013 by 3.4 times. The proportion in Shanghai increased from 10.17% in 1992 into 42.74% in 2013, increased by 4.2 times. To the situation in Guangzhou, the proportion increased from 1.806 % in 1992 to 17.77% in 2013.

d) In Chapter five, investigation of surface urban heat island effects in Beijing city which derive from land surface temperature retrieval from remote sensing data of Landsat TM

was carried out in this chapter. Spatial correlation and relationship between the urbanization level, vegetation coverage and surface urban heat island was carried out in this chapter. The analysis method in this chapter was composed of three parts: spatial relationship analysis, temporal comparison analysis and urban heat island analysis, respectively. The value of the NDVI ranges from –0.63 to 0.79 in 1995, and changes to –0.93 to 0.75 in 2009, and NDVI changed significantly due to urban expansion during this period. UHI zones were divided from the LST map in both 2005 and 2009 into four categories: heat island zone, sub-heat island zone, medium temperature zone, percentage of urban heat island zone increased from 9.3% in 1995 to 21.7% in 2009. Both the medium temperature and low temperature zones had a decrease of area proportion, especially the low temperature area which decreased from 44.0 to 35.7%

e) In Chapter seven, all the works has been summarized and a conclusion of whole thesis is deduced.

ACKNOWLEDGEMENTS

This work could not have been completed without the support, guidance, and help of many people and institutions, for providing data and insights, for which I am very grateful.

There are also a number of people without whom this thesis might not have been written and to whom I am greatly indebted.

First, I would like to extend my sincere gratitude to my supervisor, Professor Weijun Gao, for his support in many ways over the years and also for giving me the opportunity to study at the University of Kitakyushu. He has walked me through all the stages of the writing of this thesis. Thanks for his patience, motivation, and constant encouragement and guidance, besides, he also gives me much help for my daily life.

Also, I would like to thank to all university colleagues, Dr. Donny Koerniawan – who gave me the guidance and research supports, Dr. Chongyu Pengwang and Mr. Rui Wang for their help and cooperation, Dr. Jinming Jiang and Dr. Yanna Gao for numerous supports either research or daily life in Japan, and also the other fellow classmates who gave me their time in fulfilling my life along these years in Japan.

Finally, many thanks to my family for their support, encouragement and kind company which beyond words.